Cardiac Long-Axis Function. Experimental and Clinical Aspects.

Berg, Jonathan

2022

Document Version:
Publisher's PDF, also known as Version of record

Cardiac Long-Axis Function

Experimental and Clinical Aspects

JONATHAN BERG
DEPARTMENT OF CLINICAL PHYSIOLOGY | FACULTY OF MEDICINE | LUND UNIVERSITY

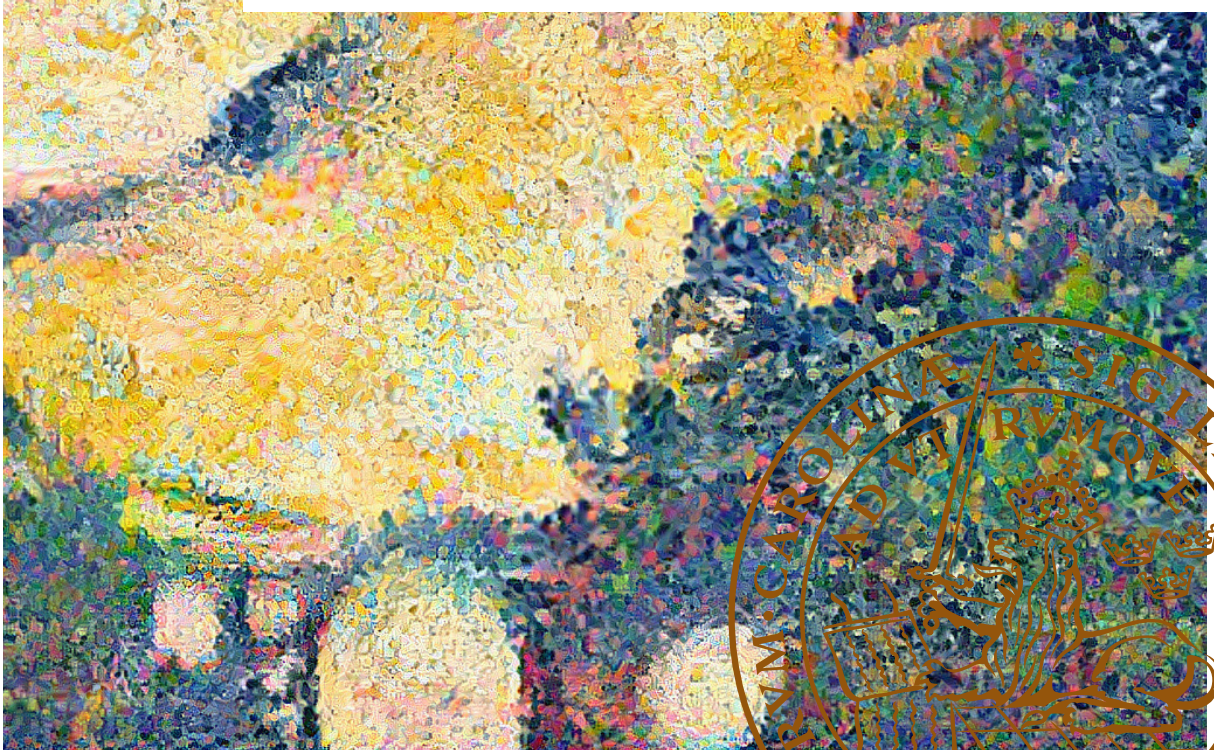

Cardiac Long-Axis Function

Experimental and Clinical Aspects

Cardiac Long-Axis Function
Experimental and Clinical Aspects

Jonathan Berg, M.D.

LUND
UNIVERSITY

Thesis for the degree of Doctor of Philosophy

Thesis advisors: Assoc. Prof. Marcus Carlsson, M.D.,Ph.D. Prof. Håkan Arheden, M.D., Ph.D. Assoc. Prof. Einar Heiberg, M.Sc. Kristian Solem, Ph.D, M.Sc.

Faculty opponent: Afshin Farzaneh-Far, M.D.

To be presented, with the permission of the Faculty of Medicine at Lund University, for public criticism in the lecture Hall 1 (Föreläsningssal 1) at Skåne University Hospital, Entrégatan 7, Lund, Swedenon Friday, 17th of June 2022 at 13:00.

Organization
LUND UNIVERSITY

Lund University, Department of Clinical Sciences Lund, Clinical Physiology, Skane University Hospital, Lund, Sweden.

Document name
DOCTORAL DISSERTATION

Date of issue 2022-06-17

Sponsoring organization
The Swedish Foundation for Strategic Research

Author(s)
Jonathan Berg

Title and subtitle

Cardiac long-axis function: Experimental and clinical aspects

Abstract

This thesis includes both experimental and clinical projects. The experimental studies investigate pathophysiological aspects of ventricular function and therapeutic hypothermia during acute myocardial infarction (AMI). The clinical projects investigate the ability of ventricular longitudinal function variables to predict mortality and morbidity in patients with heart failure and reduced ejection fraction (HFrEF).

Study I involves two experimental models of acute myocardial infarction (AMI), namely an ischemia/reperfusion model and a microembolization model. The aim is to investigate the relationship of stroke volume to ventricular longitudinal function in the two models of AMI. The main finding is that stroke volume closely follows the ventricular longitudinal function after infarction in both experimental models. This highlights the link between ventricular longitudinal function and cardiac performance.

Study II involves an experimental model of ischemia/reperfusion injury. The aim is to investigate changes in ventricular energetics using non-invasive pressure-volume loops after therapeutic hypothermia during AMI. The main finding is that hypothermia (<35°C) adjunct to reperfusion yields preserved cardiac volumes and work. Furthermore, this effect was not explained by reductions in infarction sizes.

Study III investigates the ability of ventricular longitudinal function to predict mortality in patients with HFrEF. Ventricular longitudinal function is measured as atrioventricular plane displacement (AVPD) or global longitudinal strain (GLS). The main finding is that AVPD and GLS exceed well-known clinical risk factors as predictors of mortality using standard survival analyses.

Study IV builds upon the investigation from Study III and focuses on the ability of AVPD and GLS to predict cardiovascular morbidity with methodologies that incorporates reoccurring events. The results show that AVPD and GLS are valuable predictors of morbidity when using reoccurring event analyses.

Key words: Heart Failure, Myocardial Infarction, Magnetic Resonance Imaging, Pressure-Volume loops, Hypothermia, Atrioventricular Plane Displacement, Global Longitudinal Strain

Classification system and/or index termes (if any):

Supplementary bibliographical information:

Language
English

ISSN and key title:
1652-8220

ISBN
978-91-8021-258-8

Recipient's notes

Number of pages
254

Price

Security classification

Cardiac Long-Axis Function

Experimental and Clinical Aspects

Jonathan Berg, M.D.

LUND
UNIVERSITY

Cover: A 4-chamber long-axis view of Jonathan Berg's heart in the style of the "Provence Landscape" painting by Henri-Edmond Cross. This artwork was created with the help of Artificial Intelligence in the NightCafe Creator application [https://creator.nightcafe.studio].

Typeset in LaTeX

Faculty of Medicine, Department of Clinical Physiology
ISBN: 978-91-8021-258-8
ISSN: 1652-8220
Lund University, Faculty of Medicine Doctoral Dissertation Series 2022:97

Printed in Sweden by Media-Tryck, Lund University, Lund 2022

Ithaka

As you set out for Ithaka hope your road is a long one, full of adventure, full of discovery. Laistrygonians, Cyclops, angry Poseidon—don't be afraid of them: you'll never find things like that on your way as long as you keep your thoughts raised high, as long as a rare excitement stirs your spirit and your body. Laistrygonians, Cyclops, wild Poseidon—you won't encounter them unless you bring them along inside your soul, unless your soul sets them up in front of you.

Hope your road is a long one. May there be many summer mornings when, with what pleasure, what joy, you enter harbors you're seeing for the first time; may you stop at Phoenician trading stations to buy fine things, mother of pearl and coral, amber and ebony, sensual perfume of every kind—as many sensual perfumes as you can; and may you visit many Egyptian cities to learn and go on learning from their scholars.

Keep Ithaka always in your mind. Arriving there is what you're destined for. But don't hurry the journey at all. Better if it lasts for years, so you're old by the time you reach the island, wealthy with all you've gained on the way, not expecting Ithaka to make you rich.

Ithaka gave you the marvelous journey. Without her you wouldn't have set out. She has nothing left to give you now.

And if you find her poor, Ithaka won't have fooled you. Wise as you will have become, so full of experience, you'll have understood by then what these Ithakas mean.

- C. P. CAVAFY

Contents

Studies I-IV

This thesis is based on the following publications and manuscripts:

I **Decreased atrioventricular plane displacement after acute myocardial infarction yields a concomitant decrease in stroke volume**

Jonathan Berg, Robert Jablonowski, David Nordlund, Sascha Kopic, Sebastian Bidhult, Christof G.Xanthis, Maythem Saeed, Kristian Solem, Håkan Arheden, Marcus Carlsson.

Journal of Applied Physiology 128: 252–263, 2020. First published December 19, 2019; doi:10.1152/japplphysiol.00480.2019.

II **Hypothermia yields favorable cardiac energetics in experimental ischemia/reperfusion – insights from PV loops by CMR**

Jonathan Berg, Robert Jablonowski, David Nordlund, Daniel Ryd, Einar Heiberg, Marcus Carlsson, Håkan Arheden.

Submitted manuscript

III **Ventricular longitudinal shortening is an independent predictor of death in heart failure patients with reduced ejection fraction**

Jonathan Berg, Robert Jablonowski, Mohammed Mohammad, Kristian Solem, Rasmus Borgquist, Ellen Ostenfeld, Håkan Arheden, Marcus Carlsson.

Scientific Reports. 11:20280, 2021. First published October 13, 2021; https://doi.org/10.1038/s41598-021-99613-1.

IV **Ventricular longitudinal function by cardiovascular magnetic resonance predicts cardiovascular morbidity in HFrEF patients**

Jonathan Berg, Julius Åkesson, Robert Jablonowski, Kristian Solem, Einar Heiberg, Rasmus Borgquist, Håkan Arheden, Marcus Carlsson.

ESC Heart Failure. Published online in Wiley Online Library. First published April 11, 2022; https://doi.org/10.1002/ehf2.13916

Preface

It was a chance that got me into research, as I previously had no plan to do research in any diligent manner. This chance was offered to me by my supervisor Marcus when he, in the spring of 2017, presented an upcoming Ph.D. project at a lecture in the Radiology Department. In some ways, I happened to be at the right place at the right time, have the proper education, and, perhaps most importantly, was curious enough to sign up for more information.

After graduating the medical school in Lund and spending a few months working in the surgery department at Helsingborg Hospital, I applied for this project. I was excited and curious about where this could lead. I got accepted, and my Ph.D. studies were initiated in the fall of 2017 at the Department of Clinical Physiology in Lund. The project was a collaboration between Lund University and Syntach AB, a med-tech company in Lund that develops a novel cardiac assist device for heart failure.

The project had a lot of pull factors. It sounded fascinating for a newly graduated doctor: research and development of a novel implantable cardiac assist device to help patients struggling with end-stage heart failure, experimental studies, learning research, and ultimately the chance of acquiring a Ph.D.

This collaboration between academia and industry has worked out terrifically and has provided me with many friends and experiences. As it is for many Ph.D. projects, the initial plan is malleable. Due to various circumstantial reasons, some studies that we initially planned for were substituted for the current studies in this thesis. However, we persistently managed to find new paths forward, and I am proud of the result.

This thesis was also the result of generous funding from the Swedish Foundation for Strategic Research (SSF), making it possible for me to work on this project full-time. Without their aid, we could never have carried out our work to this extent.

— Jonathan Berg, May of 2022

Syntach AB och Medicinska fakulteten på Lunds Universitet söker gemensamt en läkare för en industridoktorandtjänst.

Doktorand inom Medicinteknik/Kardiologi/ Klinisk fysiologi

Sökanden ska ha avlagt läkarexamen och ska ha intresse och acceptans för djurstudier. Erfarenhet från kardiologi, klinisk fysiologi, eller medicinteknik är meriterande men krävs ej. Syntach AB är ett medicinteknisk startupföretag, grundat 2012 i Lund, som utvecklar ett aktivt hjärtimplantat. Doktorandprojektet kommer att pågå under 5 år med början 2017 i samarbete mellan Syntach och hjärt-MR-gruppen vid Lunds universitet. Anställningen är 80% forskning på Syntach och 20% kliniskt arbete vid Skånes universitetssjukhus. Projektets mål är att förbättra hjärtfunktionen genom en nyutvecklad assist device som återställer hjärtats normala klaffplansrörelse. Doktoranden kommer att arbeta med djurförsök och kliniska studier med fokus på de fysiologiska effekterna av behandlingen av hjärtsviktspatienter.

Ansökan skickas senast 12/7 till info@syntach.com. För frågor skicka mail eller kontakta Kristian Solem (Syntach) tel 0702-718303, Marcus Carlsson (Lunds Universitet) tel 0705-212424.

Abbreviations

AHA American Heart Association. 29

AMI acute myocardial infarction. 24, 26, 27, 31, 41, 47, 53, 57, 59, 71, 76, 77, 91, 97

ANCOVA analysis of covariance. 79

AV atrioventricular. 9, 39

AVPD atrioventricular plane displacement. 20, 31, 32, 40, 53, 64, 71, 72, 84, 97, 100

bSSFP balanced steady-state free precession. 35

CABG coronary artery bypass grafting. 25, 30

CMR cardiac magnetic resonance. 23, 31, 38, 77, 84, 97, 102

CV cardiovascular. 47, 48, 53, 84, 91

EDPVR end-diastolic pressure-volume relation. 15

EDV end-diastolic volume. 71, 94

EF ejection fraction. 22, 53

ESV end-systolic volume. 71, 94

Gd gadolinium. 35, 36

GLS global longitudinal strain. 22, 31, 32, 53, 64, 84, 98

HF heart failure. 24, 28, 31, 47, 53, 91, 97

HFpEF heart failure with a preserved ejection fraction. 29, 30, 38

HFrEF heart failure with a reduced ejection fraction. 29, 30, 32, 53, 91, 97

I/R ischemia/reperfusion. 53, 57, 59, 61, 62, 71, 77, 79

ICM ischemic cardiomyopathy. 89

IS infarct size. 24, 27, 77

LAD left anterior descending artery. 9, 24, 60

LCX left circumflex artery. 9, 24

LGE late gadolinium enhancement. 35, 37, 53, 62

LV left ventricle. 9, 31, 39

LVM left ventricular mass. 74

MAP mean arterial pressure. 77, 78

MAPSE mitral annular plane systolic excursion. 22, 31, 32, 39, 40, 71, 84, 102

MaR myocardiium at risk. 24, 27, 77

MCS Mechanical circulatory support. 30

ME microembolization. 53, 59, 62, 71

MI myocardial infarction. 24, 71, 91

mPTP mitochondrial permeability transition pore. 26

MRI magnetic resonance imaging. 34

MSM multi-state model. 48

NICM non-ischemic cardiomyopathy. 89

NMR nuclear magnetic resonance. 33

NYHA New York Heart Association. 29, 84, 91

PCI percutaneous coronary intervention. 25, 27, 41

PV Pressure-Volume. 13, 41, 64, 77, 97, 102

PWP Prentice, William, and Peterson. 48

RAAS renin-angiotensin-aldosterone system. 58, 91

RCA right coronary artery. 9, 24

RV right ventricle. 39

SSFP steady-state free precession. 62

STEMI ST-elevation myocardial infarction. 24, 27, 31, 72

SV stroke volume. 41, 53, 71, 97

TAPSE tricuspid annular plane systolic excursion. 39, 64, 86

TDI tissue Doppler imaging. 39

TH therapeutic hypothermia. 27, 28

Populärvetenskaplig sammanfattning

Hjärtsjukdom är en av de vanligaste dödsorsakerna i världen. Denna avhandling är inriktad på hjärtsvikt och en av dess vanligaste orsaker – hjärtinfarkt. En hjärtinfarkt uppstår när syretillförseln till en del av hjärtmuskeln hindras, vanligtvis av en blodpropp i ett kranskärl. Denna syrebrist leder till smärta och kallas i vardagligt tal för ”hjärtattack”. I förlängningen leder detta till att den drabbade hjärtmuskeln dör, vilket kallas hjärtinfarkt. Små infarkter klarar hjärtat av, men vid en viss gräns leder den försämrade pumpförmågan till att hjärtat sviktar. Denna hjärtsvikt orsakar symptom som andfåddhet, trötthet, svullnad i underben, och kraftigt nedsatt arbetsförmåga hos individen. För patienter med hjärtsvikt är sjukhusinläggningar vanliga och dödligheten är i snitt högre än för många cancerformer. Bakgrunden till den höga dödligheten är det faktum att ett svagt och sviktande hjärta inte klarar av att tillgodose kroppens behov.

Ett vanligt sätt att tänka på hjärtat är att se det som en pump. En av de vanligaste föreställningarna om hur hjärtat pumpar är att det huvudsakligen sker med en inåtgående, ”kramande”, rörelse. Forskning med hjälp av ultraljud och magnetkamera (MR) av hjärtat har istället visat att hjärtats yttre form är relativt oförändrad under ett hjärtslag. Pumpförmågan sker istället huvudsakligen genom förflyttning av klaffplanet mellan förmak och kammare, kallat ”AV-planet”. Denna rörelse, som liknas vid upp-och-ner förflyttningen i en cykelpump, har visat sig vara sänkt vid hjärtinfarkt och hjärtsvikt och hänger samman med dödlighet i flera hjärtsjukdomar.

Det övergripande syftet med denna avhandling är att vidare utreda hur hjärtats pumpförmåga förändras vid och efter hjärtinfarkt, samt att utröna om denna pumpförmåga kan förutse prognosen hos patienter med svår hjärtsvikt. Metoden som används för att undersöka hjärtat är MR. Avhandlingen innehåller både djurexperimentella och patientbaserade studier, och består av fyra delarbeten:

- **Delarbete I** är en djurexperimentell studie som undersöker hur två olika typer av hjärtinfarkter påverkar AV-planets rörelse och hur detta är kopplat till försämring av hjärtats pumpförmåga. Fynden visar att AV-plansrörelsen har en stark koppling till hjärtats slagvolym och att dessa följer sig åt veckan efter en hjärtinfarkt.

- **Delarbete II** är en djurexperimentell studie som undersöker hur en nedkylning till en kroppstemperatur under 35°C vid en hjärtinfarkt skyddar hjärtats funktion. Detta

undersöks genom att analysera tryck-volymloopar, även kallat ”PV loopar”, från MR. Resultaten visar att nedkylningen tenderar att bevara hjärtats funktion efter en hjärtinfarkt och att detta resultat står sig även när man tar hänsyn för olika infarktstorlekar.

- **Delarbete III** är en överlevnadsstudie som undersöker hur hjärtats förkortning i den längsgående riktningen kan förutse överlevnad hos 287 patienter med hjärtsvikt och uttalat sänkt systolisk kammarfunktion. Den längsgående hjärtfunktionen analyseras via MR-undersökningar och fynden relateras till data från det nationella dödsorsaksregistret. Resultaten från överlevnadsanalyser är att AV-plansrörelsen samt hjärtmuskelns formförändring är viktiga faktorer som förutsäger överlevnaden bättre än flera vanligt förekommande mätvärden.

- **Delarbete IV** är en fortsättningsstudie till Delarbete III på samma grupp av patienter. Denna syftar till att undersöka hur hjärtats längsgående pumpfunktion kan förutse sjukligheten i denna patientgrupp med uttalad hjärtsvikt. För att besvara detta samlas data in från det Socialstyrelsens slutenvårdsregister och en mer avancerad statistisk metodik som inkluderar flera händelser per patient används. Denna studie finner att hjärtats längsgående förkortning och formförändring hänger samman med antalet sjukhusinläggningar samt är bättre på att förutse sjukligheten hos hjärtsviktspatienter än vanligt förekommande mätvärden.

Sammanfattningsvis leder dessa resultat till ökad förståelse om sjukdomsmekanismer kring hur AV-planets rörelse påverkas vid hjärtinfarkt samt understryker att hjärtats längsgående funktion är en viktig markör för både dödlighet och sjuklighet hos patienter med svår hjärtsvikt. Avhandlingen berör också effekterna av kylning som en behandlingsmetod för att minimera skador vid hjärtinfarkt samt förespråkar vidare användning av MR-baserade PV loopar i framtida studier.

Popular summary

Heart disease is one of the most common causes of death in the world. This dissertation focuses on heart failure and one of its most common causes - myocardial infarction. A myocardial infarction occurs when the oxygen supply to a part of the heart muscle is blocked, usually by a blood clot in a coronary artery. This lack of oxygen leads to pain and is colloquially called a ”heart attack.” In the long run, this leads to the affected heart muscle dying, which is called a myocardial infarction. Small infarcts are withstood by the heart, but the impaired pumping ability leads to the heart failing at a certain point. This heart failure causes symptoms such as shortness of breath, fatigue, swelling of the lower legs, and severely reduced work capacity of the individual. Hospitalizations are common for patients with heart failure, and mortality is higher than for many cancers. The basis of the high mortality rate is the fact that a weak and failing heart is unable to meet the body's needs.

A common way of thinking about the heart is to see it as a pump. A common belief about how the heart pumps is that it mainly does this by an inward ”squeezing” motion Research using ultrasound and magnetic resonance imaging (MRI) of the heart has instead shown that the external shape of the heart is relatively unchanged during a heartbeat. Instead, the heart pumps mainly by moving the valve plane located between the atrium and chamber, called the ”AV plane”. This movement, which is similar to the up-and-down stroke in a bicycle pump, has been shown to be reduced after a heart attack and in heart failure and is associated with mortality in several heart diseases.

The overall purpose of this dissertation is to further investigate how the heart's pumping changes during and after a heart attack and to find out if this pumping ability can predict the prognosis in patients with severe heart failure. The method used to examine the heart is MRI. The dissertation contains both experimental and clinical studies and consists of four parts:

- **Study I** is an experimental study that examines how two different types of heart attacks affect the AV plane's movement and how this is linked to a worsening in the heart's pumping ability. The findings show that the AV plane movement is strongly linked to the heart's stroke volume and that these follow each other during the week after a heart attack.

- **Study II** is an experimental study investigating how cooling to a body temperature below 35°C in a heart attack protects the heart's function. This is examined by analyzing pressure-volume loops, also called "PV loops," from MR. The results show that the cooling tends to preserve the heart's function after a heart attack and that this result holds up when different infarct sizes are taken into account.

- **Study III** is a survival study that examines how the shortening of the heart in the longitudinal direction can predict survival in 287 patients with heart failure and markedly reduced systolic ventricular function. The longitudinal cardiac function is analyzed via MRI examinations, and the findings are related to data from the National Cause of Death register. The survival analysis results show that the AV plane movement and the deformation of the heart muscle are important factors that predict survival better than several commonly used measured values.

- **Study IV** is a follow-up study to Study III on the same group of patients. This investigates how the heart's longitudinal function can predict the morbidity in this patient group with pronounced heart failure. To answer this, data is collected from the National Board of Health and Welfare's In-patient care register, and a more advanced statistical methodology that includes several events per patient is used. This study finds that the longitudinal shortening and deformation of the heart is related to the number of hospitalizations and is better at predicting the morbidity of heart failure patients than commonly used measurements.

In summary, these results lead to an increased understanding of disease mechanisms affecting the AV plane's movement in a heart attack and emphasize that the longitudinal function of the heart is an important marker for both mortality and morbidity in patients with severe heart failure. The dissertation also discusses the effects of cooling as a treatment method to minimize injuries after heart attacks and advocates using MRI-based PV loops in future studies.

Part I

Research Context

Chapter 1

Introduction

Form and Function of the Cardiovascular System

1.1 Cardiac Macrostructure

The anatomical morphology of the heart is essential for understanding its functional capability. The heart is a muscular organ that solves the vital problem of pumping sufficient blood throughout the circulation to sustain a functioning organism, that is, to supply and regulate the blood flow to meet the requirement of the tissues. This thesis will mainly focus on the left ventricle since this is the primary source of impairment in most patients with myocardial infarction and heart failure.

The four distinct heart chambers divide into a left and a right side by the interventricular septum. Both sides have thin-walled, low-pressure atria and thicker-walled, higher-pressure ventricles. The left side of the heart receives blood from the four pulmonary veins and ejects blood through the aorta into the systemic circulation. The right side of the heart receives blood from the large systemic veins: the inferior and superior vena cava. The right ventricle ejects blood into the pulmonary circulation through the pulmonary artery for blood oxygenation, dissipating carbon dioxide. An approximately six-fold difference between the systemic and pulmonary circulation in mean pressure requires different structural adaptations for each chamber. This is evident in the muscular wall thickness of the left ventricle (<12 mm) in contrast to the right ventricle (3-5 mm). The left ventricle typically ejects against mean aortic pressures of 75-90 mmHg at rest, while the right ventricle ejects against mean pulmonary pressure of 12-15 mmHg.

The heart with the surrounding non-distensible pericardium sits in the center of the thoracic cavity, wholly embedded by the lungs, connective tissue, and fatty contiguous tissues. Therefore, the heart's pumping is not isolated from any medium, but rather, the heart will push and pull on the surrounding tissues with each heartbeat. Thus, the soft tissues embedding the heart are displaced, equivalent to any change in heart size during

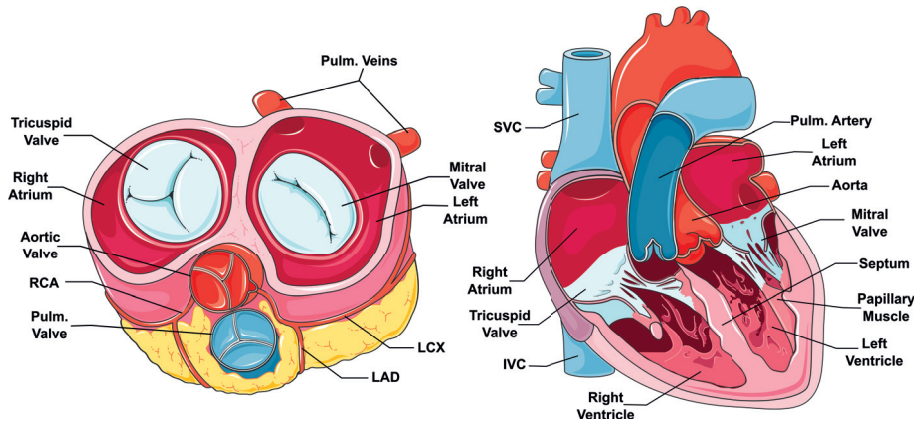

Figure 1.1: Left: the atrioventricular valve plane viewed from the atrial side. Right: the heart viewed in a long-axis cross-section. RCA, right coronary artery; LAD, left anterior descending artery; LCX, left circumflex artery; SVC, superior vena cava; IVC, inferior vena cava; *Adapted with labels from Servier Medical Art, provided by Servier, licensed under a Creative Commons (CC) Attribution 3.0 unported license*

the cardiac cycle. As it happens, the heart's outer contour changes affect the air in the lungs, and small bouts of air are pushed out from the lungs every heartbeat [1]. These are negligible during respiration but can be detected during prolonged apnea. The slight outer contour change of the heart in the order of a few percent [2], and is discussed in more detail later. This type of motion would waste energy if significant and would not be optimal for longevity. Blood pumping should theoretically be performed at optimal energetic economy while balancing the output between the pulmonary and systemic circulatory loops. The heart can perform this task primarily with a longitudinal mode of pumping, a volume-regulating septum, and a near-constant heart volume throughout the heartbeat [3]. The longitudinal mode of pumping is further discussed in later sections.

The left side of the heart supplies the systemic circulation with pressurized, nutrient-rich, and oxygenated blood. Blood pressure fundamentally exists to combat the gravitational pull following an upright posture while maintaining pressure above the lower limit of cerebral autoregulation. An adamant regulation of systemic blood pressure is vital as cerebral blood flow interruption for five seconds causes loss of consciousness [4]. The tissues need a pressure gradient enabling perfusion through the microcirculation. In contrast, the venous system does not require significant blood pressure due to valves limiting backflow.

Inside the heart, the propagation of blood flow in the forward direction is ensured by the atrioventricular (AV) valve apparatus (Figure 1.1). The semilunar valves of the major arteries (the aortic and pulmonary valves) similarly prevent the backflow of blood into the ventricles during filling. The AV valves consist of the mitral valve, situated between the left atria and ventricle, and the tricuspid valve, located between the right atria and ventricle.

The valve orifices of the AV and semilunar valves are connected with a fibrous structure known as the atrioventricular (AV) plane [5], which is of high importance to the concept of longitudinal pumping. The AV valves are also connected to the myocardium by the papillary muscles and their non-distensible fibrous strings: the chordae tendineae. This structure effectively prevents the valves from prolapsing inside the atria during ventricular systolic pressure work while remaining entirely flaccid and permitting diastolic low-pressure filling.

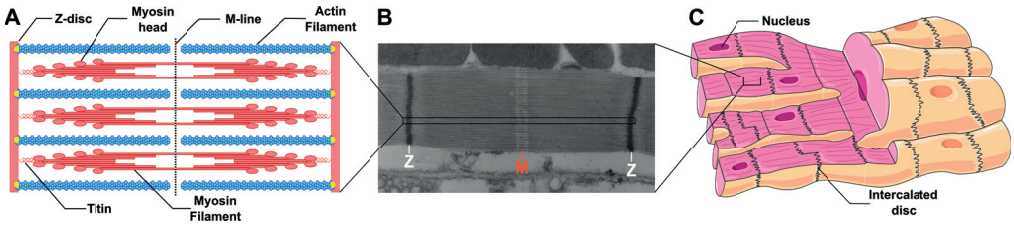

Figure 1.2: A: Schematic illustration of the intracellular proteins involved in the contractile apparatus. B: Transmission electron microscopy image of a longitudinal section of a sarcomere showing tightly packed actin-myosin complexes. C: Schematic illustration of branching myocytes. Note that unlike skeletal myocytes, cardiac myocytes only have one nucleus. *Sources: A, Adapted from David Richfield (27 July 2014), "Medical gallery of David Richfield 2014", WikiJournal of Medicine, 1 (2), licensed under Creative Commons BY 4.0; B: Reproduced from Loison et. al. PLoS Biology 2018, licensed under Creative Commons BY 4.0; C, Adapted with labels from Servier Medical Art, provided by Servier, licensed under a Creative Commons (CC) Attribution 3.0 unported license.*

1.2 Cardiac Microstructure

1.2.1 The Contractile Apparatus

The macroscopic contraction is generated, at its foundation, from a single myocardial muscle cell – i.e., the myocyte. The contractile apparatus within the myocyte, called the sarcomere, arises from arrangements of overlapping intracellular filaments (Figure 1.2). The "sliding filament theory" first described in 1954 [6, 7] explains our current understanding of the interplay between these intracellular components. The contraction occurs when two intracellular proteins, actin and myosin, partake in cycles of linking, structural re-arrangement, and releasing. Both linking and releasing activities require energy as adenosine triphosphate (ATP). The actin and myosin filaments are tightly packed and overlap. The outer anchor of the thin actin filament is the Z-disc. The middle anchor of the thick myosin filament is the M-line.

When an electrical impulse depolarizes the cardiomyocyte, Ca^{2+} floods the intracellular volume. The increase in Ca^{2+} concentration triggers additional Ca^{2+} release stored in the sarcoplasmic reticulum. When Ca^{2+} binds to troponin, which usually blocks the binding between actin and myosin, it re-arranges, leaving the binding sites open. This enables the binding of crosslinks between actin and myosin. ATP molecules carried by myosin are hydrolyzed during the crosslink formation, which causes the myosin head to pull on the actin filament – effectively shortening the sarcomere. When additional ATP is added, the myosin head coils back to its initial position and prepares for a new cycle. The force and duration of contraction depend on the calcium cycling, i.e., the contraction will continue as long as there is Ca^{2+} present. In normal homeostasis, Ca^{2+} is rapidly pumped back

into the sarcoplasmic reticulum and out of the cell upon repolarization. The contractile apparatus will undergo rigor if no new ATP is made available, such as after the organism's demise.

In addition to contraction, relaxation is an essential part of the heart cycle. The effective return of the contractile apparatus to its initial position is augmented by the gigantic protein titin [8, 9]. The titin spans between the Z-disc to the M-line and have portions resembling Hookean elastic springs that gradually compress and store potential energy upon contraction. This energy is released, contributing to swift relaxation and restoring the sarcomere to its slack length. Another key mechanism of diastolic relaxation is the effective intracellular calcium transport by the sarcoendoplasmic reticulum Ca^{2+}-ATPase "SERCA" and the level of inhibition from its regulatory protein phospholamban [10]. Thus, the diastolic relaxation is sensitive to the myofilaments' energy supply/demand balance and is an early marker of ischemia and hypertrophy [11].

The almost immediate synchronicity of the entire myocardium is the corollary of the electrical connections between cardiomyocytes through intercalated discs. These contain desmosomes and gap junctions that almost instantly propagate the electrical charges within myocytes through the branching meshwork.

1.2.2 Fiber Orientations and Sheetlets

Historical Background

Researchers and anatomists have long tried to elucidate how the heart's function is linked to the heart's structure. Part of this lack of understanding has likely come because of a scarcity of precision or non-destructive dissection methods. Historically, anatomists and pathologists were for a long time limited to investigating the heart's finer structure ex-vivo, mainly during or after rigor mortis contracture. To say nothing of the eloquent dissection studies produced by *Stensen* and *Lower* in the 1600s, *Winslow* and *Senac* in the 1700s, and *Ludwig* and *Pettigrew* in the 1800s, which are consistent in depicting a continuum of helical arranging myocardial pathways that transmurally traverse from a left-handed angle toward a right-handed angle, these ex-vivo methods hampered the understanding of how the heart was contracting inside a living organism. A detailed review of earlier studies of myocardial architecture was published by *Greenbaum et. al.* [5]. Mathematical modeling by *Sallin* in 1969 [12] showed that the only possible orientation of myocardial fibers achieving a physiological ejection fraction is helical, which follows what has been observed.

However, studies conflicting with the helical architecture did also arise. An intriguing example is the ventricular myocardial band (VMB), made famous by *Torrent-Guasp* [13]. The essence of the VMB theory is that the whole-heart 3d-architecture can be undone in a series of meticulous dissections, unwinding the heart into a continuous long strip of muscle. Although there are large-scale similarities in our current understanding, such as the oblique angulation of muscle bundles, the microstructural architecture we is not

coherent with distinct macroscopic layers of muscle. Thus, the VMB has been disproven and primarily attributed to the particular dissection procedure [5, 14, 15].

Modern Evidence

The visible deformations at the organ level are ultimately linked to events at the microscopic level. Therefore, it is of interest to go deeper into the microstructure of the heart to understand both physiological and pathophysiological mechanisms that contribute to cardiac pumping. Whereas the myocardium may seem like a homogenous tissue, the microstructure is arranged in a highly complex and organized architecture at the micro-scale. The whole heart can be seen as an ellipsoidal pressure vessel, woven with interconnected "fibers" – metaphorically cloth fibers threads – made up of interlinked myocardial cells. The term "fiber" is somewhat inaccurate since the myocytes continuously branch and merge at every few myocytes. Thus, it is impossible to talk about specific fibers per se [16], but instead, it is more accurate to speak of varying fiber orientations.

New techniques arising in the recent two decades, such as diffusion tensor imaging "DTI" by CMR, made available to researchers a view into the changes of the microarchitecture in both systole and diastole. DTI utilizes diffusion (i.e., random motion of water molecules) weighted imaging to extract the primary direction, or "eigenvector," where the diffusion is greatest. The secondary eigenvector "$\overrightarrow{E_2}$" is orthogonal to the primary eigenvector "$\overrightarrow{E_1}$" and represents the second greatest diffusion direction. A third eigenvector is orthogonal to both $\overrightarrow{E_1}$ and $\overrightarrow{E_2}$ and is where diffusion is most restricted [17]. Since the myocytes are long and thin, the water diffusion is most significant along the length of the myocyte. Thus, the $\overrightarrow{E_1}$ is equal to the long axis of myocytes while the $\overrightarrow{E_2}$ is where the aqueous diffusion orthogonal to $\overrightarrow{E_1}$ is greatest [18]. When $\overrightarrow{E_1}$ is equal to the helix angle, the $\overrightarrow{E_2}$ lies in the sheetlet/shear plane perpendicular [19], as discussed below. There are reservations to this statement since in-vivo DTI only measures mean diffusion inside a voxel (typically 3x3x8mm^3), which may include more than one sheetlet population.

The three eigenvectors together create a diffusion ellipsoid, or "tensor". If diffusion were unrestricted, this ellipsoid should instead appear as a sphere with equal eigenvectors in all directions. With a sufficient number of acquisitions covering the entirety of the heart, a visually appealing 3d-tractography of the heart can be created depicting the myocardial microstructure [20, 21]. This has heavily influenced our current understanding of the myocardial 3d-transformation during a heartbeat in health and disease.

A few myocytes in the proximity of each other are arranged in small bundles, as shown by *Streeter et.al.* in renowned histopathological studies [22]. The fiber orientation of these bundles of cells, often called fibers, transitions from an oblique angle of +60° to an almost orthogonal -60° from the endocardium towards the epicardium, referencing the ventricular equator as 0° (Figure 1.3). The double-helical orientation contributes to the ventricular torsion, like the wringing of a cloth. Furthermore, Streeter et al. also showed that the helix

angles do not change significantly over the heart cycle and that the proportion of mid-wall circumferential fibers ±(0-22.5°) dominates 10 to 1 over the more fringe longitudinal fibers ±(67.5-90°).

Another essential micro-structure significantly contributes to our understanding of how a relatively small shortening (∼15%) and thickening (∼8%) of a single myocyte can contribute to a ∼40% centripetal (i.e., towards the center) wall thickening and ∼15% decrease in apical-basal length (i.e., longitudinal shortening). This is the small myolaminar bundle in recent literature often called "sheetlet" – meaning a small sheet. The laminar re-arrangements of these small sheets help to explain the wall-thickening during the heart cycle. Electron microscopy studies by *LeGrice et. al.* [23] measured the sheetlets to be ∼50μm thick, ∼4 myocytes across, and detected distinct cleavage planes in between them. The myocytes within sheetlets are tightly packed whereas loose connective tissue in cleavage planes allows for slip and shear mechanics along these planes. The sheetlets undergo both a sheet-normal shear and a slight sheet extension and thinning during contraction [24]. In addition, *Ashikaga et. al.* [25] found not only one but two distinct populations of sheetlets approximately perpendicular to each other in canine hearts. The view of two sheetlet populations of opposite polarity scattered throughout the myocardium has been further validated by *Gilbert et. al.* [26]. Their presence contributes to centripetal and longitudinal displacement of ventricular muscle mass [27], and like intertwined fibers in a rope, they rapidly distribute stresses during deformation in all directions [16].

In the last decades, research using histopathology and CMR with DTI [17, 20, 28] has corroborated the function of the sheetlets in-vivo. The inter-sheet shear and slippage result in an accordion-like re-arrangement from diastole to systole (Figure 1.3). This means that they both increase their angulation relative to each other and slide over one another. This mechanism extends the myocardium in the centripetal direction which significantly augments systolic wall-thickening and longitudinal shortening.

In disease, helix angles and sheetlet re-arrangement can be disturbed due to myocyte damage and disarray. Infarcted myocardium exhibits increased diffusion due to myocyte necrosis and swelling [29] and disturbed propagation of myocardial fibers [30]. Ventricular dilatation after a large myocardial infarction causes circumferential re-angulation of epicardial longitudinal fibers in remote regions of the heart [28]. Failed systolic conformations of sheetlets have been identified in dilated cardiomyopathy [21]. In addition, computer simulations have shown that more circumferential fiber orientations detrimentally impact longitudinal function [31] and myocardial strain [32]. Although many diseases exhibit microstructural disturbances, the novel measurements by DTI have not yet gained a large evidence base. To summarize, it is highly expected that disease progression, e.g. with poor apical-basal function, for a big part has its foundation in disturbed microstructural function such as restricted sheetlet re-arrangement and fiber disarray [33].

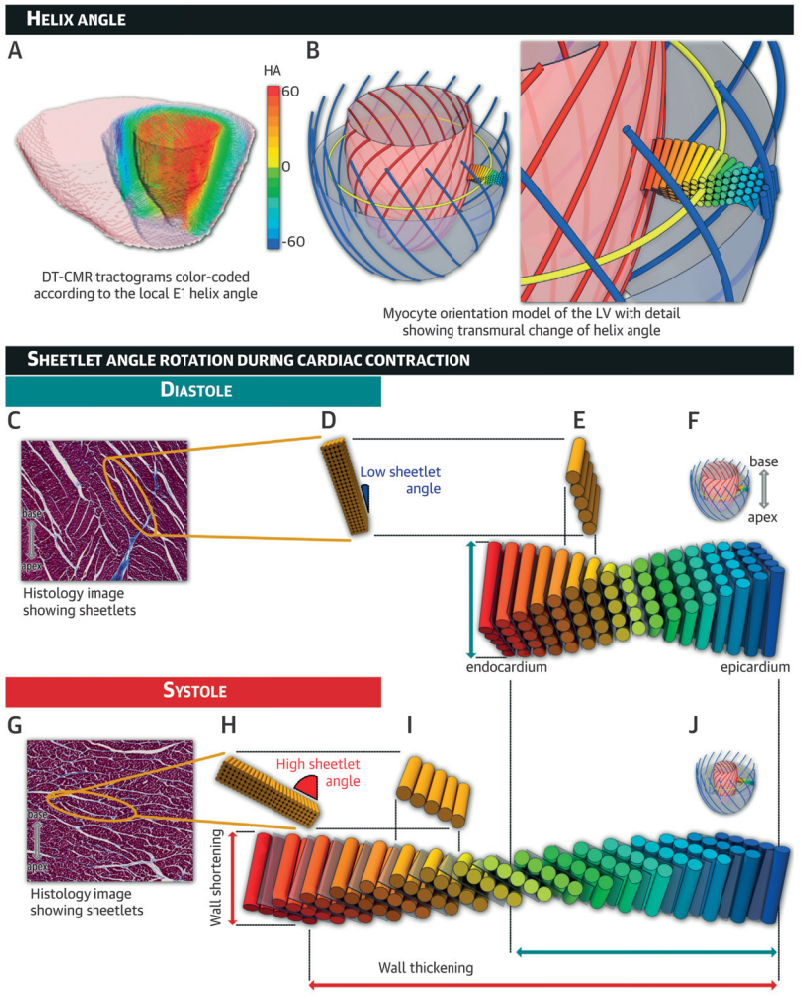

Figure 1.3: A: 3d-tractography showing helix angle orientations derived from diffusion tensor imaging. B: Illustration of the transmural change in helix angles. C: Histology section of a myolaminar "sheetlet" and surrounding cleavage planes in its diastolic conformation. D&E: Illustration of tightly packed myocytes inside sheetlets. Note the low sheetlet angulation away from the vertical axis in diastole. F&J: Illustration of helix angles in systole and diastole. Note the relatively constant helix angles from diastole to systole. G: Histology section of a myolaminar "sheetlet" and surrounding cleavage planes in its systolic conformation. H&I: Illustration of the systolic inter-sheetlet rearrangement and increase in sheetlet angles during systole. *Reproduced from Nielles-Vallespin et. al. J Am Coll Cardiol 2017 [21]. through a Creative Commons BY-NC-ND 4.0 license.*

1.2.3 Coronary Arteries and Perfusion

Cardiac pumping is an oxygen-consuming process. Therefore, the myocardium is supplied with blood through an intricate network of coronary vessels. There is much complex variability in the coronary anatomy. What follows is a representation of the most common form found in humans (Figure 1.4). The coronary arteries originate from the sinus Valsalva of the aortic root, which splits into the right, left, and non-coronary sinus.

In most cases, the right coronary artery (RCA) originates from the right sinus Valsalva and travels in the right atrioventricular groove to the posterior interventricular tract. When the RCA supplies the posterior descending artery in the interventricular groove, the coronary circulation is called a "right dominant" system, although misleading because it does not contain information about the rest of the RCA and how much myocardial mass it supplies. If the PDA originates from the left circumflex artery (LCX), the system is "left dominant." A right dominant system is present in 79% of humans [34].

The left coronary main stem originates from the left sinus Valsalva, which branches to left anterior descending artery (LAD) and the LCX. The LAD branches from the main stem typically after 10 mm [35] and travels in the anterior interventricular groove. Small transmural branches along with the artery supply the septal wall. Larger epicardial branches called diagonals transverse diagonally over the left ventricle (LV). The LAD can feather out near the ventricular apex but often wraps around it, up the posterior interventricular groove. The LCX passes along the left atrioventricular (AV) groove, and the first branches are called the obtuse marginal arteries, which supply the lateral part of the LV and also the posterolateral papillary muscle in a left dominant system.

The coronary arteries are typically 0.3-5.0 mm in diameter. The vessels consist of three layers: The outer adventitia, containing small nerves and blood vessels that supply the artery itself; The central media, containing smooth muscle cells; and the innermost intima, containing the vascular endothelium. Even smaller vessels are called arterioles and range from 15-300μm. The arterioles are essential components of the coronary circulation because of their pre-capillary sphincters that open and close the finer capillary beds in response to tissue requirements.

Experimental studies using Micro-Computed Tomography and microsphere injections found a strong relation between vessel size and perfusion volume [36]. The terminal arterioles (8-10μm) each perfuse a myocardial volume of $\sim$0.008mm^3 which corresponds to the basic unit of a capillary with its surrounding tissue cylinder where oxygen is exchanged (Krogh cylinder). Arterioles of 100μm instead each perfuse a volume of $\sim$0.65 mm^3, an increase by a factor of 1,000.

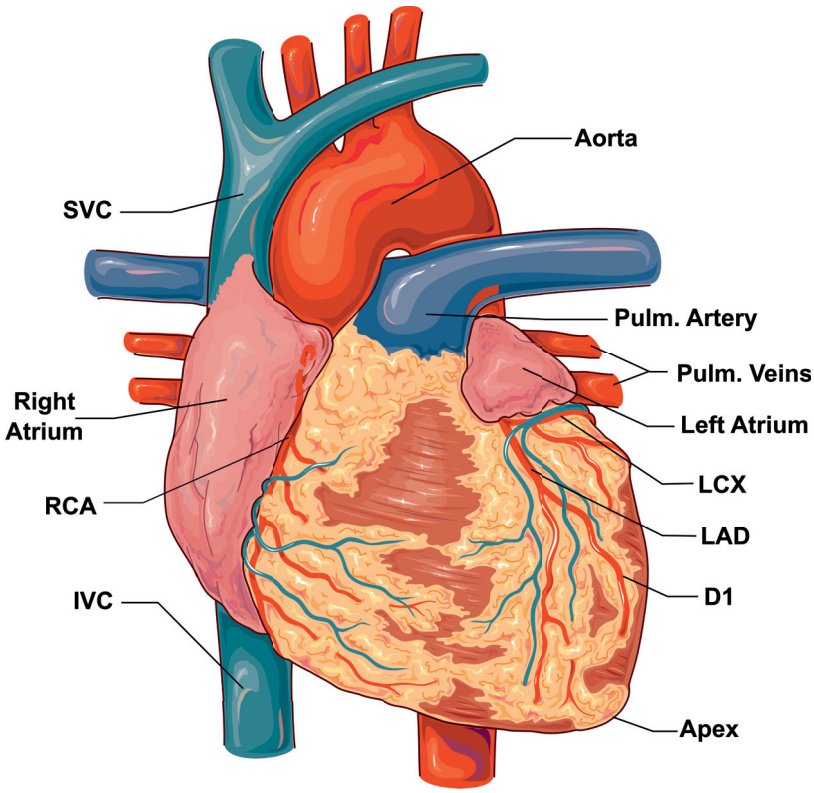

Figure 1.4: The heart, major vessels, and coronary arteries. SVC, superior vena cava; RCA, right coronary artery; IVC, inferior vena cava; D1, first diagonal branch; LAD, left anterior descending artery; LCX, left circumflex artery. *Adapted with labels from Servier Medical Art, provided by Servier, licensed under a Creative Commons (CC) Attribution 3.0 unported license.*

1.3 Cardiac physiology

Understanding the governing laws of fluid flow through a closed-loop system is a common starting point for investigating the flow-related phenomena in the living organism. Blood flow is the result of a pressure gradient overcoming resistance. Ohm's law (equation 1.1), initially applied in electrical circuitry, is generally adequate for modeling blood flow in the circulatory system at a global level.

$$Q = \Delta P/R \tag{1.1}$$

where Q = Flow rate; Δ P = pressure gradient; R = resistance.

In the case of the heart, the flow of cardiac output per minute (Q) is the result of stroke volume (SV) times the heart rate (HR). The resistance the arterial flow encountered is often termed "total peripheral resistance" (TPR) and is mainly regulated by the adaptable constriction of arterioles and precapillary sphincters. Hagen-Poiseuille's equation 1.2 states that the resistance is inversely related to the radius of the fourth power.

$$\Delta P = \frac{8\mu LQ}{\pi r^4} \tag{1.2}$$

where ΔP = pressure gradient along vessel; μ = blood viscosity; L = length of vessel; Q = flow rate; r = radius of vessel; π = mathematical constant.

The heart can impossibly generate any more output than what it receives as input. Therefore, a fundamental regulating mechanism is the "law of the heart" proposed by *Frank* and *Starling* [37] which in simple terms is stated, "the heart pumps what it receives." This is based on a phenomenon seen when an increased filling, yielding an increased end-diastolic sarcomere stretch results, in a more forceful contraction. The effect of this law is evident considering that the primary governing factor of stroke volume is the end-diastolic volume, and of cardiac output is the venous return flow.

1.3.1 Cardiac Cycle

The classic "Wiggers" diagram depicts relevant cardiac variables in the time domain and provides a helpful overview of hemodynamic events, including their relative timing (Figure 1.5). The cardiac cycle describes the sequence of events during one complete heartbeat. The cardiac cycle can be divided into two main phases: systole and diastole. Systole refers to the phase during which the ventricles contract and eject blood out of the ventricles. Diastole refers to the period during which the ventricles relax and fill. Since a reciprocal filling and emptying pattern exists between the ventricles and atria, atrial systole and diastole occur in ventricular diastole and systole, respectively.

Each ventricular beat includes four sequential ventricular events: isovolumetric ventricular contraction, ejection, isovolumetric ventricular relaxation, and filling. Diastole

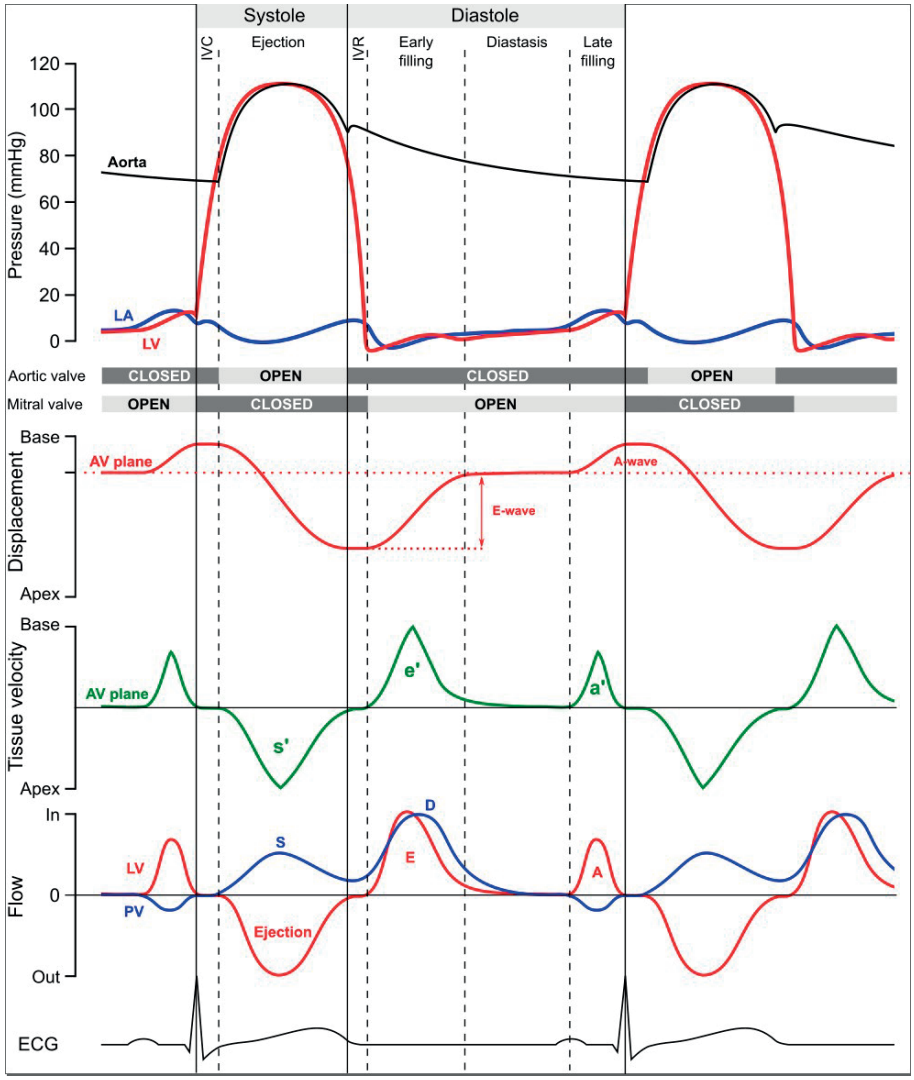

Figure 1.5: This adapted Wiggers diagram represents the pressure, displacement, tissue velocity, and blood flow of the left side of the heart in the time domain. LA, left atrium; LV, left ventricle; AV, atrioventricular; IVC, isovolumetric contraction; IVR, isovolumetric relaxation; PV, pulmonary veins. *Adapted with permission from original by Per Arvidsson.*

comprises three phases: early rapid filling (E-wave), diastasis, and late atrial filling (A-wave). Both systolic and diastolic duration depends on heart rate (HR). Specifically, systolic and diastolic durations are ∼400ms and ∼600ms at an HR of 60 whereas durations of ∼315msand ∼300ms are measured at an HR of 100 [38]. Further, E- and A-wave dura-

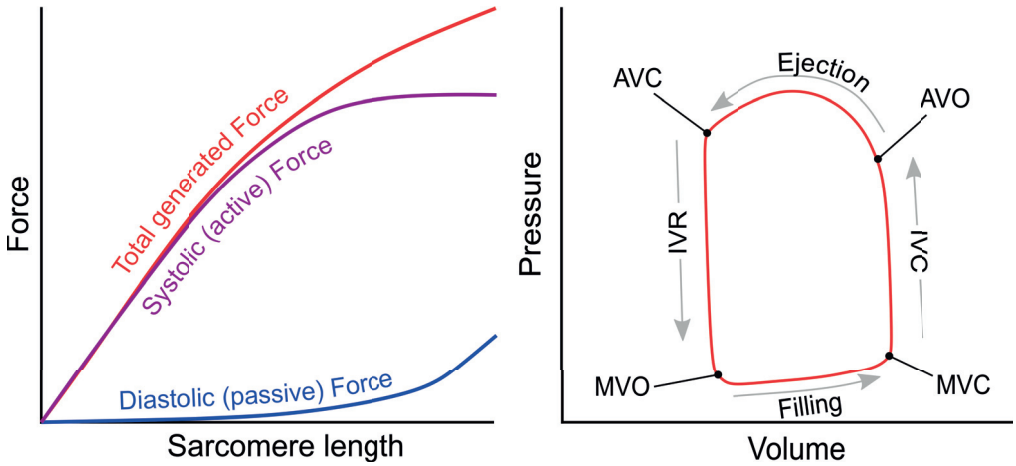

Figure 1.6: Left: The diastolic passive resting force results from diastolic stretch boundaries and heart filling. The peak activating force from the sarcomere is the systolic force. The total generated force (red) is the systolic peak force (purple) added by the diastolic resting (blue) force. Right: The left ventricular cycle from a pressure-volume loop perspective. IVR, isovolumetric relaxation; IVC, isovolumetric contraction.

tions show negligible dependencies of HR. Thus, diastolic shortening at higher heart rates results from a diminished diastasis and merging of E- and A-wave.

1.3.2 Pressure-Volume loops

Pressure-Volume (PV) loops assess hemodynamic relations in a pressure-volume dimension rather than a time dimension. Such PV constructions exist in all four heart chambers, and while differences exist, all the main concepts apply to each compartment. Here, we consider that the cardiac cycle begins in end-diastole and follows a predefined sequence of events (Figure 1.6). The major heart valves also close and open at specific time points. A PV approach can depict many aspects of cardiovascular physiology and including its interaction with the arterial tree. Thus, PV loops can supply many indexes and variables concerning preload, afterload, contractility, and lusitropy - being the myocardial relaxation during diastole.

Cellular Level

Although pressure-volume loops view the heart and the cardiovascular physiology from a macroscopic perspective, what is observed at the whole heart level has its basis in the cellular mechanics and the sarcomere's function. For example, the myocyte force-length relationship has a natural extension to the pressure-volume relationship in a 3d heart structure. Simplified, the pressure-volume relation is the force-length relation in three dimensions

(Figure 1.6). The ascending limb of the force-length relationship shows that with an increase in sarcomere length, there is an increase in force generated, and relates to "the law of the heart". Because of the cardiomyocyte structure, cellular boundaries, extracellular matrix proteins, and pericardium, the heart never reaches the descending limb of the force-length relationship in-vivo.

Organ Level

The pressure and volume change during one heartbeat due to heart contractions, valve openings, and valve closings. The outer limits of the pressure-volume loops observed at multiple beats will follow both an end-systolic (ESPVR) and an end-diastolic pressure-volume relationship (EDPVR). ESPVR is roughly linear in humans at normal states and in most clinically observed working conditions and describes the maximal elastance, or stiffness, the heart produces for specific inotropic states. Where the ESPVR intercepts the volume axis is known as "V_0" and can differ from zero-volume. V_0 is the largest volume in the heart that does not give rise to pressure or the largest unloaded volume in a relaxed heart. Where V0 exists is dependent on the method of extrapolation [39] and has shown to be positively correlated with inotropy and negatively correlated with afterload in rats [40]. EDPVR is nonlinear and is determined by the passive stiffness inherent to the heart in its relaxed state and external constraints, such as the pericardium.

In a given instant of time, the ESPVR and EDPVR define the boundaries of space that the PV loop theoretically can occupy, irrespective of preload or afterload. At the same time, the placement of the PV loop in the PV space is determined by the preload and afterload. Still, ESPVR, and with a slower rate EDPVR, changes over time due to hemodynamic circumstances. The upper boundary of the PV loops, the ESPVR, is assumed mostly linear. However, while that linearity is mainly preserved in normal states, it can become markedly curvilinear towards low or high contractility states [41–43]. A linear extrapolated intercept "V_0" regularly yields nonsensical negative values. This is likely due to non-linearization produced by interventions or disease states.

Preload is the load imposed on the heart at end-diastole, with the most common surrogate measures being end-diastolic pressure (EDP) or end-diastolic volume (EDV). In another sense, the preload - following LaPlace law (eq.1.3) - is the wall stress at end-diastole.

$$T = \frac{Pr}{2u} \tag{1.3}$$

where T = Wall tension; P = Pressure; r = Radius; u = Wall thickness.

EDV is highly dependent on size, which can vary widely in different species or conditions. In PV loop research with small sample sizes, EDV is preferable in detecting changes within an individual, such as after a cardiac support device intervention. However, end-diastolic pressure is more suitable for objective comparisons of preload between individuals, groups, or species. Non-invasive methods of obtaining PV loops, which are later discussed in more detail, are currently limited in estimating the diastolic properties of the loop.

Afterload is the load imposed on the heart under ejection. In principle, it is a measure to characterize the arterial system independent of preload and contractility. One such index based on Ohm's law is total peripheral resistance (eq. 1.4), representing the ratio between the pressure and the mean flow across the system.

$$TPR = \frac{MAP - CVP}{CO} \tag{1.4}$$

where MAP = Mean arterial pressure; CVP = Central venous pressure; CO = Cardiac output.

Indexes of ventricular afterload are several: Myocardial wall stress according to LaPlace law (eq.1.3); central arterial pressure, which is most commonly used; arterial resistance; and arterial impedance. Arterial impedance is a measure of TPR that incorporates instantaneous pressure to instantaneous flow and can be analyzed in the frequency domain by Fourier analysis [44, 45].

Contractility are often estimated by the ESPVR and have been used as a relatively preload and afterload insensitive measure of contractility. However, experimental studies indicate that ESPVR is affected by heart rate towards extreme values [46]. A change in contractility will theoretically pivot the end-systolic pressure-volume relation around its "V_0" intercept. Changes in contractility are almost exclusively due to changes in calcium concentration and sensitivity to the calcium available, which can be influenced by beta-adrenergic stimuli, inotropic drugs, pH, temperature, or loss of myocyte function.

Lusitropy is the rate of the heart's diastolic relaxation and is derived from ventricular pressure curves. The end-diastolic pressure-volume relation (EDPVR) is both the measure of elastance and its inverse: compliance. EDPVR estimation may be limited in normal working ranges and since measuring pressure-volume loops in wide working ranges is not always feasible, interpretation can benefit from looking at the volume at a specific filling pressure [47]. For extreme working ranges, an experimental setting is needed. While the systolic relationship can change on a beat-by-beat basis, due to arrhythmias or cardiovascular drugs, the diastolic relationship more accurately represents the geometrical and structural state of the heart and is less sensitive to quick alterations. Diastolic properties do worsen in progressive heart failure or improve with high-performance athletes. The athlete's heart permits a remarkable early filling and high compliance arising from cardiovascular conditioning. Other common PV loop metrics are the pressure decay known as "tau," or the pressure derivatives "dP/dt".

Effective arterial elastance "Ea" estimates the stiffness of the arterial compartment, and it incorporates both pulsatile and resistive components. *Sunagawa et. al.* proposed the concept in a 3-windkessel model [48] that depicted the afterload with a proximal impedance parameter (aortic distensibility), the arterioles' opposition to flow through a mean resistance parameter (systemic vascular resistance), and a capacitance parameter (upstream total arterial compliance). Aortic elastance is dynamic over the heart cycle. It increases when the

aorta becomes stiffer when receiving blood during the ejection phase and decreases when the elastic aorta drives the stored blood forward during diastole.

Ventricular Energetics

During the cyclical changes in ventricular pressure, the ventricle ejects blood when pressure overcomes the diastolic arterial load. The contractile myocardium can be depicted as a global ventricular stiffness, or ventricular elastance, that waxes and wanes during each heartbeat (Figure 1.7A). Implicit in the PV loop model is, therefore, that ventricular contractility can be quantified in terms of elastance, which increases during systolic contraction, reaches a peak near end-systole (Emax), and decreases during relaxation, and repeats. As pressure multiplied by volume equals energy, the total energy expenditure of each heartbeat can be quantified as the net effective work utilized for expelling blood (i.e., stroke work) and the potential energy (PE) stored in the sarcomere after contraction. The area under the ESPVR, i.e., the pressure-volume area (PVA), amounts to the sum of PE and SW (Figure 1.7B), and the net work exerted over time, i.e., external power (EW), is quantified as SW·Heartrate. The Emax has been widely used to measure contractility as it shows strong independence from pre and afterload conditions (Burkhoff AJP 2005). For a given inotropic state, the Emax measured from a family of PV loops at stepwise reduced afterloads at a fixed preload (Figure 1.7C) would equal the same Emax as obtained by reducing preload at a fixed afterload (Figure 1.7D). However, there are reservations to this statement as Emax is slightly influenced by afterload impedance [49, 50] and length-dependent activation [51, 52], indicating an intrinsic load dependence of the cellular actin-myosin interaction.

Suga et. al. demonstrated a linear correlation between total mechanical expenditure and left ventricular oxygen consumption (VO2) [53]. This relationship is characterized by an internal and an external O2 cost, corresponding to 1) the basal metabolic rate independent of the PVA and 2) the cost that increases linearly with PVA (Figure 1.7E). Furthermore, the 02 cost of PVA for a given contractile state is largely independent of the type of beat, heart rate, or loading condition [54, 55]. The original research underlying these findings was performed in well-defined conditions of instrumented canine hearts. Due to a multitude of influencing hemodynamic variables, the correlations in-vivo are weaker [56]. Ventricular efficiency refers to the proportion of mechanical work output to chemical energy input [57]. Direct measurements of myocardial oxygen consumption from the large cardiac veins have been performed by experimentalists, yielding efficiency as the ratio of SW to VO2. Using the previous assumption that PVA strongly relates to the MVO2, a common approach to efficiency is using the SW to PVA ratio. Both SW and efficiency are within a few percent of their respective maxima in many conditions [58]; however, they can severely deteriorate in heart failure with systolic dysfunction [59].

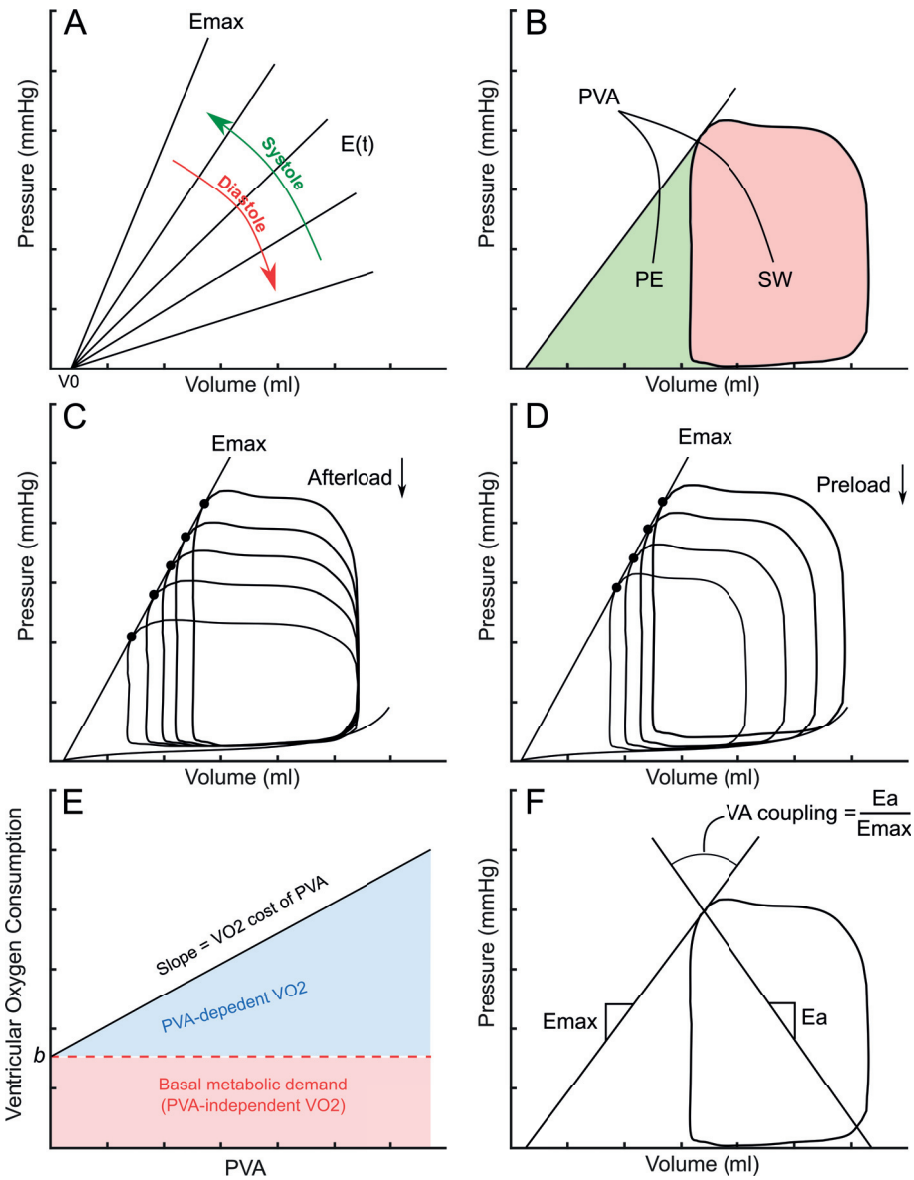
A
Emax
E(t)
Systole
Diastole
Pressure (mmHg)
V0
Volume (ml)
B
PVA
PE
SW
Pressure (mmHg)
Volume (ml)
C
Emax
Afterload
Pressure (mmHg)
Volume (ml)
D
Emax
Preload
Pressure (mmHg)
Volume (ml)
E
Slope = VO2 cost of PVA
PVA-depedent VO2
b
Basal metabolic demand
(PVA-independent VO2)
Ventricular Oxygen Consumption
PVA
F
VA coupling = Ea/Emax
Emax
Ea
Pressure (mmHg)
Volume (ml)

Figure 1.7

Ventricular-Arterial Interaction

A complex equilibrium arises from the pressure generated from the ventricle and the flow in the arterial compartment, which can be estimated with pressure-volume loops. The hemodynamic concept of ventricular-arterial (VA) coupling was initially developed by *Sunagawa et. al.* [48]. The VA coupling describes the relationship between the vasculature and ventricle as two elastic chambers, using units of volume and pressure. The coupling is a balance between the "stiffness," or elastance, of the receiving chamber and the "stiffness" of the ejecting chamber, with the ratio $\frac{Ea}{Emax}$ (Figure 1.7F). Further, it was predicted that the most efficient energy transfer between the ventricle and arterial compartment without excessive pressure differences occurs when the VA coupling is near 1 [60].

In health, there is reasonable matching between the ventricular and arterial elastance. Average ratios of Ea/Emax at rest are between 0.6-1.2 in healthy humans [61]. By contrast, severe afterload mismatch is present in systolic heart failure, which can be seen in VA coupling ranging between 1.3-4.3 [62, 63]. When the etiology is of an ischemic basis, it is commonly associated with a stiff and diseased aorta, aggravating the mismatch resulting in an increased proportion of stroke work exerted is wasted. Solely focusing on the VA number itself seldom gives sufficient hemodynamic insight, especially when fixating the V_0 to zero, as it provides $Ea/Emax = \frac{1}{EF} - 1$ [64]. Instead, explicitly examining the individual components of the Ea/Emax or their changes after an intervention provides information on whether the hemodynamic alterations are due to properties of the left ventricle, arteries, or both [65].

1.4 Ventricular Longitudinal Function

1.4.1 Historical Background

The heart's longitudinal motion was, like many things, early described by *Leonardo da Vinci.* He depicted how a needle-like instrument inserted into a pig's heart had a significant movement if inserted at the base and less movement when inserted at the apex [66]. This indicated that the heart's pumping action was a shortening in systole and lengthening in diastole in the longitudinal – or "caudal-cephalad" - axis. Subsequently, animal experimentation by *Hamilton* and *Rompf* [67] in the 1930s observed several essential concepts such as the relatively constant total heart volume, a stationary apex, and even the reciprocal filling pattern between the ventricles and atria. *Inge Edler* briefly mentioned the first recordings of the mitral ring motion in 1965 [66]. However, Zaky et al. in 1967 [68] studied 25 healthy volunteers as the first study focusing on the mitral ring movement in humans. The average amplitude was 16 mm.

Stig Lundbäck was a cardiologist and entrepreneur who compiled a comprehensive thesis on cardiac longitudinal movement and the function of the ventricular septum in 1986 [3]. He states that the heart needs to overcome two bioengineering problems: The optimal pumping of blood from an energy conservation perspective and the balance between the systemic and pulmonary circulatory loops. The energetically optimal pumping problem, he ascribed to the longitudinal pumping. If the apex is stationary, congruent with previous research, and if the heart does not want to pull on the surrounding tissues resulting in wasted energy, there must be minimal volume variations during the heart cycle. Thus, the longitudinal pumping has to be essential. The thesis also states that the ventricular septum is the critical regulator between the two circulatory loops, acting as a membrane-like pump. Furthermore, he also developed new types of pumps based on the principles of longitudinal pumping and the ventricular septum.

These foundational concepts briefly mentioned have been observed and expanded upon by modern imaging techniques such as CMR and echocardiography and are further described in later sections.

1.4.2 Atrioventricular Plane Displacement

This section revisits the anatomical AV plane and views its functional implications for cardiac pumping. Firstly, the microstructural components during the cardiac cycle, i.e., myocyte contraction, relaxation, and sheetlet reorientation, are the drivers of the apical-basal ventricular systolic longitudinal shortening and diastolic lengthening. Secondly, a non-compressible myocardium that becomes shorter must also become thicker to preserve the membrane stability of cardiomyocytes. What follows is that the external boundary conditions are prerequisites of normal ventricular longitudinal function and the near-constant total heart volume during the heart cycle. The heart is anchored at the atrial roof, connecting to the major arteries. The pericardium is the side and bottom anchors of the heart,

which effectively renders the apex stationary during the heart cycle [67, 69]. The pericardial adherence forces result from the surface tension of the pericardial liquid multiplied by the area of contact with the epicardium. The pericardial-normal constraint while allowing sliding of the epicardial surface is shown to positively influence longitudinal pumping in computer simulations [31]. The pericardium also often adheres to the sternum, securing the heart relatively immobile.

With the function, anchoring, and boundaries in place, the AV-plane and valvory movementnit with their oscillatory movement. The ventricular shortening pulls the base of the heart towards the apex and simultaneously lengthens the atria (Figure 1.8). Therefore, the atrioventricular plane displacement (AVPD) causes aspiration of blood from caval and pulmonary veins into the atria during systole [70] since the heart and vessels act as a closed-loop system at this level. The atria receive and store this aspirated volume before entering the ventricle during the early ventricular filling phase. This volume is known as the atrial reservoir volume. The AVPD is directly coupled with the atria in this regard and can thus be considered a measure of both ventricular and atrial function.

Since the heart is simultaneous emptying and filling, the total heart volume varies only slightly. However, there is no exact temporal matching of blood inflow and outflow; instead, the ventricle succeeds in emptying a larger volume than what the AVPD is pulling into the atria during systole [71]. This is due to the slight inward outer contour change of the ventricle during systole [2, 72, 73] and explains why the total heart volume has been shown to vary from 4-11% in humans [71, 74, 75]. This volume debt, generated by the epicardial outer contour change, is accounted for during ventricular diastole by a small portion of blood directly bypassing the atria into the ventricle caused by the centrifugal – i.e., outward from the center - rebounding during relaxation. This volume is known as the atrial conduit volume [76].

In early diastole, the AV plane rapidly rebounds to its equilibrium position at diastasis and oscillates [77, 78] after releasing the stored potential energy in the myocardium during initial relaxation. The amplitude of the AV plane during this phase is here referred to as ”E-wave AVPD”, and its velocity as e’. As a result of the early upward movement of the AV plane, the atrial reservoir volume is now placed in the ventricle. This mode of blood transfer is not detectable by Doppler echocardiography since it is a ventricular wall movement relative to stationary blood. However, the pressure gradient between the ventricle and atria caused by diastolic suction generates blood flow represented through the Doppler E-wave. After the diastasis, the atrial systole causes atrial pressure to increase and augments filling by an additional flow of blood, seen by the Doppler A-wave. The atrial systole also lifts the AV plane to a small degree and stretches the myocardium, preparing for subsequent ventricular contraction. This last stretch is here called ”A-wave AVPD”, and its velocity a’.

The volume that the AVPD encompasses can be calculated by multiplying the end-diastolic short-axis area of the ventricle by the AVPD. The remainder of the stroke volume is accounted for by the radial mode of pumping, which can be calculated as the inward movement of the epicardium multiplied by the surface area. Furthermore, the radial con-

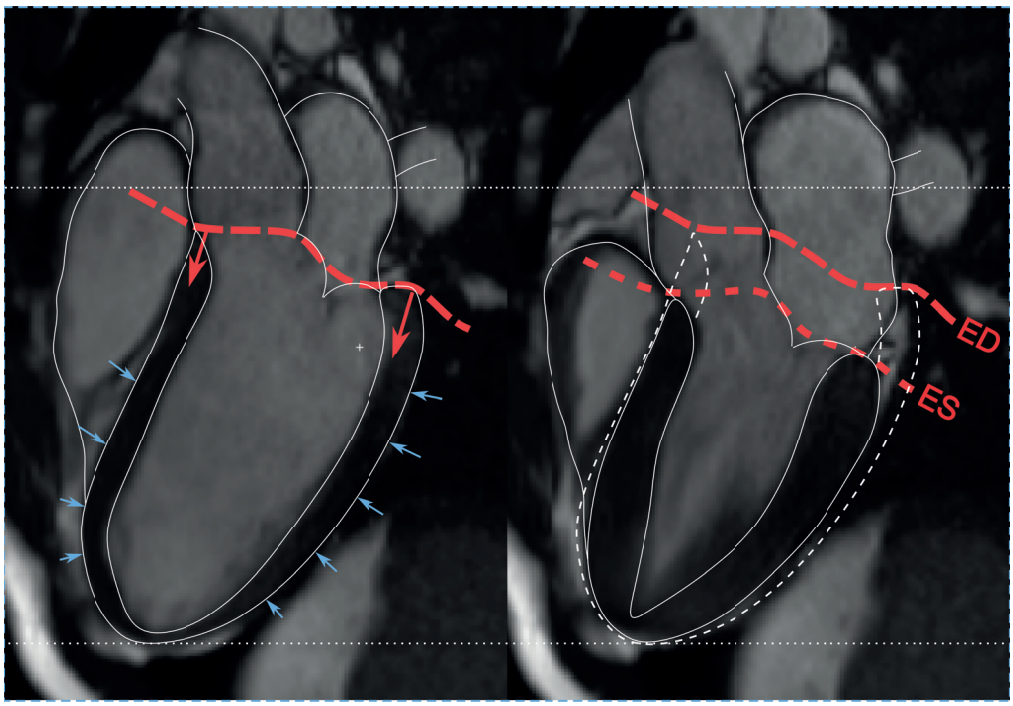

Figure 1.8: A 3-chamber view of a heart. Left: The heart is in end-diastole (ED), and the atrioventricular plane will begin its descent toward the apex (*red arrows*). Simultaneously, a small inward epicardial contour change (*blue arrows*) will occur, representing the radial "squeezing" motion. Right: The left ventricle has shortened and thickened due to both longitudinal and radial functions. The contour at end-systole (ES) is shown with the solid line and at ED with the dashed line. The ventricular longitudinal function generates the majority of stroke volume. See text for further details.

tribution can also be divided into septal and lateral parts. The relative contribution of longitudinal and radial pumping to total stroke volume is approximately 60/40% for the left ventricle and 80/20% for the right ventricle [72], which remains relatively unchanged in myocardial infarction [79], dilated cardiomyopathy, and athletes [80]. Average values of AVPD, or the near-equivalent metric "mitral annular plane systolic excursion (MAPSE)", depend on methodology and age but are for six-wall measurements in adults typically: 16.7±3.4 mm <40 years;15.1±3.4 mm 40-60 years; 13.2±3.2 mm >60 years [81].

Unaccounting for disease, AVPD typically decreases slightly with age, correlates negatively with heart rate, positively with height, but has no or minimal correlation with weight, body surface area, or sex [82, 83]. With increasing body size, there is a similar increase in heart size. However, the left ventricular length and end-diastolic diameter ratio do not change significantly [84]. The volumetric contribution of AVPD to stroke volume will therefore be relatively insensitive to symmetrical changes in heart size. In simplified terms, AVPD/MAPSE normalized to LV length approximately equals the relative deformation in the longitudinal axis, i.e., the global longitudinal strain (GLS). However, this normalization induces an inverse correlation with heart enlargement. Although longitudinal strain can offer detailed information on regional myocardial function, the insensitivity to heart size of AVPD/MAPSE may contribute to the apparent prognostic value in many different conditions, albeit being a "simple" variable.

1.4.3 Global Longitudinal Strain

The microstructural rearrangements of sheetlets and myocyte contractions from systole to diastole produce significant longitudinal shortening, centripetal thickening, and twisting motion of the base relative to the apex. The myocardial 3d-syncytium undergoes geometrical deformation in all directions, and strain metrics are thus available in longitudinal, radial, and circumferential directions. This thesis focuses on the apical-basal shortening and lengthening of the ventricle, which can be assessed through myocardial longitudinal deformation on a global level. This global estimate is known as GLS. The most straightforward strain equation can be described as the relative length change at the contracted state "L_1" from a starting end-diastolic length "L_0" (eq. 1.5). GLS measures the myocardial deformation in the longitudinal direction, while AVPD can be conceptualized as the result of this deformation acting on the AV plane.

$$GLS(\%) = \frac{L_1 - L_0}{L_0} \tag{1.5}$$

ejection fraction (EF) is an omnipresent parameter used in modern medicine and has gained an extensive evidence base. The relationship between EF and GLS is highly correlated, although more complicated than a simple linear correlation. In addition to only incorporating volume change, like EF, GLS is affected by differences in LV shape and wall thickness [85]. The EF and GLS relationship also differs depending on the pathology at

hand. In most cases of normal heart function, the equation 1.6 holds – as long as the LV shape, e.g., sphericity, elongation, or regional abnormalities, does not vary throughout the cardiac cycle [86].

$$GLS = (1 - EF)^{1/3} - 1 \tag{1.6}$$

Generally, a more spherical end-systolic shape results in larger GLS amplitudes than an elongated shape, even with identical EF. This is evident in good correlations between GLS and EF in normal conditions and heart disease with dilatation. However, an abnormal GLS can be detected in pathologies while EF remains unchanged, like concentric hypertrophy or heart failure with preserved EF [87]. GLS provides some insight into how the shape of the LV changes during the heartbeat, and its incremental value over EF partly corresponds to how much shape change is occurring.

Over the last decade, there has been significant interest in developing new cardiac technologies to evaluate the contraction and relaxation of the heart. One promising development was speckle-tracking echocardiography, which allows clinicians to measure the heart's strain or deformation. More recently, cardiac magnetic resonance (CMR) feature-tracking technology enables the measurement of GLS with specialized software by recognizing "patterns of irregularities" in the myocardium that are tracked in successive frames. More details on GLS imaging are provided in later sections.

1.5 Heart disease

Ischemic heart disease is a disease originating in the coronary circulation that can cause microvascular dysfunction, poor myocardial perfusion, and myocardial infarction (MI). There are over 600,000 new and 200,000 recurrent cases of acute myocardial infarction (AMI) per year in the US, and MI is a significant cause of heart failure (HF) globally [88]. Most MIs are nonfatal; however, many patients suffer reinfarctions, angina, and progress towards heart failure. Furthermore, a growing and aging population have increased ischemic heart disease's global burden [89]. Because of the severity of the situation, research on ischemic heart disease is continuously warranted.

1.5.1 Myocardial Infarction

Pathophysiology

MI is caused by a prolonged lack of blood flow, known as ischemia, in myocardial tissue. The basis for the reduction in blood flow can be either of a progressive or an acute nature. Most cases of acute myocardial infarction are caused by the sudden rupture of an atherosclerotic plaque, causing an acute occlusion of a coronary artery. The ischemic region at risk of demise is herein referred to as the myocardiium at risk (MaR). When a plaque ruptures and extra-intimal tissues and plaque fragments are exposed to the bloodstream, a thrombus quickly builds, blocking the passage of blood downstream. The pathophysiological progression from ischemia to manifested infarction is known as the ischemic cascade [90]. The term "cascade" may be misleading as it underlines that one event casually triggers the next in a preordained fashion. Instead, the usage of an ischemic "constellation" has been proposed to disband the confusion arising from temporally mismatched events, for example relating to the onsets of chest pain, wall abnormalities, or ECG changes [91].

The manifest infarct size (IS) is the most important predictor of poor outcomes after AMI [92]. The main determinants of myocardial IS are 1) the extent of the MaR, 2) the duration of ischemia, and 3) the amount of residual collateral blood flow [93]. Additional aggravating elements influencing the severity of myocardial ischemia include factors that further increase myocardial oxygen demand beyond supply, e.g., increased pressure work, inotropy, wall tension, temperature, and heart rate. A consummated MI is synonymous with loss of viable myocardium and reduced cardiac function. Ultimately, this means poor cardiac output when facing ordinary afterload, failure to recruit reserve capacity when required, or only being able to do so at the expense of increased filling pressures. During the initial ischemia, ventricular diastolic and then systolic dysfunction ensues. After that, ECG abnormalities become present, and their appearance depends on the ischemic locale. In LAD's perfusion territory, transmural ischemia leads to an ST-elevation on ECG, hence the term "ST-elevation myocardial infarction (STEMI)" [94]. Ischemia originating from other vessels, i.e., LCX or RCA, can result in STEMI but may also present with non-typical

or minimal ECG changes. This latter case is labeled non-STEMI. Further ischemia ultimately leads to myocyte death.

Myocardial contractile tissues subjected to transient or repetitive ischemia can sometimes stay in intermediate states between viable and dead. Dysfunctional but viable myocardial tissues are often targets for reperfusion therapies and are essential to detect [95]. Stress-induced ischemia occurs when the metabolic demands at stress exceed the blood supply, resulting in poor function and perfusion. Stunning, induced by ischemic bouts, is a low-functioning state at rest and stress, but at normal perfusion [96]. Repetitive stunning can also elicit histopathological changes and a deteriorated perfusion at stress. Hibernation is another poor contractile and perfusion state without widespread cell death. Abnormal histopathological changes, such as dedifferentiation of myocytes, are often present in hibernating myocardium [97, 98].

The rupture of plaques can also cause *microembolization* of debris, e.g., plaque material, cellular, and platelet aggregates, which travel downstream and occlude smaller vessels and riddle the myocardium with small regions of ischemia. Microembolization can also be iatrogenically caused and is one of the periprocedural risks associated with percutaneous coronary intervention (PCI) [99].

Treatment

The single most important treatment for ongoing myocardial ischemia is reperfusion. This is most often accomplished by a PCI. Since its advent and widespread use, it has dramatically improved mortality and morbidity for patients with acute myocardial infarction [100]. Formerly, drug-mediated thrombolysis was the recommended choice.

Other therapies beyond percutaneous reperfusion in the acute setting exist. Reduced coronary flow reserves in dysfunctional but viable myocardium can be treated by coronary artery bypass grafting (CABG) [101], which is especially suitable in patients with diabetes or multi-vessel disease. Medical treatment for ischemic heart disease includes the use of dual antiplatelet therapy [102], Beta-blockers [103], angiotensin-converting enzyme or angiotensin II inhibitors [104], depending on tolerance and risk-benefit ratio. Amiodarone may remedy associated arrhythmias [105]. IHD remains a significant cause of acute and chronic HF, and recommended medical therapies for HF do not differ significantly. The two types of drugs that most recently have shown survival benefits and are adjudicated for widespread use in HF are angiotensin-neprilysin inhibitors [106, 107] and sodium-glucose cotransporter 2 inhibitors [108, 109].

Reperfusion Injury

Although seemingly unintuitive, the reestablishment of blood flow of ischemic myocardial tissue can cause additional damage (Figure 1.9). Reperfusion is, therefore, a double-edged sword that has gained the interest of many researchers. A theoretically optimal cardioprotective therapy would instantly stop any further ischemic injury. However, no such

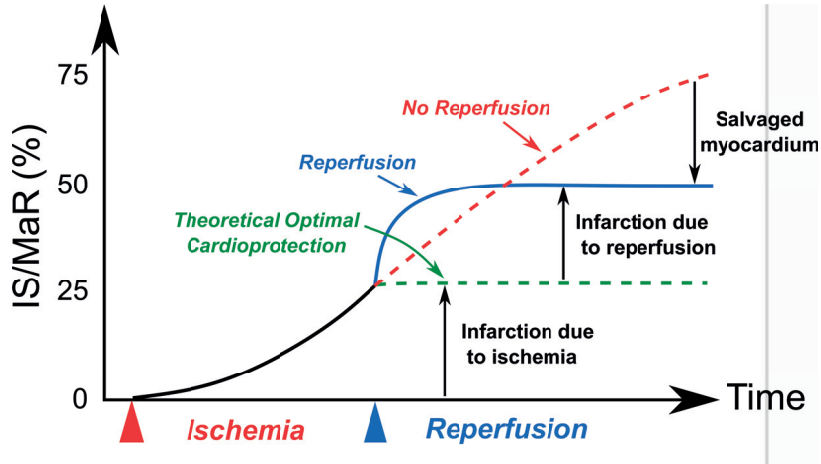

Figure 1.9: Schematic illustration of reperfusion injury. Without reperfusion, the infarct size (IS) will, in time, devour a larger piece of the myocardium at risk (MaR). Reperfusion by percutaneous coronary intervention salvages some myocardium from succumbing to ischemia while inadvertently causing additional myocardial injury, compared to theoretical optimal cardioprotection. *Adapted from Garcia-Dorado and Piper, Cardiovascular Research 2006 [112].*

treatment exists to date. The view of reperfusion injury is supported by evidence that interventions applied at the end of the ischemic period (i.e., coinciding with reperfusion) can reduce infarct size. This was exemplified in the 1980s, showing that gentle reperfusion was superior to abrupt reperfusion [110]. Other modes of controlled reperfusion, also known as post-conditioning, which is a series of brief episodes of ischemia and reperfusion after a prolonged bout of ischemia, have been refined and shown effective [111].

Reperfusion injury refers to damage caused by restoring blood flow to an area that has been deprived of it, such as in AMI. There is currently no complete understanding of the pathophysiological mechanisms involved. However, it is generally accepted that it is characterized by a complicated series of events, both inside and outside the myocyte, including the generation of free radicals, calcium overload, mitochondrial dysfunction, inflammation, complement cascade activation, platelet aggregation, microvascular injury, hemorrhage, and edema [113, 114]. Several of these mechanisms have directed researchers to potential targets for ameliorating reperfusion injury. For example, the ability of Cyclosporin A to combat the ramifications of mitochondrial dysfunction has been investigated [115]. The mitochondria are the cell's powerhouses and balance ATP production with ATP demand by sensing calcium levels. During reperfusion after ischemia, the cells and mitochondria are overloaded with calcium and oxidative stress. This, in turn, induces the opening of large-conductance non-specific pores in the inner mitochondrial membrane known as the "mitochondrial permeability transition pore (mPTP)" [116]. mPTP production is associ-

ated with mitochondrial swelling and cell death and has been the aim for cardioprotective drugs, such as Cyclosporin A.

Hypothermia

As previously stated, the myocardial temperature is a determinant of ischemic severity. therapeutic hypothermia (TH) in ranges of 32-35°C has been shown to reduce the size of MI in pre-clinical models [117, 118]. This has been demonstrated in rabbits [119], dogs [120], sheep [121], and pigs [122–124], and the potency of the ischemia-limiting effect seems to be directly linked to the temperature reduction and shortening of normothermic ischemia. In patients who have suffered from cardiac arrest, hypothermia has been shown to reduce the incidence of neurological deficits following resuscitation and is implemented in clinical guidelines [125, 126]. TH has therefore been considered a promising therapeutic approach adjunct to PCI for AMI.

Although many potential targets exist, cardiovascular drugs have a low likelihood of gaining approval for clinical use (∼7%) after clearing the experimental phase [127]. The allure of hypothermia might be the "catch-all" mechanism of enzymatic deceleration that involves known and still unknown pathways for reducing ischemic injuries that aid the heart's recovery.

Despite promising results from experimental studies, TH is still hampered by the larger clinical trials' moderate and varied results. In meta-analyses [128–130] of completed randomized clinical trials, including "RAPID-MI-ICE" [131], "CHILL-MI" [132], "VELOCITY" [133], "STATIM" [134], "COOL-MI-InCor" [135], "COOL AMI EU pivotal trial" [136], the combined results failed to significantly show reductions in IS or IS/MaR. However, significant reductions in infarct sizes were seen in specific subgroups of patients achieving core temperature ≤35°C at the time of reperfusion for both anterior ($p=0.03$) and inferior infarcts ($p=0.04$) [137].

The slow cooling rate currently achievable by hypothermia-inducing devices could contribute to this lack of results. It is important to reach an adequate level of cooling before reperfusion to achieve a potent IS reduction. A central temperature goal of <35°C reached in minutes has been stated as a sweet spot [132], balancing the clinical feasibility and cardioprotective efficacy. Still, this level remains challenging to achieve in human patients without prolonged cooling (45-90 min) [128]. Faster cooling devices without increasing adverse side effects are likely needed to instate this approach into the clinical setting. Systemic hypothermia is associated with some side effects and complications. These are mainly extra intravenous access points that could lead to infections, a higher incidence of atrial fibrillation, a prolonged door-to-balloon and ischemic time, and discomfort. To overcome this, novel strategies to cool the myocardium, such as intracoronary cooling, have been proposed [130]. It has been shown in experimental models that cooling directly inside the culprit's vessel before and during reperfusion may improve outcomes for STEMI patients

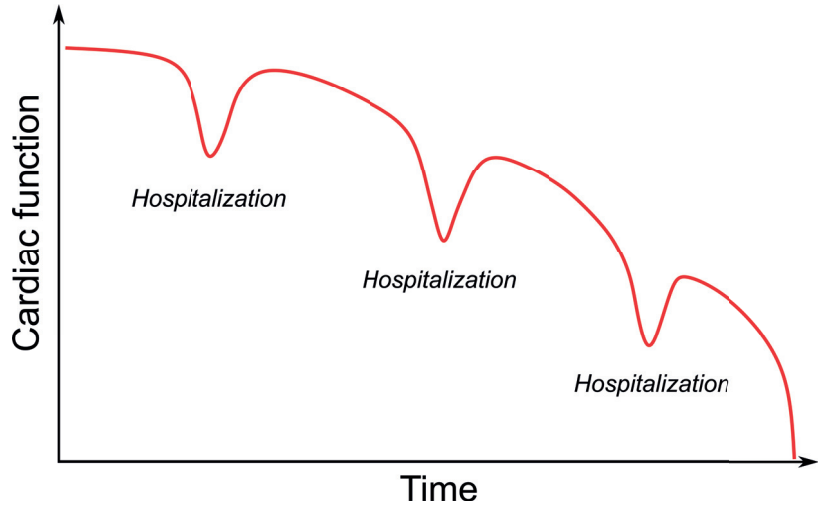

Figure 1.10: Illustration of the typical progression of heart failure leading to reocurring hospitalizations and unrecovered cardiac function. *Adapted from Gheorghiade and Mebazaa, Am J Cardiol, 2005 [142].*

[138]. Some researchers propose intracoronary cooling for reducing reperfusion injuries as the new stage for TH, and the randomized clinical trial "EURO-ICE" is ongoing [139].

1.5.2 Heart failure

Epidemiology

HF represents a significant burden on healthcare systems worldwide. According to estimates from the Centers for Disease Control and Prevention in the United States, HF affects approximately 3.5 million to 5.8 million people annually. It is a leading cause of hospitalization in adults aged over 65 years, and HF is responsible for about one of every nine deaths involving cardiovascular disease in the United States [88, 140]. To enumerate, 26 million people suffer from HF globally [89]. One in five people is expected to develop HF in a lifetime [141]. Furthermore, the typical trajectory of an HF patient is a recurrent series of gradual or abrupt clinical deteriorations leading to hospitalization, each associated with unrecovered cardiac function and quality of life (Figure 1.10).

Pathophysiology

HF is a collection of symptoms that manifests when the heart cannot perform its duties. The underlying cause can be a failure in any foundational pillars: contraction, relaxation, filling, emptying, heart rate, or a combination thereof. Chronic HF manifests from an inability of the heart to produce sufficient blood flow and pressure to meet the metabolic

demands of the body, leading to a buildup of fluid in the lungs, shortness of breath, and fatigue. While the two forms of chronic heart failure — heart failure with a reduced ejection fraction (HFrEF) and heart failure with a preserved ejection fraction (HFpEF) — have similar symptoms, they are characterized by different pathophysiological findings [143]. In HFrEF, a high degree of cardiomyocyte injury, evident in increased injury biomarker troponin T, and replacement fibrosis results in left ventricle enlargement and increased wall stress apparent in increased N-terminal pro-B-type natriuretic peptide levels. Activation of neurohormonal systems leads to sodium retention and systemic vasoconstriction [144]. The neurohormonal activation maintains hemodynamic homeostasis and contributes to myocardial fibrosis and remodeling, resulting in progressive ventricular dilation and pump dysfunction. The loss of myocytes and thus contractility can be caused by various adverse reasons such as ischemia, myopathy, inflammation, or culprit gene disorders. On the other hand, HFpEF is characterized by systemic inflammation, epicardial accumulation of fatty tissue, diminished microcirculation, myocardial fibrosis, and vascular stiffness [145].

Classification

The universal definition of HF states that: "HF is a clinical syndrome with symptoms and/or signs caused by a structural and/or functional cardiac abnormality and corroborated by elevated natriuretic peptide levels and/or objective evidence of pulmonary or systemic congestion" [146]. Contemporary definitions of HF is based on cut-points of EF. For instance, the European Society of Cardiology (ESC) has the following definitions: HFrEF = EF<40%; HF with mid-range EF "HFmrEF" = EF 40-49%; and HFpEF = EF≥50%; with the additional requirements of symptoms and signs such as elevated natriuretic peptides.

There are several other systems used to classify heart failure. Two of the most common are the New York Heart Association (NYHA) and the American Heart Association (AHA) classifications. The NYHA classification has four categories, ranging from patients who experience no symptoms of heart failure to those who experience severe symptoms at rest. In general, patients in Class I experience no symptoms. Class II patients experience symptoms of heart failure during physical activity, such as walking or climbing stairs. Patients in Class III experience symptoms of heart failure during low levels of activity, like walking or climbing one flight of stairs. Patients in Class IV cannot undertake any physical activity without experiencing symptoms.

The AHA system has four stages that are generally used to describe damage progression. Stage A describes patients at risk for developing heart failure without current manifest signs. Stage B describes patients with pre-HF indicating existing structural damage, abnormal cardiac function, or elevated natriuretic peptides but without symptoms. Stage C describes patients with existing structural damage and currently experiencing signs or symptoms of that damage. Stage D describes patients with advanced structural damage and chronic symptomatic heart failure or reoccurring hospitalization despite optimal medical treatment.

In addition to these classifications based on symptoms, structure, and activity levels, there is also the "Interagency Registry for Mechanically Assisted Circulatory Support (INTERMACS)" system. This is based on the severity of illness and treatment urgency and allows physicians to track changes in these factors over time. It consists of seven stages that are divided into early (1-3), advanced (4-5), and end-stage (6-7) HF.

HF can also be divided into different pathophysiological or symptomatic categories depending on context. These include: systolic vs. diastolic HF, which are often used unanimously with HFrEF and HFpEF; left vs. right-sided HF, referring to which ventricle predominantly fails; and HF with forward vs. backward failure, highlighting if insufficient perfusion or congestion dominates the symptomatology. The combination of tissue perfusion and pulmonary congestion is exemplified as the four hemodynamic subsets of acute heart failure developed by *Forrester et. al.* in 1976, i.e., combinations of "Warm/Cold" and "Wet/Dry," respectively [147]. When perfusion is inadequate, the patient is "Cold," and when congestion causes pulmonary edema, the patient is "Wet." A patient exhibiting simultaneous "Cold" and "Wet" clinical characteristics has a grim prognosis. This framework can be used as a guide for clinical decision-making.

Treatment

Treatment for heart failure is multi-faceted and always builds on top of the best medical therapy available. Patients should also participate in exercise rehabilitation and be managed by a multi-professional team of healthcare professionals. The optimal medical treatment shown to reduce mortality in all HF patients includes a regimen of ACE-inhibitors/angiotensin receptor neprilysin "ARNIs", beta-blockers, mineralocorticoid antagonists "MRAs", and sodium-glucose cotransporter 2 inhibitors "SGLT2s", at tolerated dosages.

The underlying cause of HF should be treated whenever possible in both acute and chronic onsets of HF. Acute etiologies can be remembered from the "CHAMP" acronym (acute **C**oronary syndrome, **H**ypertension, **A**rrhythmia, **M**echanical cause, **P**ulmonary embolism). Patients with an established ischemic burden, and particularly those with diabetes and multi-vessel involvement, benefit from CABG revascularization surgery [148]; patients with arrhythmias or intra-ventricular conduction delays can be treated with cardiac resynchronization therapy (CRT) pacemaker [149] or implantable cardioverter-defibrillator (ICD) [150]. Open surgery or percutaneous interventions may be performed to treat manifest mitral regurgitation or aortic stenosis [151]; in severe cases, however, heart transplantation remains the gold standard in patients without contraindications. Post-transplant 1-year survival is above 80%, with a median survival of about 11 years [152]. Still, transplantation remains only available to a small number of patients. Mechanical circulatory support (MCS) is a specialized form of treatment for patients with advanced HF ineligible for heart transplantation. Although an MCS device is not a cure, it can sustain blood

perfusion to vital organs and improve the quality of life for many patients [153]. An MCS device can be used as a bridge to therapy, bridge to candidacy, or as destination therapy.

1.5.3 Ventricular Longitudinal Function in AMI and HF

An impaired ventricular longitudinal function is a common feature of heart disease, including AMI and HF [154], and renders the ventricles' contraction and relaxation inadequate. Thus, this functional impairment can be detected as dysfunctions in both systole and diastole. Two non-invasively measured entities of ventricular longitudinal function are AVPD/MAPSE, which measures the amplitude of the oscillatory atrioventricular ring motion during a heartbeat in the longitudinal direction, and GLS, which measures the deformation innate to the myocardium in that same direction.

Both echocardiography and CMR have been utilized when studying ventricular longitudinal function. Echocardiographic studies toward the end of the 20th century found MAPSE to be depressed after AMI [155, 156] with recovery after thrombolysis, highlighting its link to contractile function [157]. Furthermore, MAPSE was shown to be low in patients with stable coronary artery disease [158], in chronic congestive HF [159], be associated with diastolic dysfunction in HF [160], and the degree of aortic stenosis [161]. MAPSE was reported to predict mortality in HF [162], AMI [163], chronic atrial fibrillation [164], and in patients with stable coronary artery disease [165].

AVPD/MAPSE and GLS decrease with age, even without CV disease [81], such as most indices of ventricular function. Be that as it may, the heart's long-axis function is early and significantly reduced in myocardial infarction and heart failure. Intriguingly, both experimental [166] and clinical studies [167] report that regional ischemic injuries cause globally depressed AVPD. The longitudinal contribution to stroke volume varies at the individual level, and may even be above 100% in patients with paradoxical wall motion. However, it is largely unchanged at around 60% at group levels, even when left ventricular dilation [80] or remodeling after MI is present [79]. A reduced AVPD in HF is often compensated by an increased short-axis area from LV dilation, retaining the longitudinal contribution to stroke volume.

CMR studies in the last years have shown that MAPSE has prognostic value for major cardiac events (MACE) in patients undergoing routine CMR examination [168] and in STEMI patients [169, 170]. Further, MAPSE was shown an independent predictor of all-cause mortality with high significance in patients with reduced EF (<50%) [171] and hypertension [172]. MAPSE normalized to LV length was shown to independently predict MACE in a large population without cardiovascular disease at inclusion [173].

Likewise, GLS has amounted to a large evidence base in AMI and HF [174]. GLS measurements signal myocardial abnormalities in HF earlier than do EF [175, 176]. GLS correlates with exercise capacity in HF [177]. GLS also predicts progression in subclinical HF [178], HF-readmissions in acute HF [179], and HF-associated morbidity [180, 181]. It was recently shown that a feeble GLS response during vasodilator stress predicted ad-

verse cardiovascular events in patients undergoing stress CMR [182] and treadmill-exercise echocardiography [183]. For mortality endpoints, GLS has shown prognostic merit in several patient populations, including dilated cardiomyopathy [184, 185], acute HF [186], HFrEF [187, 188], and hypertension [184]. GLS also carries prognostic value in ventricular hypertrophy [87]. Although pitfalls exist, the coupling of strain imaging with myocardial function, its growing evidence base, and technical feasibility have resulted in it being increasingly used clinically.

AVPD, which can be calculated from standard echocardiographic or CMR-acquired long-axis views of the heart, is relatively easy to measure. GLS, on the other hand, relies on more specialized sequences or software but may carry information about additional aspects of cardiac function such as regional contractility when using accurate methods. Much of the GLS intricacies related to software algorithms and postprocessing are proprietary secrets of companies that elicit vendor dependency [189]. Both AVPD and GLS seem to have similar prognostic information and are valid methods to assess long-axis function. Certain patients may be better classified by one over the other, as indicated by discrepant results between studies [170, 187]. However, it is more apparent that AVPD/MAPSE and GLS seem to be better carriers of prognosis than ejection fraction, as evident in several extensive imaging studies regardless of imaging technique [168–171, 174, 176, 180, 184, 187, 190, 191].

1.6 Cardiac Imaging

Imaging the heart can be performed with many different techniques, and all modalities have their benefits and limitations. Furthermore, the innovations that enable imaging originates from a wide range of physical properties (e.g., echolocation, electromagnetism, ionizing radiation, etc.) Here is a short overview of the cardiac imaging methods relevant to this thesis.

1.6.1 Cardiac Magnetic Resonance

The MRI Hardware

The MRI system contains three main components. 1) A magnet that produces a strong and homogenous magnetic field. The main magnet consists of a metal coil which is cooled until superconducting properties emerge. This enables a near-zero resistance for any imposed current. The main magnetic field produced, B_0, is measured in Tesla (T), and its direction is along the MRI scanner bore. A cartesian coordinate system with three orthogonal axes (x, y, and z) is used to define the magnetic fields, and the z-axis is always parallel to B_0. Specific strengths for clinically used MRI scanners are typically 1.5T or 3T. 2) Three additional minor electromagnets, called gradient coils, are used to manipulate and vary the magnetic fields in known magnitudes in three different directions. The function of the gradient coils is the spatial localization of the MR signal. 3) Two radiofrequency (RF) coils, one transmitting and one receiving, are used to send and receive radio pulses. The RF transmitter sends radio waves at specific known frequencies and durations. The RF receiver detects the MR signal generated by the "NMR" process discussed below.

The Physics and Encoding of the MR Signal

The MR signal results from the physical phenomenon of nuclear magnetic resonance (NMR). Hydrogen (H^+) is the nucleus almost exclusively used clinically since its vast abundance in humans, particularly in water and fat. The NMR process can be achieved because hydrogen atoms (protons) have an unevenly spatially distributed nuclear mass. The protons also have specific quantum mechanical properties called spin and thus a magnetic moment. Simplified, they behave as magnetic dipoles, which electromagnetic fields can influence. When B_0 is applied, the protons align parallel or antiparallel with a slight predisposition in one direction resulting in a net magnetization vector. In addition to this, the protons precess around B_0 with a specific frequency which can be calculated with the Larmor equation (eq. 1.7).

$$\omega = \gamma B_0 \tag{1.7}$$

where γ = 42.6 MHz/T for hydrogen. The precession frequency "ω" is dependent on the element-specific gyromagnetic ratio "γ" and the strength of the magnetic field "B_0".

Since the strengths of the magnetic fields are known and thoroughly calibrated, this equation is the foundation for calculating which frequencies specific protons precess with and at which frequency the RF pulses need to resonate with those protons, hence the term magnetic resonance. When the RF pulses and the precessing protons resonate, the net magnetization vector tilts away from B_0 at a certain flip angle. The gradient coils create linear variations in the magnetic fields along with one of the orthogonal axes "x, y, or z" and thus yield gradual changes in γ in the same direction. When a gradient is applied on the z-axis, the protons' precessing frequencies in the body now depend on their location on the z-axis. Therefore, a narrow group of RF pulses can target a thin slice's γ to acquire the MR signal and achieve *slice selection*.

Once flipped away from the B_0 and z-axis, the net magnetization vector can now be described by three components, or vectors, in the z, x, and y-axis. After RF pulse cessation, the magnetization vector will rapidly return to the z-axis, which is called relaxation. The relaxation in the longitudinal, z-component, and transverse xy-component occurs independently and can be described using exponential functions. The regrowth of magnetization in the z-axis is defined by the time constant called "T1" and the decay of magnetization in the xy-axis by the time constant "T2". T1 is the time it takes for 63% of the z-component to recover. T2 is the time it takes for the xy-component to decrease to 37% of its initial value. Simplified, the contrast in the MR image results from different T1 and T2 properties and different proton densities of the imaged tissues. Sequences can be designed to exaggerate the signal of one relaxation over the other.

One dimension of the MR signal can now be manipulated. To further the selection in two additional dimensions, the protons' properties need to change in the other two orthogonal directions, "y and x." This is accomplished by phase encoding (y-axis) and frequency encoding (x-axis). Phase encoding means that a magnetic gradient is played out directly after the first slice-selecting gradient along the y-axis that accelerates and decelerates the protons' precessing frequencies, thus causing phase shift. The phase-encoding gradient would interfere with the slice-selecting gradient and is therefore set apart in time. A third frequency-encoding gradient is applied during the acquisition period and alters the frequencies in the x-direction during readout.

The resulting signal is recorded in the spatial frequency domain, called k-space. It is an intricate waveform pattern resulting from frequencies manipulated in three dimensions. The k-space is encoded in phase and frequency. It is represented as a 2D grid, and each signal sampled results in one line of k-space. The number of lines and points limits the spatial resolution of the image. The k-space data is ultimately transformed into a digital image through the Fourier transform.

MRI Contrast Media

All imaging modalities present their results in digital images. The two most essential components in a digital image are contrast and resolution. The signal in magnetic resonance

imaging (MRI) can be augmented by different elements, the most common being gadolinium (Gd). MRI-contrast agents are magnetic or paramagnetic, referring to whether they themselves are detected or affect surrounding tissues to alter their magnetic properties. Gd-based contrast agents are paramagnetic and cause protons in their immediate surroundings to shorten their T1 time. Free Gd ions are toxic and therefore chelated with small carrier molecules, most commonly "diethylenetriaminepentaacetic acid (DTPA)" or "dodecane tetraacetic acid (DOTA)", which the kidneys can excrete. Gd-chelates passively diffuse into extracellular spaces but are unable to enter viable myocytes. This property is utilized in late gadolinium enhancement imaging discussed below.

Sequences

Cine Imaging

"Cine" imaging refers to the resulting "video" or moving image used to view the heart function over time, most often as one heartbeat. This is commonly achieved by synchronizing the MR acquisition with the subject's ECG rhythm. Since the acquisition of multiple slices requires time and the heart moves by itself, and with respiratory motion, a reconstructed heartbeat "cine" is a merged sampling of typically ten heartbeats during end-expiratory breath holds. Multiple breath holds are often needed to cover the entire heart. Heart rhythm irregularities or failed breath holds during acquisition is a common cause of image artifacts. The sequence used for cine imaging in this thesis is the balanced steady-state free precession (bSSFP) [192], either with or without contrast. When bSSFP is used, the net magnetization vector is flipped in an oscillatory manner along the z-axis, giving a relatively steady-state xy-transverse magnetization over several heartbeats. It provides an excellent difference between the myocardium (dark) and blood (bright) even without contrast and is based on the T1 and T2 relaxation ratio.

Late Gadolinium Enhancement Imaging

Myocardial infarction and fibrosis can be visualized and accurately quantified by CMR using late gadolinium enhancement (LGE) [193, 194]. LGE is also commonly used for detecting other pathologies such as myocarditis, hypertrophic myopathy, or sarcoidosis. The mechanism of LGE is the increasing distribution volume of Gd-contrast in pathological tissues [195, 196]. The term "late" refers to the time delay of typically 10-30 minutes between contrast injection and imaging. Healthy and injured myocardial tissue exhibit different contrast kinetics, i.e., the contrast washes out unevenly (Figure 1.11), yielding a kinetic pathological basis for using LGE imaging to differentiate ischemic, infarcted, and normal myocardium. Gd-based contrast agents do not pass the lipid membranes of cells, although they enter the extracellular volume that contains the fluid and proteins between the cells.

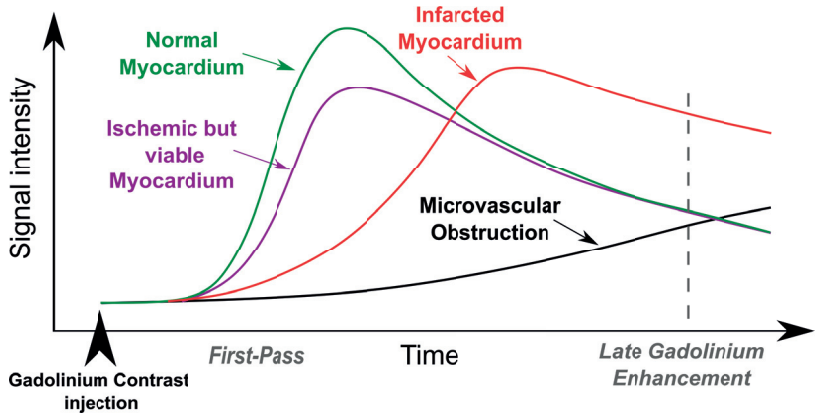

Figure 1.11: Schematic illustration of the temporal relationship between contrast wash-out of different tissues. Late gadolinium enhancement imaging is typically performed 10-30 minutes after contrast injection. *Adapted from Kellman & Arai J Magn Reson Imaging, 2012 [197].*

When myocardial tissue damage occurs in the acute phase (hours), loss of myocyte integrity leads to intracellular fluid and proteins leaking into the extracellular space, increasing its proportion. An influx of inflammatory cells and subsequent swelling by fluid inflow also contribute to an increased extracellular volume fraction. At later stages (days), the acute swelling reduces as cell debris are being handled by inflammatory cells such as macrophages [198, 199]. At a week and beyond, fibroblasts start increasing matrix protein deposition in the injured areas to replace the injured tissues with fibrosis. Thus, after a Gd-based contrast bolus is injected, there is an increased distribution volume with a slower contrast washout in injury locales following myocardial infarction. The contrast will enter all extracellular space but quickly wash out in viable tissues, unlike in non-viable, infarcted, or fibrotic tissues, where the contrast media will linger and exhibit a transient steady-state condition [200–202]. Microvascular obstruction is a minimal to no-reflow phenomenon after ischemia/reperfusion with blockage of small arterioles by debris, cell swelling, and vessel damage [203].

The LGE imaging is considered the gold standard for assessing myocardial infarction [197, 204] and was already developed in the 1980s [205, 206]. An LGE image is typically displayed such that non-viable tissue appears hyperintense, i.e., "bright," while normal myocardium appears dark (Figure 1.12). Dark regions near or inside infarctions may appear and can be due to microvascular obstruction, fat, ventricular thrombus, or calcifications. To acquire an LGE, an inversion recovery (IR) pulse sequence is used to enhance the contrast between Gd-accumulated tissues with short T1 and normal T1 relaxation. An IR pulse flips the net magnetization vector 180° in the myocardium before acquisition. This is followed

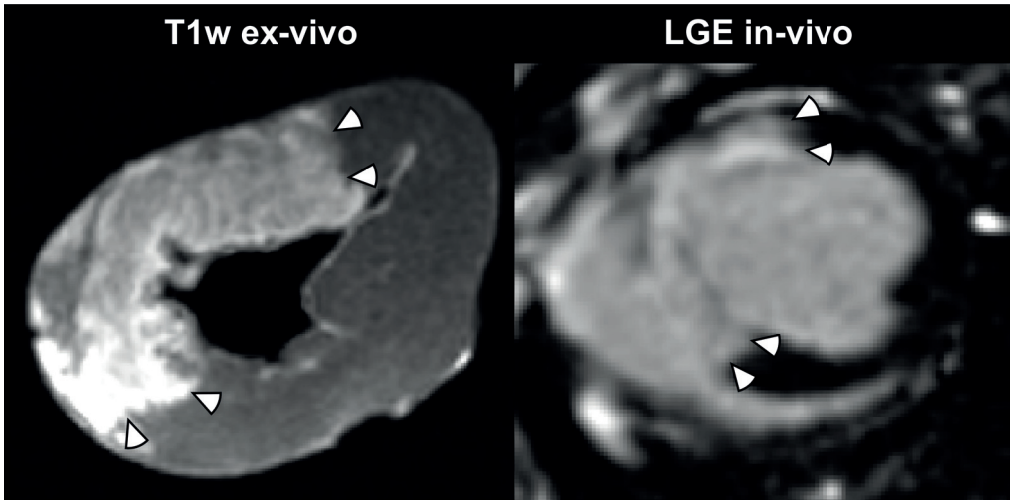

Figure 1.12: Left: A Short-axis slice of an infarction imaged with a high-resolution ex-vivo late gadolinium enhancement (LGE). Right: An image of the same slice location in the same animal using in-vivo LGE. White pointers demarcate infarction edges.

by a time delay, called "inversion time," which can be adjusted to effectively null the signal from the normal myocardium, thus appearing dark in images.

LGE imaging has historically been performed using multiple breath-holds of 12-16 heartbeats with a segmented fast low-angle shot "FLASH" gradient echo "GRE" sequence [196, 202]. To improve speed and quality, new sequences have been developed, including phase-sensitive inversion recovery "PSIR" [207], PSIR single-shot using bSSFP [208], and free-breathing motion-corrected "MOCO" LGE [209, 210]. The superiority of MOCO LGE over breath-hold LGE pertains to faster scan times, improved image quality, and less discomfort for patients [211]. LGE can be performed in 2D or 3D, where 2D segmental LGE has shorter breath-holds but longer total acquisition time, while 3D LGE has shorter imaging sessions but a higher risk of image artifacts. Newer "dark-blood" LGE techniques has also been developed where the contrast between blood and hyperintense regions is improved [212].

Ex-vivo LGE imaging for experimental research can be performed to achieve excellent infarct quantification with high accuracy (Figure 1.12), and validation studies using histological staining with triphenyl tetrazolium chloride (TTC) correspond well with ex-vivo LGE [194, 213, 214]. The contrast media is administered intravenously and circulated for typically 15 minutes before termination. The heart is most often explanted and suspended in an MRI-compatible container. MRI acquisition is thus unhindered by any motion or time restraints allowing high-resolution images.

1.6.2 Echocardiography

Ultrasound imaging, or sonography, utilizes the reflection of sound waves at frequencies above 20kHz to generate images. The frequencies applied in medical imaging are often several megahertz, and the human hearing threshold is approximately 20kHz in young adults. The mechanism of detecting reflecting sound waves is called echolocation and is not uncommon in the animal world.

The cardiac applications of ultrasound imaging originated from the collaboration between *Inge Edler*, a cardiologist, and *Helmuth Hertz*, a physicist, both from Lund University [215]. In 1953, *Edler* assessed patients before surgical repair of mitral stenosis, and X-ray imaging or cardiac catheterization failed to give comprehensive information on the patients' valve pathologies. *Hertz*, who already had some experience with a device using ultrasound to detect cracks in the metal of ship hulls and tanks, met Edler at Lund University. They both started collaborating on imaging the heart. Their first publication appeared in 1954 [216] and echocardiography was slowly adopted throughout the cardiology domain.

Today, echocardiography is widely used for assessing ventricular volumes, valve pathologies, flow measurements, and guiding interventions. It can be performed transthoracically, transesophageally, intravascularly, or intracardially. It is absent of ionizing radiation, relatively cheap, and quick to use. Therefore, it has become the most common imaging method for investigating patients with suspected heart disease. Limitations of echocardiography include high dependence on the sonographer's skill and variations in patient thoracic anatomy (e.g., spaces between ribs, adipose tissue, and lung anatomy). As a result, the variability in image quality is often higher than for other modalities. Current guidelines from the ESC recommend echocardiography as the primary imaging method for assessing heart failure [101]. CMR is recommended over echocardiography in patients with poor acoustic windows or with the need for tissue characterization in infiltrative or inflammatory cardiomyopathies. CMR should also be used to distinguish between ischemic and non-ischemic etiologies.

1.6.3 Imaging of Ventricular Longitudinal Function

Imaging of cardiac function is one of the cornerstones of clinical assessment. Ventricular longitudinal displacement and deformation metrics are valuable because they contain both systolic and diastolic information. Displacement measurement is relatively intuitive and comprehensible. On the other hand, deformation imaging is heavily reliable on the specific image postprocessing algorithm, which varies between techniques and modalities.

Ejection fraction (EF) is the most common variable to report and guide therapy today. However, limitations for EF include that 1) a considerable proportion of symptomatic HF patients with diastolic dysfunction exhibit "normal" EF, i.e., HFpEF [217, 218], 2) longitudinal dysfunction can be masked by an increase in circumferential function rendering a "pseudonormalized" EF, and 3) that EF solely is a global parameter. In contrast, ven-

tricular longitudinal function measurements are more sensitive to detect diastolic function [219, 220], are less affected by LV geometry, and can be used to measure regional function.

Deformation tracking algorithms generally need a definition of the myocardium of interest. This is supplied by human or automatic segmentation. The segmentation is critical and defines which pixels should be tracked. The tissue of interest is then tracked throughout the cardiac cycle, and strain curves are computed. Deformation imaging software employs different tracking algorithms, of which some are modality-specific (e.g., strain encoding "SENC" and displacement encoding with stimulated echoes "DENSE" in CMR), and some are generic (e.g., image block-matching for speckle-tracking echocardiography "STE" and feature tracking "FT"). Detailed discussions of tissue tracking algorithms are beyond the scope of this thesis. General limitations of strain methods are that normal values differ between techniques, and even vendors, such that validation studies are needed for each application. In general, normal values for GLS ranges from -15% to -22% [189, 221]. Additionally, a low temporal resolution will yield falsely low strain values, which is often the case for CMR-based techniques.

Both echocardiography and CMR are clinically used to measure ventricular longitudinal function. Other modalities, such as computed tomography and fluoroscopy, can measure longitudinal displacement, as the most basic methods only require a moving image of a heartbeat in the longitudinal axis. Still, this thesis mainly focuses on different methods for echocardiography and CMR.

Echocardiograhpy

Transthoracic echocardiography (TTE) is used to measure ventricular longitudinal function to a great extent. The earliest form of echocardiography where image information is gathered in a single line at a very high frame rate, the "M-mode," is a valuable method to measure the basal-apical movement of the AV plane. The MAPSE and tricuspid annular plane systolic excursion (TAPSE) are the most commonly used terms to measure ventricular longitudinal function for the LV and the right ventricle (RV). TAPSE is primarily used as a surrogate for RV ventricular function since adequate RV visualization is often not attainable due to poor acoustic windows due to anatomy.

Strain imaging is widely used in echocardiography. The two primary imaging methods used are tissue Doppler imaging (TDI) and speckle tracking (STE) imaging. TDI relies on detecting the Doppler shift in the acoustic signal caused by the myocardial movement [222]. It has a good spatial and excellent temporal resolution (>100 frames per second). Limitations of TDI are angle dependency and limited regional reliability. STE is a post-processing technique that estimates deformation by tracking naturally occurring fiducial markers called "speckles" in the myocardium. It is currently the most available technique since it can be performed on standard cine images of sufficient quality [223]. It is angle independent but not as robust for assessing regional function.

CMR

Displacement, such as AVPD or MAPSE, can be measured in standard cine images. SSFP-based image stacks in both short and long-axis were obtained in the current studies, and the long-axis images were used to visualize and calculate AVPD as previously published [72, 79, 80, 224]. The main advantages of using AVPD compared to the commonly used MAPSE include that 1) the annotation points for AVPD are placed at the top of the basal ventricular ring vs. at the mitral valve hinge for MAPSE, providing easier tracking in CMR. In addition. 2) Six measuring points for AVPD compared to fewer locations commonly used for MAPSE increases reproducibility and resistance to measurement errors. 3) The perpendicular distance from an end-diastolic fiducial plane used in AVPD vs. the beeline route commonly used in MAPSE avoids biases due to lateral translation of the ventricle.

Cine images often have temporal resolutions in the order of 20-30 frames per heartbeat. Measurements of valve plane velocities in the long-axis from standard cine images can therefore yield underestimated values. Sequences with temporal resolutions of >200 frames per heartbeat [225], similar to Doppler echocardiography, exist and are more suitable for measuring tissue velocities.

CMR offers several techniques for deformation imaging. Since the tissues' magnetization properties are visualized and manipulated, this combination is utilized to create CMR-unique deformation tracking. MR-"tagging" is widely considered the reference standard and has been validated both in-vitro [226] and in-vivo [227]. A locally induced grid is produced by selectively perturbing the magnetization by RF pulses [228]. The square grid creates visual "tags" in the myocardium. Since the magnetization is intrinsic to the myocardium, they move according to the tissue. A variation of tagging is the HARmonic phase "HARP" technique [229]. Two other related techniques are "SENC" [230] and "DENSE" [231]. Unlike DENSE which uses phase contrast, SENC is calculated from magnitude images. Both SENC and DENSE measure the modulation in the through-plane direction and create a pixel-wise map in which the intensities are directly related to the deformation. Additionally, a fast-SENC "fSENC" [232] has been gaining popularity which has a very high temporal resolution which is beneficial in deformation imaging. Deformation can also be extracted from phase-contrast velocity data [233].

While a standard limitation of the mentioned CMR techniques is that they require specialized pulse sequences not widely available, CMR feature tracking (FT) can be applied in all standard cine images of sufficient quality. Several commercial software offers this method, and FT has therefore been widely adopted. Although tagging, DENSE, SENC, and fSENC are more consistent and accurate for segmental and regional deformation, it appears that FT is sufficient for the assessment of global deformation measures [234].

1.6.4 Coronary Angiography

Coronary angiography is the visualization of the coronary circulation. This is most often done by injecting an iodine-based contrast media through a guiding catheter visualized by

fluoroscopy imaging. Of note, it is not the vessels themselves that are observed but only the lumens of the arteries filled with contrast media are depicted. Coronary angiography is performed by placing a guide catheter of suitable shape and orientation to access the coronary circulation. Different catheter shapes are used depending on the entry site (e.g., radial or femoral artery) and the desired destination. The guide catheter supports the injection of contrast media and the introduction of smaller procedural instruments into the arteries, such as PCI balloons and stents for treating AMI.

Invasive catheterization is widespread in clinical use today and is the basis for many procedures involving coronary circulation, systemic or pulmonary circulation, or intraventricular procedures. The commonplace approach to gaining access to either arterial or venous vessels is the "Seldinger technique." This method of obtaining safe access to blood vessels is named after the Swedish radiologist *Sven Ivar Seldinger*. Briefly, a sharp hollow needle punctures the blood vessel of interest, after which a flexible guidewire is inserted through the needle. The needle is withdrawn, leaving the guidewire inside the blood vessel, and a hollow introducer sheath or catheter can be inserted over the guidewire into the blood vessel.

1.6.5 Invasive Pressure-Volume Loops

Invasive PV loops are excellent for studying the short-term effect of interventions such as cardiovascular drugs or cardiac assist devices on ventricular performance. Due to their invasiveness, however, they have primarily been used for experimental research. One aspect rarely mentioned is that real-world data is of variable quality and sometimes insufficient for interpretation (Figure 1.13). This is especially noticeable in large animal models such as sheep and pigs. Correct method and calibration is therefore important.

Measuring a PV loop invasively involves placing a catheter inside the left ventricle by retrograde insertion through the aortic valve. A PV catheter has one pressure sensor, and two proximal excitatory and two distal recording electrodes that handle the electrical communication. Several heartbeats are often recorded in apnea to limit the respiratory effects on cardiac volumes. Pressure calibration is performed before insertion. The volume output data is a mathematically calculated value using admittance theory and Wei's equation (eq. 1.8).

$$Volume = \frac{1}{1 - \frac{G_b}{\gamma}} \rho L^2 G_b \tag{1.8}$$

where ρ = Blood resistivity; L = Electrode distance; G_b = Blood conductance; γ = field correlation factor.

Three factors are important for correct absolute values: the stroke volume (SV) calibration factor, blood resistivity, and heart muscle type (conductivity and permittivity). The SV calibration factor has to be derived from external methods. Variables of importance to guide the placement inside the ventricle are magnitude and phase angle. Briefly, magnitude

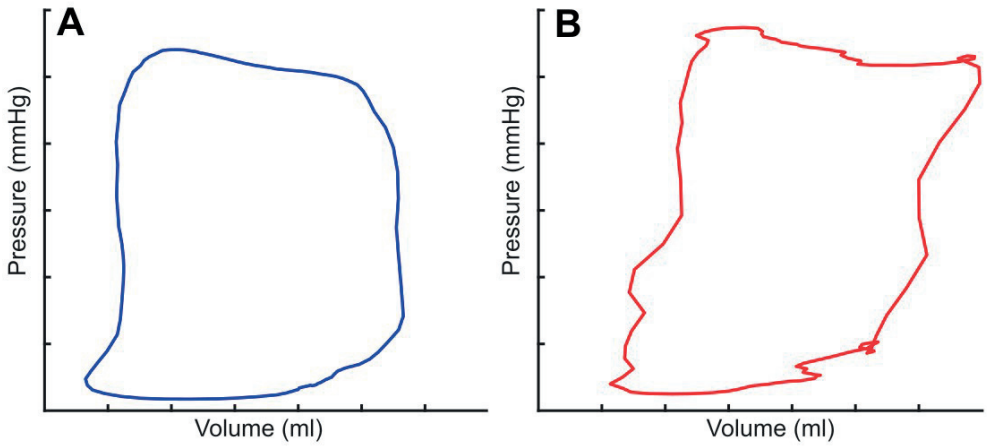

Figure 1.13: Real examples of invasive pressure-volume loops measurements in sheep. An acceptable acquisition is shown in panel A, whereas B shows a PV loop of less quality. *Reproduced with permission from Syntach AB.*

is similar to conductance (direct current) or admittance (alternate current) and is correlated to the surrounding blood volume. The phase angle measures the lag between outgoing and incoming sinusoidal waves and estimates the parallel conductance, which is the part of the signal that travels in the myocardium instead of blood. The phase angle combined with the heart muscle resistivity is used to subtract the signal traveling through the myocardium to isolate the blood signal in the blood. In general, a low oscillatory phase angle indicates a central position.

1.7 Statistics

Two common paradigms of statistical frameworks are rank-based non-parametric methods and value-based parametric methods [235]. The non-parametric tests are appropriate for data that exhibit a non-normal, non-Gaussian distribution. The parametric tests are suitable for data distributed according to a normal distribution. A normal distribution, also known as Gaussian, or bell curve, can be determined by evaluating histograms for symmetry and skewness. We can also assess outliers in boxplots or perform specific normality tests. All tests are based on assumptions, and the primary assumption of parametric tests is that the data is normally distributed. In contrast, non-parametric methods do not rely on data shape and distribution assumptions. Although it is possible to apply the tests on whatever data the researchers find adequate, results could be misleading if assumptions are not reasonably met. The decision of what statistical tests to use is ultimately the researchers', and knowledge of pitfalls and assumptions will help recommend a suitable method.

Two drawbacks of the non-parametric tests are that they are less powerful than parametric tests and are most often rank-based rather than based on actual data. Less powerful means that a larger sample size is required to meet the power of a corresponding parametric test. Rank-based methods are more challenging to interpret as we do not readily understand what, for example, a mean rank difference of "five" between two groups means for a given variable.

1.7.1 Survival Analyses

Statistical survival analyses have historically been employed in several fields of medicine since its advent in the 20th century, with formidable developments in the latter half of it [236]. Today, survival analyses are fundamental to modern clinical trials to investigate medical drugs, devices, therapies, and biomarkers. Although the term "survival" indicates that the methods are used in data with terminal events, the same statistics can also be applied in non-terminal circumstances as well as in engineering, electronic and material sciences.

Out of many significant contributions to this field, some developments have profoundly impacted it and amassed many thousand citations since publication. The most famous and impactful studies are the *Kaplan–Meier* method for estimating the survival function [237] and the *Log–Rank test* for assessing the differences between two survival distributions [238]. Another fundamental method worth mentioning is the *Cox proportional hazards (PH) regression* model [239] for quantifying the impacts of covariates on the survival time.

The survival curve and the hazard rate are crucial aspects of survival data. The survival curve, modeled by the survival function $S(t)$, is primarily descriptive. The survival function is the probability that an individual survives from the time origin (e.g., cancer diagnosis) to a specified future time t. The hazard rate, modeled by the hazard function $h(t)$, mainly analyzes the magnitude of change in hazard between groups. The hazard function estimates

the probability that an individual under observation has an event at time t. Put another way; it represents the instantaneous event rate for an individual who has already survived to time t, compared to a reference individual or group.

1.7.2 Single Event

Survival data is rarely normally distributed but generally skewed with many early and few late events. Further, survival analyses supersede standard regression models for survival data because they are able to handle individuals without events through "censoring". Censoring occurs when an observation is interrupted before the event of interest occurs. The dropout can be due to the end of study follow-up, event occurrence of non-interest, or individuals lost to follow-up. Censored study participants are removed from the analysis after the censoring and their time to event is, therefore, unknown. However, unlike standard statistical regression models, survival analyses make use of the time under risk before censoring.

Most studies in the cardiovascular domain focus on a single event. Therefore, the apparent endpoint is mortality, which a patient only experiences once. There is non-specific mortality, such as all-cause mortality, and cause-specific, such as cardiovascular mortality. In general terms, a non-specific mortality endpoint is appropriate when the objective is the net benefit for the patient. This endpoint is blunt and unrelated deaths may dilute the effect resulting in reduced statistical power. Cause-specific mortality, like CV mortality, is appropriate when the objective is to show a more pathophysiological linked benefit [240]. The advantage is reduced noise from unwanted and unrelated events. Both types of mortality should be reported to avoid the pitfall of obscuring an increase of unwanted events caused by the intervention of interest. The choice of an endpoint is essential, and factors to consider include the underlying event rate, which relates to the expected number of events. Because many of the survival-statistical calculations only update at event times, this determines much of the statistical power. More events equal higher power and precision. Further, the availability of credible cause-specific registries, the feasibility of external adjudication, and pathophysiological considerations also impact the choice of endpoints.

Kaplan-Meier

The most used method of estimating the survival function and describing the survival probability is the Kaplan-Meier method [237], also sometimes called the "product limit estimate." First, time is divided into multiple small intervals demarcated by events. After that, the probabilities of surviving from one interval to the next are multiplied to give the cumulative survival probability (eq. 1.9). Therefore, the estimated probability is a step function that changes value only at an event (Figure 1.14). This method allows each patient to contribute information to the calculations for as long as they are known to be event-free. This gives that any censuring should be non-informative and not subject to systematic bias. Life tables are similar but divide the time intervals into discrete periods, which can be helpful when the exact time of an event is unknown.

ID	Month	Event
1	2	1
2	5	1
3	6	0
4	7	1
5	4	1
6	2	1
7	3	1
8	2	0
9	5	1
10	2	1

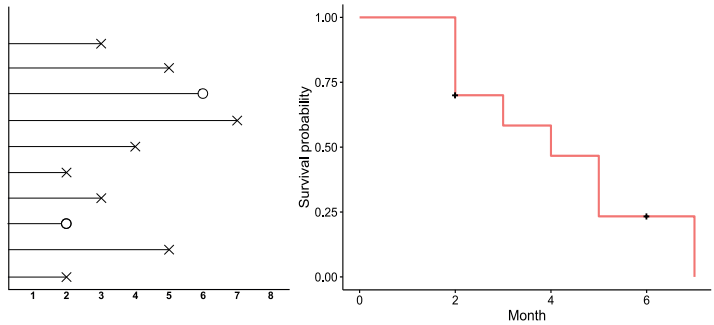

Figure 1.14: Left: Example data of 10 study individuals. Middle: Individual paths during the follow-up period. Right: The resulting Kaplan-Meier graph.

$$\hat{S}(t) = \prod_{t(i)<t} \frac{n_i - d_i}{n_i} \tag{1.9}$$

where t = time; n = number at risk; d = events.

The Log-Rank Test

The Log-rank test is a non-parametric test often used to compare the survival distributions between groups or strata [238]. The method calculates at each event time, for each group, the number of events one would expect since the previous event if there were no difference between the groups. These values are then summed over all event times to give each group the predicted number of events. When only two groups are compared, the Log-rank test tests the null hypothesis the two groups' survival curves are equal. The Log-rank calculation (eq. 1.10) of the expected E vs. observed O values in the different groups follows a χ^2 distribution, thus a p-value can be derived. The p-value refers to the probability of seeing this difference or greater if one would perform the study again.

$$\sum_{j=1}^{J} \left(\frac{(\sum_{t=1}^{T} O_{tj} - \sum_{t=1}^{T} E_{tj})^2}{\sum_{t=1}^{T} E_{tj}} \right) = \chi^2 \tag{1.10}$$

where O = Observed; E = Expected.

Cox Proportional Hazards Regression

The Cox PH regression "semi-parametric" model describes the relationship between the event incidence and a set of covariates as expressed by the hazard function [239]. The term "semi-parametric" refers to that the baseline hazard is unknown and that the model quantifies the influence of the covariates of the hazard excessive to the baseline. The hazard is the

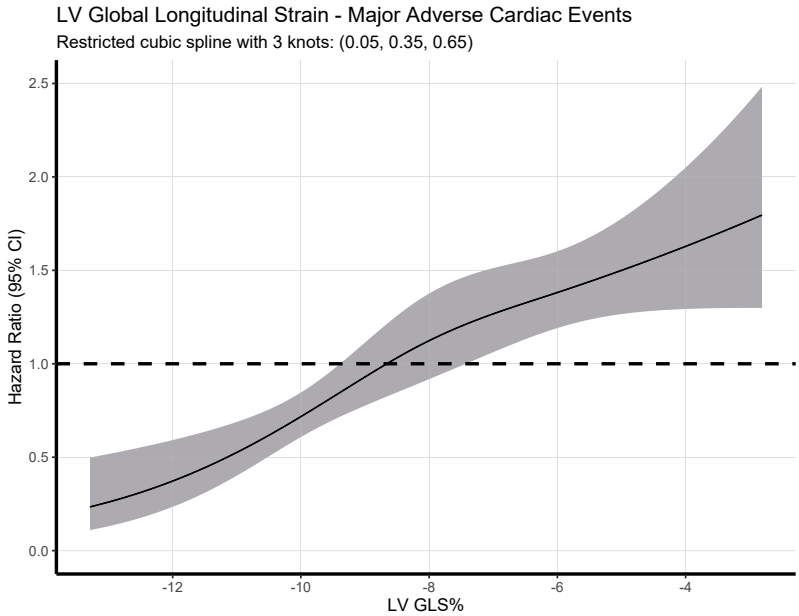

Figure 1.15: The hazard ratios for left ventricular (LV) global longitudinal strain values displayed using restricted cubic spline modeling.

instantaneous event probability at a given time t. The hazard function $h(t)$ is dependent on (or determined by) a set of covariates whose impact is measured by the size of the respective coefficients and a baseline hazard (eq. 1.11). In essence, the Cox model is a multiple linear regression of the logarithm of the hazard of the variables, with the baseline hazard being an 'intercept' term that varies with time. The predicted hazard ratios for a variable can then be displayed (Figure 1.15).

$$\mathrm{h(t)} = \mathrm{h_0}(t) \cdot e^{b_1 x_1 + b_2 x_2 + \cdots + b_n x_n} \tag{1.11}$$

where h_0 = Baseline hazard (unknown); b = Coefficients; x = Predictors.

The log-rank test and Cox regression both look at the difference between observed and expected events. Unlike the log-rank test, the Cox regression looks at the incidence (event per time unit) and can handle multiple predictors at once. An important assumption is that the hazards are proportional over time, which is different from the Kaplan-Meier estimation. Proportionality implies that the coefficients e^b are called hazard rate ratios, most often only referred to as "hazard ratio" (HR). An HR above 1 indicates a covariate that is positively associated with the event probability and thus negatively related to the length of survival. This proportionality assumption is often appropriate for survival time data, but it is important to verify it. Plotting the difference between expected and observed events over time gives you partial residuals, such as Schoenfeld residuals, and should not

deviate with time if proportionality exists. Nevertheless, a covariate may exhibit a non-proportional hazard over time. Two different circumvention approaches are 1) to include an interaction term between time and the covariate, or 2) to stratify the Cox regression using the non-proportional covariate. A Cox PH model with time-dependent covariates implemented allows the effect of the relevant covariates to change with time.

Composite Endpoints

It is common practice to use the first event only, although this ignores information beyond this point. A *composite endpoint* is often chosen since the numerosity of events determines statistical power. In cardiovascular research, a set of prespecified events of pathophysiological relevance can be integrated and used as a substitute, or in addition, to a mortality event. A common triplet of major adverse cardiovascular events is cardiovascular (CV) death, AMI, and HF hospitalization. A higher event occurrence is traded at the expense of specificity. Widespread use of composite endpoints has benefitted cardiovascular research greatly, but limitations of composite endpoints are often not addressed. One limitation is that standard analyses of combined events ascribe the same value to all the included events. This might influence the conclusions if mortality events are considered equal to more trivial events.

Competing risks

Another pitfall related to composite endpoints, other than lost specificity and equal-valued events, is not addressing the presence of *competing risks* from other causes [241]. When the survival duration is ended by the first of several events, it is called competing events. The problem occurs when one event inhibits the occurrence of others. As a result, censoring might be informational. Consider an example: A study is investigating tumor-related death after treatment and is not considering other deaths. If the therapy inadvertently causes other deaths, such as frailty-related, the treatment causes censoring and decreases the number of patients in the treatment arm. Consequent events will have a relatively greater impact on the remaining patients. Thus, the risk of tumor-related deaths may be exaggerated. Competing risks often exaggerate Kaplan-Meier estimates such that when adding each component, they amount to an artificially high number [242].

Instead of Kaplan-Meier, one can use the Cumulative incidence function when analyzing competing events. Cumulative incidence is defined as the cumulative probability of an event having occurred in the presence of other competing events. The cumulative incidence function keeps all study participants in the risk set even after having experienced a censoring or competing event. *Gray's test* [243] can then be used to evaluate the equality of cause-specific cumulative incidence functions between two groups. In the absence of censoring, Gray's test is identical to the log-rank test. A regression model appropriate for evaluating a covariate's effect on the absolute risk in presence of competing risks is the *Fine and Gray* model [244].

1.7.3 Multiple Events

Unlike mortality which is a clearly defined end-point, morbidity is not. For example, there are no official guidelines on how to best study the morbidity endpoint in heart failure [240]. Methods of including multiple events for every patient aim to represent the morbidity endpoint better than inefficient "time-to-first-event" methods. This is impactful for future clinical CV research since many diseases have multiple, non-terminal, and reoccurring events, which all are carriers of information. The primary benefit of using data from several events is increased statistical power. Some areas in need of future research include determining which methods to best handle multiple events, weighting the relative importance of components in composite endpoints, and accruing the value of numerous events of lesser importance or severity. Two metrics that imply reoccurring events and relate to the extent of hospitalization, and without needing specific statistical methods, are "Days alive and out of hospital" [245] and the win ratio [246].

The visual description of the survival function is an intuitive way of presenting survival data. The *Mean cumulative function (MCF)* [247, 248] is similar to the Kaplan-Meier plot in its appearance but includes reoccurring events. The MCF shows the average number of events that a group's individual has experienced during the follow-up period. The MCF can be divided into groups similar to a Kaplan-Meier graph.

Prentice, Williams, and Peterson model

The *Prentice, William, and Peterson (PWP)* model [249] extends the Cox proportional hazards model to incorporate reoccurring events by stratifying the model with an event sequence indicator and connecting patients in different strata using a cluster parameter. Future events depend only on the immediate past. Hence, two stratified PWP models can be fitted: PWP-tt (total time), which evaluates the effect of a covariate for the k-th event since the entry time in the study; the PWP-gt (gap time), which assesses the impact of a covariate for the k-th event since the time from the previous "$k-1$" event. These stratified cox-based conditional models incorporate the order of events in the definition of the risk sets. Usually, the number of individuals and events in subsequent strata declines significantly with an increasing number of strata. As the statistical power is tied to the number of events in each stratum, there is often a need to truncate the dataset to counter this risk. The number of strata should be selected specifically for each study with this in mind. Other extensions of the Cox regression model which slightly differ from PWP include the *Andersen-Gill model* [250] and the *Wei, Lin, and Weissfeld model* [251].

Multi-State Models

A multi-state model (MSM) is a network of nodes or states that models transitions between states generated by events [252]. The simplest MSM is defined as two states: alive (a transient state) and dead (an absorbing state). A more complex MSM is when individuals

move between one state, e.g., "healthy," and another state, e.g., "hospitalized," through time, with or without absorbing states. A "healthy-illness-death" MSM may be considered for analyzing reoccurring events in HF. Of note, MSMs can be arbitrarily complex with an increasing number of possible states − at the expense of intuitive interpretations. The results yield estimations of transition probabilities between states and transition intensities defined as instantaneous hazards, or hazard ratios, of transitioning between states. The possible distinction between different types of events benefits this framework.

Poisson Regression

The Poisson regression is a generalized linear model that estimates the count or rate of event occurrences. The Poisson distribution is a discrete distribution that is useful for estimating the expected distribution of a number of events occurring in a fixed interval of time or space. In a strict Poisson distribution, the mean is equal to the variance, and a Poisson regression assumes that the response variable "Y", e.g., hospitalizations, follows a Poisson distribution. Other assumptions of the Poisson regression are that the events should occur at a constant rate, be independent of each other and that all individuals carry the same underlying event rate. Although in heart failure, subsequent hospitalizations are likely not independent from the previous. The Poisson regression gives estimates of a variable's coefficient "x". This means that for each one-unit increase in a variable, e.g., age, the expected log count or rate of "Y" (hospitalizations) changes by "x." This information can be used to calculate risk ratios of different groups and variables.

The Joint Frailty model

The joint frailty model [253], also called the "random-effects" approach, was used to analyze mortality and reoccurring HF events in the recent "EMPEROR-Preserved" trial [109]. It simultaneously analyses reoccurring events whilst taking into account the link between different types of events by introducing a subject-specific random covariate into the model. The idea is that the random effect term describes the excess risk or frailty for distinct individuals, taking into account unmeasured heterogeneity that cannot be explained by observed covariates alone and inducing dependence between reoccurring event times. The frailty model can be applied when there are multiple events, different types of events, and if the relationship between different events is of interest.

1.7.4 Evaluating Models

Overall Model Fit

The term "model" or "modeling" is often used in survival analysis. In essence, a model is a map of risk predictions of individuals in the risk set generated from the collection of individual covariates. A survival model is adequate if it represents the survival patterns in the data to an acceptable degree. A good model must be able to 1) distinguish between

higher and lower-risk patients and 2) make unbiased predictions and give predicted probabilities that match closely those observed in terms of absolute risks. These are the two components of predictive ability called discrimination and calibration [254]. A model that closely mirrors the survival patterns of the data is said to have internal validity. However, for a predictive model to be of broader use, it should perform well in other patients separate from the training dataset – i.e., be externally valid. In addition, both discrimination and calibration should be assessed before a model is implemented in clinical decision-making.

Likelihood

Statistical models are often assessed by their improvement in *likelihood*, and some researchers argue that one likelihood-based test might be sufficient for evaluating new predictors [255]. However, implementation of models into clinical practice mostly requires further evaluation in terms of discrimination and calibration, as discussed later. The likelihood function reflects the probability, or "likelihood," of obtaining the observed data in a specified model and the best estimate is called the maximum likelihood estimation. For easier calculations, the log of the likelihood function is used.

A common approach to evaluating a new diagnostic or prognostic marker is to test if the new variable's inclusion in a model already containing well-known predictors yields a significant increase in likelihood. The likelihood ratio test achieves this and measures the difference in unexplained error between a full and a reduced model, which follow a χ^2 distribution. Only nested models can be compared using the likelihood ratio test. Accepting the new biomarker as having predictive value entails significant association with the outcome in the multivariable model after adjusting for the established biomarkers. If so, it is commonly referred to as having an "independent" predictive value. If the new marker does not improve the likelihood of the outcome, it probably is not a valid predictor of outcome. However, a significant improvement in likelihood is not necessarily translated into clinical significance.

The *Wald* statistic can be calculated as (b/standard error of b)^2 and is assumed to follow a χ^2 distribution. It can be used for dimensionless comparisons between variables and corresponds to whether the β-coefficient of a variable is statistically significantly different from 0. A higher value indicates a more significant deviation from the null hypothesis. Other likelihood-based metrics for model assessments are the *score test* or penalty-based information criteria such as the *Akaike information criterion "AIC"* and *Bayes information criterion "BIC"*. The latter both give penalties for added variables and can be used when comparing non-nested models.

Discrimination and Calibration

The *concordance index* [256], or C-index, measures how well a model can **discriminate** between high and low-risk individuals while regarding time. It tests if the model conforms

to the statement: "greater scores should be attributed to subjects at a higher risk of experiencing an event" [257]. The C-index is a generalization of the area under the receiver operating characteristic (ROC) curve. The number represents the probability of concordance between observed and predicted survival based on pairs of individuals, with $C = 0.5$ for random predictions and $C = 1$ for a perfectly discriminating model. A caveat of the C-statistic is that it might not translate to clinical meaningfulness. A model which has a good discriminatory ability (high C-index) can accurately state that a patient has a five-fold increase in risk. However, if the predicted risks are 1% and 5% when the actual absolute risks are 10% and 50%, the model is not clinically accurate and needs **calibration**. One limitation of the C-index is that it can be insensitive to detect improvements in the model's calibration when adding new predictors.

Calibration is more challenging than discrimination and should contain validation against separate datasets. The visual assessment of the relationship between predicted vs. observed events is likely the most intuitive marker for calibration. Decent calibration can be inferred if computed survival curves for given risk groups agree between a derivation and a validation dataset [258].

A popular method of assessing a predictive model is the *net reclassification index (NRI)* [259], which quantifies how a new model correctly reclassifies patients compared to an old model. For NRI, the choice of cut points and thresholds is of critical value and should ideally reflect important clinical risk strata so that any changes have clinical implications. A positive NRI when adding a predictor indicates an increase in true-positive or decrease in false-positive cases with respect to the older model. The *integrated discrimination improvement (IDI)* [260] is a metric that assesses risk classification without categories. However, the IDI values can be difficult to interpret.

Chapter 2

Aims

The accumulated impact of acute myocardial infarction (AMI) and heart failure (HF) is immensely severe and common such that any improvement in cardioprotection, therapy, and understanding could lead to massive cardiovascular health benefits for patients. Thus, there is a need for better pathophysiological knowledge of these conditions. This thesis focuses on the ventricular longitudinal function, hypothermia, and non-invasive pressure-volume loops as promising tools for such applications.

The specific aims for studies I - IV are listed below:

I To determine the relationship between atrioventricular plane displacement (AVPD) and stroke volume (SV) before and after AMI, whether the relationship between AVPD and SV differs between ischemia/reperfusion (I/R) and microembolization (ME) experimental AMI models, and how diastolic longitudinal function changes after an AMI.

II To elucidate the cardioprotective effects of hypothermia adjunct to reperfusion on cardiac energy mechanics in an experimental AMI model through a non-invasive PV loop algorithm by cardiovascular magnetic resonance (CMR) imaging during the initial week.

III To determine if ventricular longitudinal shortening variables, AVPD and global longitudinal strain (GLS), predicts cardiovascular (CV) and all-cause death in patients with heart failure with a reduced ejection fraction (HFrEF), independently of well-known risk factors such as ejection fraction (EF) and late gadolinium enhancement (LGE).

IV To determine if AVPD or GLS can predict the composite endpoint of CV mortality and morbidity in HFrEF patients, and to investigate the relationship of AVPD or GLS with the number of and length of HF-associated events.

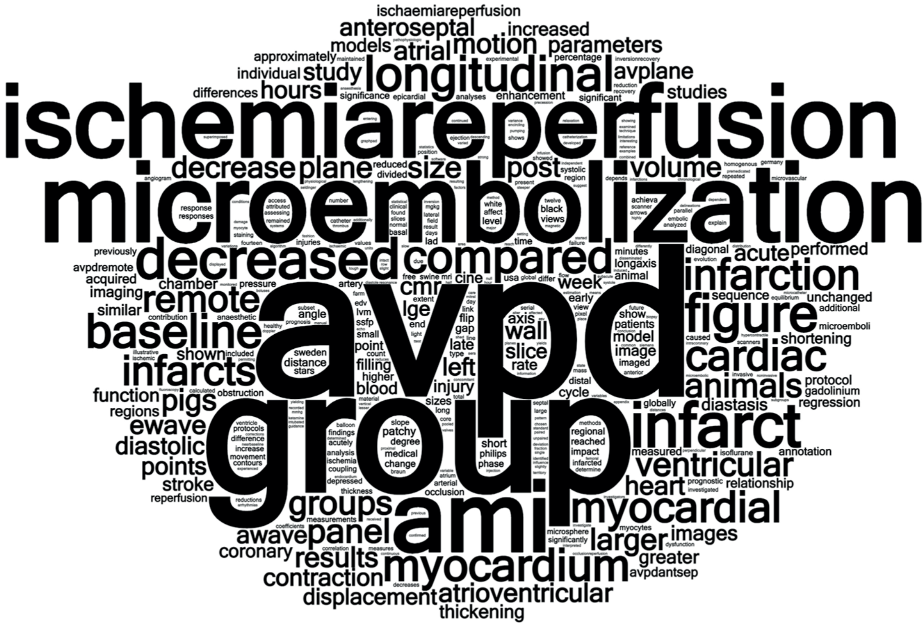
avpd
group
microembolization
ischemiareperfusion
ami
infarct
longitudinal
decreased
compared
infarction
figure
baseline
cardiac
myocardium
myocardial
infarcts
remote
ventricular
animals
groups
panel
decrease
plane
size
post
volume
motion
atrial
anteroseptal
parameters
increased
avplane
study
hours
studies
heart
larger
images
results
awave
ewave
diastolic
points
stroke
pigs
function
regions
contraction
displacement
atrioventricular
thickening
coronary
greater
avpdantsep
diastasis
shortening
acute
performed
unchanged
protocol
gadolinium
regression
relationship
annotation
ischaemiareperfusion
approximately
individual
differences
models
cmr
lge
left
wall
slice
axis
injury
blood
filling
week
previously
avpdremote
acquired
imaging
similar
chamber
reperfusion
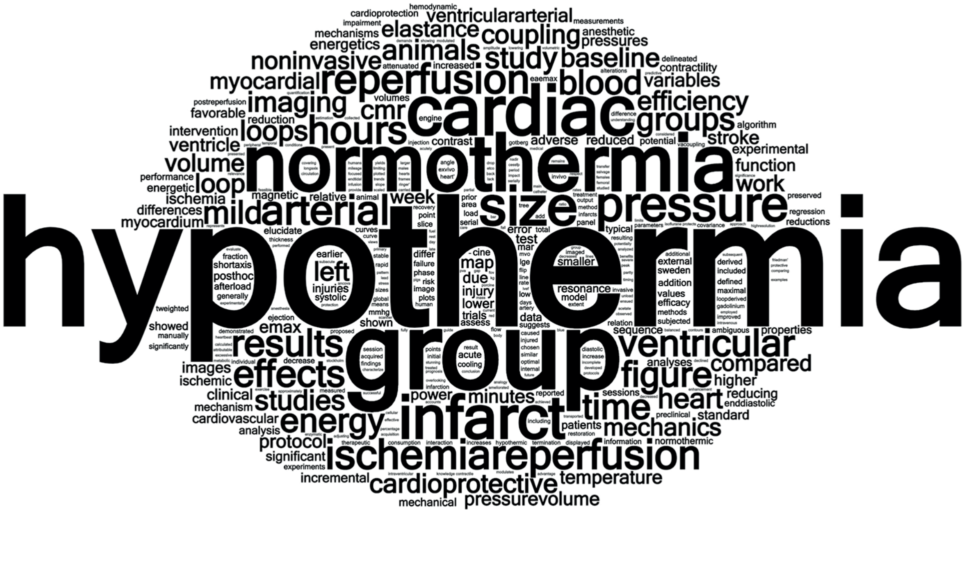
hypothermia
normothermia
group
cardiac
reperfusion
pressure
size
infarct
ischemiareperfusion
arterial
hours
ventricular
results
effects
energy
figure
heart
time
studies
mechanics
cardioprotective
pressurevolume
temperature
blood
baseline
study
animals
coupling
elastance
ventriculararterial
noninvasive
myocardial
imaging
cmr
loops
efficiency
groups
stroke
function
work
loop
volume
mild
ventricle
experimental
compared
higher
reducing
standard
protocol
significant
incremental
mechanical
clinical
mechanism
cardiovascular
images
ischemic
power
minutes
emax
left
week
myocardium
differences
energetic
ischemia
energetics
mechanisms
pressures
variables
cardioprotection
hemodynamic

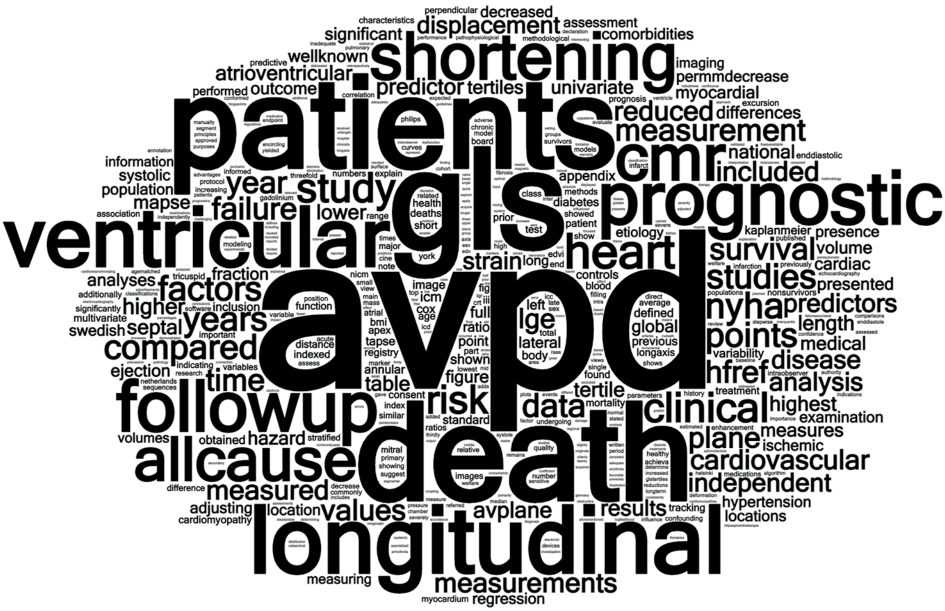
avpd
patients
gls
death
longitudinal
ventricular
prognostic
shortening
followup
allcause
cmr
heart
study
factors
compared
clinical
points
nyha
studies
predictors
risk
displacement
measurements
measured
values
cardiovascular
independent
reduced
measurement
included
survival
failure
years
year
time
data
analysis
disease
hfref
plane
tertile
strain
lge
predictor
tertiles
univariate
atrioventricular
outcome
myocardial
wellknown
significant
decreased
comorbidities
assessment
differences
national
septal
higher
analyses
ejection
mapse
population
systolic
information
fraction
lower
table
hazard
results
avplane
location
adjusting
regression
highest
measures
ischemic
examination
hypertension
locations
cardiomyopathy
length
medical
presence
volume
cardiac
presented
imaging
permmdecrease
kaplanmeier
etiology
appendix

events
patients
longitudinal
ventricular
avpdgls
event
function
cardiovascular
hospitalizations
number
plane
hfref
study
mortality
morbidity
reoccurring
cmr
heart
patient
variables
data
analysis
models
hospital
myocardial
systolic
endpoint
global
hazard
standard
experienced
values
statistical
displacement
cumulative
timetoevent
hyponatremia
hospitalization
risk
days
strain
model
index
pwptt
predictors
multivariate
failure
outcome
atrioventricular
death
predictive
tertiles
followup
included
important
final
quality
results
lower
higher
tertile
figure
analyses
measured
disease
measurements
accumulated
assessed
diagnoses
prognostic
covariates
table
diastolic
clinical
volume
deaths
longer
valve
total
stay
cine
cms
year
prior
years
image
ratios
etiology
reduced
highest
association
algorithm
enddiastolic
proportional
increased
inclusion
methods
significant
compared
velocities
predict
combined
including
specific
national
appendix

Chapter 3

Materials and Methods

3.1 Thesis at a Glance

Thesis at a glance	
Study I	
Aim	To assess the relationship between stroke volume and atrioventricular plane displacement in two types of myocardial infarction: 1) microembolization and 2) ischemia/reperfusion.
Study design	Two-group experimental intervention with before and after CMR imaging
Study participants	N=9+12 pigs
Analyses	Descriptive statistics, regression analyses.
Study II	
Aim	Elucidate the potential benefits of mild hypothermia as a cardioprotective therapy from a perspective of cardiac work and power using non-invasive PV loops.
Study design	Two-group experimental intervention with serial CMR imaging
Study participants	N=7+7 pigs
Analyses	Descriptive statistics, regression analyses, analysis of covariance
Study III	
Aim	Determine the prognostic value of ventricular longitudinal shortening for mortality in HFrEF
Study design	Retrospective Survival analysis
Study participants	287 HFrEF patients; 20 Age-matched controls
Analyses	Single event survival analyses: Kaplan-Meier; Cox PH regression; ANOVA
Endpoint	Cardiovascular and all-cause mortality.
Study IV	
Aim	Determine the prognostic value of the ventricular longitudinal function for morbidity in HFrEF
Study design	Retrospective Survival analysis
Study participants	287 HFrEF patients; 20 Age-matched controls
Analyses	Single event survival analyses: Kaplan-Meier Multiple event survival analyses: Mean cumulative function; Prentice-William & Peterson-Total time regression.
Endpoint	Composite endpoint with heart failure-associated morbidity and mortality.

3.2 Study Populations

3.2.1 Animals

The experimental *studies I & II* was performed in agreement with the Guide for the Care and Use of Laboratory Animals 8th edition [261] and was approved by the Swedish Agricultural Board (*studies I & II*), the Regional Ethics Review Board in Lund (*studies I & II*; registration number: 5.8.18- 70 11702/2019), and the Institutional Animal Care and Use Committee at the University of California, San Francisco (*study I*).

In *study I*, two models of acute myocardial infarction were used: ischemia/reperfusion (I/R) and microembolization (ME). For I/R, fourteen healthy Landrace and Yorkshire pigs (sus scrofa domesticus) weighing approximately 40 kgs were used. This model was carried out at Lund University. For ME, twelve healthy farm pigs, 33±1 kgs, were used. This model was carried out at the University of California, San Francisco.

In *study II*, two groups, Normothermia and Hypothermia, of seven landrace pigs weighing 40±3 kgs, approximately three months old, were included. The seven pigs in the Normothermia group were also part of the twelve pigs of the I/R group in *study I*. They were subjected to an acute myocardial infarction (AMI) model of type ischemia/reperfusion that was carried out at Lund University.

3.2.2 Patients

The Regional Ethics Review Board originally approved the inclusion of patients for *studies III-IV* in Lund, Sweden, in 2004. Additional application to gather detailed information on causes of death and hospital admission was approved in 2019 by the Swedish National Review Authority and the Swedish National Board of Health and Welfare. The studies were carried out following the principles of the Declaration of Helsinki. *Study III & IV* included the same patient population of two hundred ninety-five patients diagnosed with HFrEF who underwent CMR examinations at Lund University Hospital between 2003-2015. They were included if they gave informed written consent to have their CMR scan and subsequent data available for future research purposes and did not fulfill any exclusion criteria. Criteria for exclusion were an EF above 40% measured from the CMR examination, poor image quality on CMR, and significant valve insufficiencies or stenoses. Eight patients were excluded due to poor cine image quality leaving 287 patients eligible for analysis of ventricular longitudinal function, shown in Figure 3.1.

The CMR examinations were part of the regular clinical workflow, and indications were typically investigations of ventricular volumes and function, infarcts, fibrosis, or assessment prior to implantation of cardioverter-defibrillator (ICD) or cardio-resynchronizing therapy (CRT). The basis for decreased EF was separated into ischemic (ICM) or non-ischemic (NICM) etiology based on the patients' charts and the clinical CMR reports of observed pathologies.

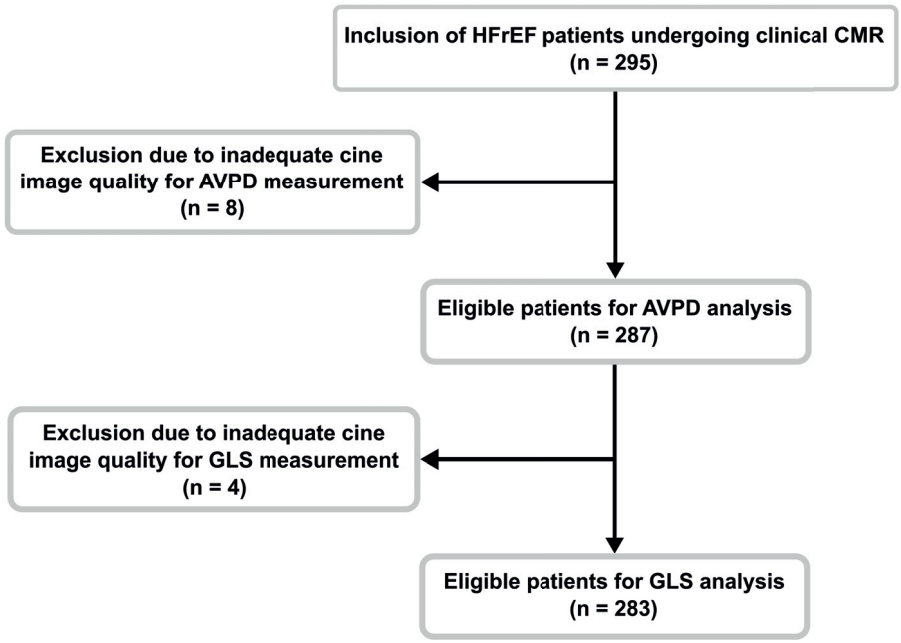

Figure 3.1: Patient flowchart for studies III & IV.

Study III contains data on causes of death, whereas Study IV also contains information on hospital admission and diagnoses. The patients' causes of death were obtained from the Swedish National Board of Health and Welfare's registries of Causes of Death. Previous medical history, hospital admissions, and diagnoses were collected from the Swedish National Board of Health and Welfare's Hospital registry. The patients' biochemical laboratory data between 2003-2019 were collated from manual reviews of the electronic medical journals. Laboratory results were used if they were gathered closer than one year from the CMR examination.

The prescribed cardiovascular medications of the patients at the time of CMR in descending order of use were: Betablockers (92%), renin-angiotensin-aldosterone system (RAAS) antagonists (90%), Spironolactone (52%),

3.2.3 Age-matched Controls

Study III & IV contain an age-matched control group of 20 healthy volunteers recruited from advertising, portraying ventricular longitudinal function reference values. The healthy volunteers signed an informed consent form before CMR examinations which accepts the inclusion of their scans for research purposes. There were twelve males and eight females. They were 62±11 years, had an EF of 60±5%, and were free from any history or presence of cardiovascular diseases such as diabetes, hypertension (blood pressure below 140/90

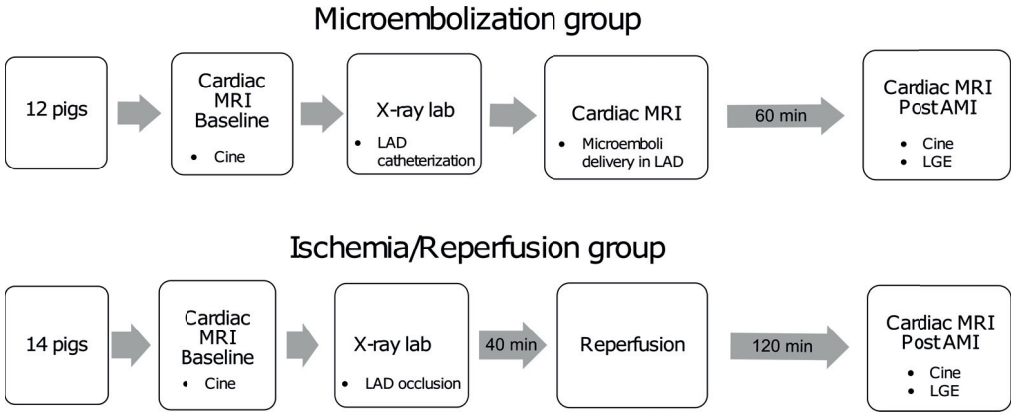

Figure 3.2: Study I flowchart.

mmHg), ischemic heart disease, other systemic diseases, cardiovascular medication, or evidence of pathology on electrocardiogram or CMR.

3.3 Animal Experimental Setup

Animal models and non-invasive diagnostic technologies are valuable when studying cardiac pathophysiology in order to further the understanding of AMI and HF. Porcine and ovine models of myocardial ischemia are particularly used for studying AMI and HF pathophysiology because of the many similarities in cardiac morphology and hemodynamic responses with humans [262, 263].

3.3.1 Study I

In *study I*, two models of AMI were employed. Firstly, an I/R infarction model that results in a more homogenous infarct and injury in the myocardium. Secondly, a microembolization (ME) infarction model that produces a patchy and heterogeneous infarct without reperfusion. An overview of the study protocol is shown in Figure 3.2.

Ischemia/Reperfusion

The animals were premedicated intramuscularly with 0.5 mg/kg midazolam (Dormicum; Roche, Stockholm, Sweden) and 15 mL/kg ketamine (Ketaminol; Intervet, Dandery, Sweden). The pigs were intubated in a prone position, and anesthesia was maintained with isoflurane (Baxter Medical, Kista, Sweden) through an anesthetic conserving device (AnaConDa; Sedana Medical, Sweden) during transportation, imaging, and instrumentation. Expiratory gases (anesthetic agent and CO2) were monitored alongside blood pressure, temperature, heart rate, and oxygen saturation. Intravenous access was obtained through

the Seldinger technique in a sterile manner (Catheter: Intradyn; B. Braun, Germany), and Heparin (15,000 IE units) was given to prevent blood clotting.

After transportation, baseline CMR imaging in a 1.5T scanner (MAGNETOM Aera, Siemens Healthcare GmbH, Erlangen, Germany) ensued in a supine position to assess ventricular function. After that, the animals were transported to a fluoroscopy suite adjacent to the MR-scanner for instrumentation.

After an antiarrhythmic amiodarone infusion (300 mg) 30 minutes prior to ischemia-reperfusion, a 6F coronary guiding catheter (HS Serpia; B. Braun, Germany) was used to access the left anterior descending artery (LAD) under fluoroscopy guidance. The animals were subjected to 40-minute ischemia by percutaneous transluminal coronary angioplasty balloon (SeQuent NEO; B. Braun, Germany) occlusion. The occlusion was placed at varied distances downstream in LAD depending on individual vessel anatomy but typically between the first and second diagonal branches. A coronary angiogram confirmed reperfusion of coronary blood flow. The pigs were defibrillated in case of ventricular arrhythmias. Intravenous boluses (5–15 µg) of norepinephrine were administered if mean arterial pressure decreased below 50 mmHg. The anesthesia protocol, including drug administration and ventilator settings, was adamantly controlled to minimize alterations. The pigs were then awakened and extubated in the stables. The sedation and anesthetic regimes were repeated for animals undergoing additional CMR scans. Animal husbandry was in accordance with national regulations. The animals had free access to water and were examined daily by animal caretakers.

Microembolization

Animals were premedicated with acepromazine (1.1 mg/kg) and ketamine (22–33 mg/kg) and then intubated and anesthetized with isoflurane (2–5%). A 6F introducer (Avanti; Cordis, Miami, FL) was placed in the femoral artery by the Seldinger technique. Access to the LAD artery was acquired under fluoroscopy guidance. After that, a 3F microcatheter (Cook, Chicago, IL) was placed distal to the first diagonal branch. The animal was transported into the CMR scanner with the catheter in place. The twelve animals were divided into subgroups of six pigs each and received two different microemboli sizes (40–120 µm, 250,000 microsphere count, and 100–300 µm, 7,200 microsphere count, respectively). The two microembolization interventions began with a slow infusion through the microcatheter. A 60-min pause ensued before the following imaging allowed infarct development to take place. The embolic quantities for the two subgroups were calculated to occlude the same volume of myocardial tissue, assuming one microsphere occludes one corresponding arteriole [36]. Both 0.25-mL embolic solutions (Embosphere; Biosphere Medical, Rockland, MA) were diluted with 0.75 mL of NaCl solution.

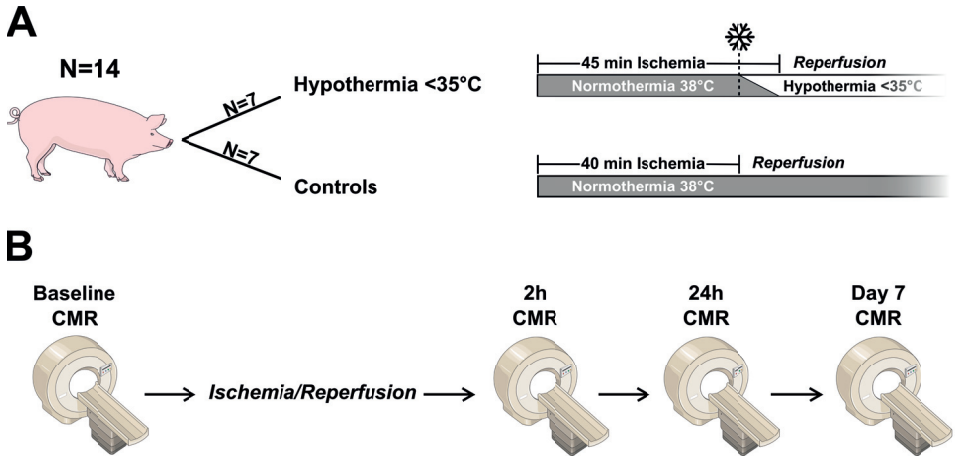

Figure 3.3: Study II flowchart.

3.3.2 Study II

In *study II*, the I/R model was identical to the I/R model in *study I* except for the hypothermia intervention. An overview of the study protocol is shown in Figure 3.3. To isolate the reperfusion injury from infarct development, the Hypothermia group experienced the same *normothermic time* under ischemia as the Normothermia group. At 40 minutes in the Hypothermia group, however, induction of hypothermia began by infusion of 1L near zero-degree Ringer's Acetate for five minutes before reperfusion, aiming for the central temperature to decrease below 35°C. The Normothermia group received a similar fluid challenge of 1L ∼37°C Ringer's Acetate. The animals with extended follow-up were images on three sequent occasions, namely at two hours, 24 hours, and seven days.

3.4 Imaging Analyses

3.4.1 Animal Studies

In *study I*, The I/R group was imaged at baseline and two hours post-reperfusion. Two different scanners were used for this group. A Philips Achieva 1.5T was used for 7 of 14 animals with the following image parameters: steady-state free precession (SSFP) sequence: echo time (T_{Echo}) 1.5 ms; repetition time (T_{Rep}) 3 ms; flip angle 60°; and slice thickness 8 mm; no slice gap. The remaining seven animals, also representing the Normothermia group in study II, were imaged with a Siemens Aera 1.5T. The parameters: SSFP sequence: T_{Echo} 1.2 ms; T_{Rep} 2.7 ms; flip angle 60°, slice thickness 8 mm, no slice gap. The Hypothermia group in study II was also scanned with the Siemens Aera 1.5T camera with an identical protocol. LGE images were acquired for the estimation of infarct size. The inversion time was chosen to null remote myocardium. LGE parameters for the Philips Achieva 1.5T scanner: T_{Rep} 4.1 ms; T_{Echo} 1.3 ms; flip angle 15°; field of view (FoV) 122x122 mm; pixel size 1.52x1.52 mm; no slice gap. LGE parameters for the Siemens Aera 1.5T scanner: T_{Rep} 2.8 ms; T_{Echo} 1.2 ms; flip angle 50°; FoV 159x154 mm; pixel size 1.41x1.41 mm; no slice gap.

The ME group was imaged with a Philips Achieva 1.5T at baseline and one-two hour post-embolization with an SSFP sequence: T_{Echo} 1.8 ms; T_{Rep} 3.5 ms; flip angle 70°; slice thickness 10 mm, no slice gap; FoV 250x250 mm^2; heart phases = 16. late gadolinium enhancement (LGE) images were acquired in short and long-axis views with an inversion-recovery gradient-echo sequence: T_{Rep} 5.2 ms; T_{Echo} 1.5 ms; flip angle 15°; pixel size 1.0x1.6 mm^2; no slice gap. The inversion time was chosen to null remote myocardium.

The main imaging differences between the I/R and ME group protocols were that 1) the ME group was imaged with two perpendicular vertical and horizontal long-axis views for cine and LGE. In contrast, the I/R group was imaged with 2-, 3-, and 4-chamber views. Therefore, the annotation points for AVPD are four instead of six in the ME group. 2) An inversion-recovery gradient-recalled echo sequence for LGE images was used in the ME group and 7 of 14 animals in the I/R group [196, 202]. LGE was acquired in the remaining seven animals in the I/R group with a motion-corrected, phase-sensitive inversion-recovery single-shot SSFP sequence in free-breathing [209]. 3) The ME group's slice thickness was 10 mm, whereas the I/R group had 8 mm.

In *study II*, A T1-weighted sequence was employed to image the explanted heart ex-vivo with high resolution and the following parameters: voxel size 0.5x0.5x0.5 mm; T_{Echo} 3.6 ms; T_{Rep} 20 ms; flip angle 70°; slice thickness 2.5 mm; no slice gap.

3.4.2 Human Studies

In *study III & IV*, imaging was carried out with three clinical MRI scanners: A 1.5T Philips Achieva (Best, the Netherlands), A 3T Philips Achieva (Best, the Netherlands), and a 1.5T Siemens Aera (Erlangen, Germany). Standard short and long-axis cine images (2ch, 3ch,

and 4ch) were acquired using SSFP sequences with the following parameters: T_{Echo} 1.5 ms, T_{Rep} 3.0 ms, flip angle 60° (Philips Achieva 1.5T); T_{Echo} 1.8 ms, T_{Rep} 3.7 ms, flip angle 45° (Philips Achieva 3T); T_{Echo} 1.2 ms, T_{Rep} 2.7 ms, flip angle 60° (Siemens Aera 1.5T). Temporal resolution was approximately 32 ms, and reconstructed spatial resolution was approximately 0.75x0.75x8 mm^3. LGE sequence parameters were identical to clinical workflow protocols. A 2D phase-sensitive inversion-recovery (PSIR) or a 3D inversion-recovery sequence was used for Philips scanners. The Siemens scanner used a 2D PSIR sequence. LGE parameters were: T_{Echo} 4 ms, effective T_{Rep} every second heartbeat, flip angle 25° (Philips 2D PSIR); T_{Echo} 1.3 ms, effective T_{Rep} every heartbeat, flip angle 15° (Philips 3D IR); T_{Echo} 3 ms, effective T_{Rep} every second heartbeat, flip angle 25° (Siemens 2D PSIR). Inversion time was approximately 280-350 ms.

3.4.3 Analysis of Infarcts and Myocardium at Risk

In *study I*, the infarct sizes resulting from ischemia were calculated from LGE images. The "EWA" algorithm with manual corrections at two hours post-reperfusion was used in the I/R group. This method has been validated against ex vivo histochemical staining [264]. For the ME group, a method using a signal intensity threshold three standard deviations above remote myocardium, i.e the "SD method", was used [214]. This method has been validated with microembolization infarct models [265, 266]. The SD method is can be affected by varying contrast in the image and warrants cautious interpretation [267].

In *study II*, detailed infarct quantification on day seven was achieved through analyzing high-resolution T1-weighted images. The extent of scar and microvascular obstruction (MVO) was manually delineated with aid from in-vivo LGE, cine images, and photographs of triphenyl tetrazolium chloride (TTC)-stained hearts, and delineations were mutually agreed upon between six observers. Myocardium at risk (MaR) was manually traced from contrast enhanced-SSFP images. MaR, infarct size, and MVO were presented as a percentage of left ventricular mass. Myocardial salvage was calculated as $100 - (\frac{IS}{MaR} * 100)$

In *study III & IV*, the presence of LGE hyperintensity was determined from the reports by the attending clinician. In addition, the patients were dichotomized into non-ischemic or ischemic etiology of LGE based on the patients' charts and LGE characteristics by the attending clinician. The patients were scanned between 2003-2015. This meant different LGE sequences and varying image quality, which hindered reliable assessments of LGE as exact percentages. Therefore, only the presence of LGE was included.

3.4.4 Venticular Volume Analysis

All cardiac variables were analyzed with the image-processing software Segment v.2.2-v.3.1 [268] (Medviso, Lund, Sweden) in all studies. LV volumes and mass was calculated by manually tracing endo and epicardial borders at end-diastolic and end-systolic time frames. However, endocardial borders were traced in every time frame for *study II* to get time-resolved volume curves. Heart rates were obtained from the CMR scanner. Tracings from

midventricular sections were used to assess wall thickening for *study I*. Left atrial volume was estimated using the area-length method in *study III* (eq. 3.1) [269].

$$\mathrm{V} = 8 \,/\, 3\pi \cdot \left(\frac{A_{2ch} \cdot A_{4ch}}{L} \right) \tag{3.1}$$

where A = atrial area; L = shortest length from the 2ch or 4ch-view.

3.4.5 Ventricular Longitudinal Function Analysis

Ventricular longitudinal variables of interest in the current studies were: atrioventricular plane displacement (AVPD) in *study I*; AVPD, 4ch-tricuspid annular plane systolic excursion (TAPSE), and global longitudinal strain (GLS) in *study III*; AVPD, valve plane velocities, and GLS in *study IV*.

AVPD was measured with the aid of a semi-tracking algorithm that has been developed and validated by *Seeman et. al.* [270]. Fiducial markers are placed at the top of the myocardial wall and the epicardial apex point in all long-axis views in end-diastole. Ideally, six positions around the LV are used. In each long-axis view, an end-diastolic reference plane is created. After that, the shortening and lengthening of the myocardial walls are tracked throughout the cardiac cycle by the placement of annotations markers in all long-axis views in each time frame. The maximal perpendicular length of systolic descent from the end-diastolic plane in each long-axis view is AVPD (Figure 3.4). AVPD is typically defined as the mean displacement of these six LV points. However, in *study I*, the six LV points were divided into two three-point regions corresponding to the injured-anteroseptal and remote-inferolateral myocardium. In *study III*, mean AVPD was indexed to LV length, and LV length was defined as the distance from the apex to a point intersecting the end-diastolic plane at a perpendicular angle. In *study IV*, the maximal valve plane velocities were obtained from a velocity curve derived from the time-resolved AV plane displacement curve at three time points of interest: systole (LV s'), early ventricular filling (LV e'), and atrial systole (LV a'). The tricuspid annular plane systolic excursion (TAPSE) used in *Study III* was defined as the right ventricular lateral wall displacement from the 4-chamber view.

Studies III & IV includes GLS, which refers to the global myocardial deformation in the longitudinal direction. GLS was measured in CMR cine images in each long-axis view by the feature-tracking algorithm implemented in Segment [271]. This algorithm utilizes manual tracings of the myocardial borders in end-diastole as input and automatically tracks the deformation in each pixel over the cardiac cycle. Re-tracking after manual corrections of tracings in end-diastole were applied if necessary. Both AVPD and GLS measurements required at least two long-axis images with satisfactory image qualities for inclusion.

3.4.6 Non-Invasive Pressure-Volume Loop Analysis

In *study II*, a non-invasive Pressure-Volume (PV) loop algorithm was used. This algorithm uses ventricular volume curves derived from tracings of cine short-axis images and non-invasively measured systolic and diastolic blood pressures to estimate the PV loops. The

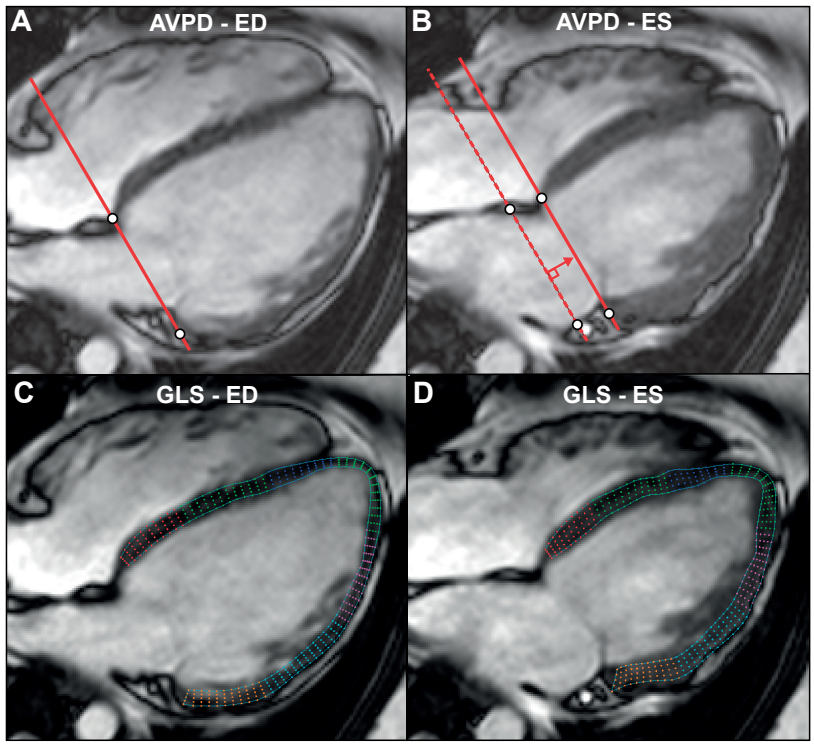

Figure 3.4: Measurement illustration of atrioventricular plane displacement (AVPD) and global longitudinal strain (GLS). ED, end-diastole; ES, end-systole.

conversion from discrete peripheral pressures to continuous ventricular pressure curves is made possible through a generalization of the time-varying elastance curve. It has been demonstrated that the elastance curve is consistent through multiple disease conditions and species when scaled in amplitude and time. The original algorithm, mathematical equations, and validation against invasive pressure-volume loop measurements was described in detail by *Seeman et. al.* [272]. *Study II* uses an updated algorithm that includes physiological modifications for varying heart rates [273]. The algorithm estimates the energy exerted by the heart in one heartbeat, known as stroke work (SW), which can be calculated as the area within the PV loop.

Measurements derived from non-invasive PV loops do not differ significantly from their invasive ditto. A line drawn from zero volume and zero pressure to the point of maximal elastance denotes a relatively load-independent measure of contractility called Emax. This origin is often referred to as V_0, here assumed to be at zero volume.

The mechanical potential energy (PE) is defined as the triangular area beneath the Emax line. It pertains to the remaining energy stored in the contractile apparatus at the end of systole that is not dissipated as SW [274]. The total mechanical energy consumption during a heartbeat equals the combined area of SW and PE, known as PV area (PVA). Thus, the ventricular efficiency in this algorithm is calculated as $\frac{SW}{SW+PE} \cdot 100$. The ventricular efficiency represents the proportion of the cardiac energy consumption dissipated as useful work to generate stroke volume.

Furthermore, total external power output is calculated as $SW \cdot \frac{HR}{60}$. The effective arterial elastance (Ea) estimates arterial afterload, which is defined as the ratio of pressure at end-systole to stroke volume. Theoretically, this is the slope from the point of maximal elastance to the point of end-diastolic volume at zero pressure. The relationship between the two interacting chambers, that is, the ventricle and the arterial tree, can be appreciated by the ventricular-arterial (VA) coupling, which is defined as the ratio of Ea over Emax (Figure 3.5).

There are two central reservations concerning the use of non-invasive PV loops. First, the end-diastolic pressure is not measured but chosen by the user, and hence the diastolic part of the PV loop is less accurate. Although this can be of interest if the diastolic properties are the main focus, the impact of the end-diastolic pressure level will ultimately be minimal when analyzing global PV loop variables concerning work and energy. Secondly, the "V_0" parameter is fixed at a zero value. This could be a simplification since V_0 is dependent on the method of extrapolation [39] and has shown to be influenced by inotropy and afterload in rats [40]. However, the values of V_0 are small, and the impact of fixating V_0 is, therefore, relatively minor.

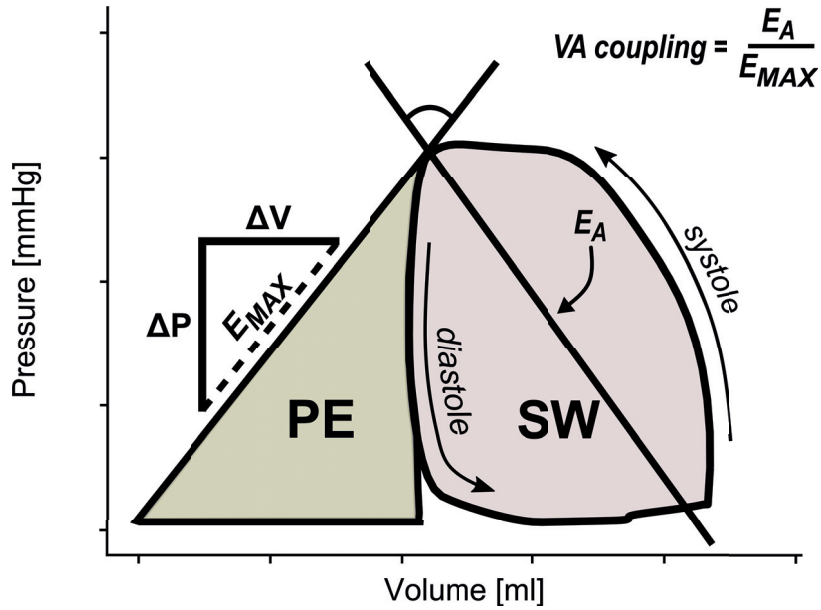

Figure 3.5: Non-invasive pressure-volume loops can be used to estimate information about cardiac energy mechanics, such as potential energy (PE), stroke work (SW), contractility (Emax), and the interaction with the arterial load (ventricular-arterial (VA) coupling; Ea, arterial elastance).

3.5 Statistical Analyses

3.5.1 Statistical Methods

The statistical methods described in the thesis can be separated into descriptive statistics, regression models, and survival analyses. Statistical software used was GraphPad (La Jolla, CA, USA; *study I*), SPSS statistics v.25-v.27 (IBM, Armonk, NY; *Study I, III & IV*), and R v.4.0.3 (*Study II & IV*).

Study I

In *study I*, a parametric approach was chosen. Student's paired and unpaired t-tests were used to assess differences between groups and time points. Paired t-test was used within an individual between baseline and two hours for the same myocardial region (e.g., anteroseptal region). Different myocardial areas (e.g., anteroseptal vs. remote region) were compared using unpaired t-tests. Differences of variables spanning four time points were compared using repeated-measures analysis of variance (ANOVA). Additionally, Pearson's regression coefficient was calculated, and results were presented in mean±standard deviations (SD) or as changes (Δ) in percentage units.

Study II

In *study II*, a largely non-parametric approach was chosen. Mann-Whitney U tests are used to compare variables between groups. Differences within groups over time were assessed with the Friedman test. In addition, Dunn's test for post-hoc multiple comparisons with the Holm correction was used to compare differences at specific time points. Linear regression modeling of the change from baseline to 24-hours and infarct size was calculated for each group. The analysis of covariance (ANCOVA) was used to test whether the differences between baseline and 24-hours in PV loop variables in each group were significant when adjusting for infarct size. Results were presented as mean±SD in tables. Error bar plots show mean±standard error of the mean (SEM).

Study III & IV

In *studies III & IV*, survival analyses, are the primary approaches. The main difference between these studies is that *study III* uses a standard time-to-first-event approach with a mortality-centered outcome, and *study IV* uses reoccurring event analysis with a morbidity-centered outcome. Differences between groups were assessed with student's t-test and ANOVA with the least significant difference post-hoc test for normally distributed variables (*studies III & IV*) and Mann-Whitney U or Kruskal-Wallis tests for non-normally distributed variables (*study IV*). Normality assumptions were checked with histograms and descriptive statistics. Categorical variables were compared with the χ^2-test. The bias be-

tween the same and different observers was tested in a subset of 43 patients, according to Bland and Altman [275].

Single-event survival analyses with Kaplan-Meier were used in both studies, with the log-rank test for comparing differences between tertiles of ventricular longitudinal function. In *Study III*, cox proportional hazards (PH) modeling was used to calculate the hazard rate ratios (HR) for cardiovascular and all-cause death with a backward elimination variable selection process (entry criterion of p-value≤0.10). In *study IV*, Prentice, William & Peterson-Total time (PWP-tt), an extension of the Cox PH regression to incorporate reoccurring events, was used to determine univariate and multivariate prognostic values. A criterion-based forward selection process optimized for maximum Wald statistic pre-inclusion and the p-value≥0.05 post-inclusion. Furthermore, the mean cumulative function (MCF) was used to describe the average number of events patients in each tertile of ventricular longitudinal function experienced. Differences were tested with two-sample pseudo-score tests with the Poisson variance estimation.

For both studies, multicollinearity between variables was limited by a cut-off criterion for inclusion: Pearson's regression coefficient <0.8 [276]. The likelihood ratio tests assessed incremental prognostic values by comparing nested-reduced models with full models. In addition, the concordance index was used to compare the final models' discriminatory abilities in *study IV*.

3.5.2 Registry Data Analysis

Detailed data on hospitalizations and causes of death were obtained from The Swedish National Board of Health and Welfare registries. To extract and handle the extensive data directory and minimize man-made errors, we developed an algorithm for data extraction in MATLAB (R2019a. Natick, Massachusetts: The MathWorks Inc. United States). The algorithm searches a patient's medical history for all hospital admissions spanning the years of interest (2003-2018). It collates the data of interest within the period between the date of the CMR exam and the 5-year follow-up end date. The start dates for each patient are the CMR acquisition dates. The end of follow-up was five years after CMR, at which the patients that had not yet encountered an event were right-censored. The algorithm uses predefined categories and associated ICD-10 codes (Table 3.1) for detecting matching events. Data collected for each event are the primary diagnosis of the hospitalization, the time to event, and the total days of hospital length of stay. All data is accumulated in each category and totaled.

The composite heart failure morbidity outcome used comprises several cardiovascular diagnoses and procedures. The event data used for time-to-first-event analyses are selected from the earliest event encountered in the different categories. Special considerations were taken with adjacent hospitalizations. Namely, events are combined when two or more hospitalizations are immediately adjacent (the end of the first event is within a day of the second event). Otherwise, a new event would be created if a patient is relocated from

Major adverse cardiovascular events	*ICD-10 codes*
Cardiovascular death	-
AMI	I21-I24
Revascularization	FNG, FNA, FNC
Heart failure hospitalization	I25, I420, I50
Heart transplant	FQA, FQB
Cardiac arrest	I46
Ventricular arrythmia	I472B, I472C, I490
Lung edema	J81
Ventricular Assist device	FXL, FXN
Comorbidities	***ICD-10 codes***
Diabetes Mellitus T1	E10
Diabetes Mellitus T2	E11-E13
Any Diabetes	E10-E14
Hypertension	I10-I13
COPD	J44
Liver failure	K72
Kidney failure	N18, N199, I20
Anemia	D649, D509
Atrial fib or flutter	I48
Stroke	I60-I64, I69
+ All event categories	

Table 3.1: ICD-10 codes for *study IV* endpoints.

one hospital facility to another. Without combing adjacent hospitalizations, the algorithm which aims to only count unique events would falsely detect multiple events instead of one in these situations. Data on comorbidities were searched for in all available hospitalizations before the CMR date and dichotomized.

Chapter 4

Results and Comments

4.1 Study I

Heart failure (HF) is a severe condition and affects millions of adults in Europe and the United States alone. Accompanying HF is often low quality of life, high morbidity, and high mortality. A common cause of HF is AMI, which often leads to dysfunction of cardiac pumping and progressive remodeling. Patients with HF due to AMI have a low ventricular longitudinal function measured as AVPD or mitral annular plane systolic excursion (MAPSE) [79, 155, 156, 167]. The most common type of myocardial infarction (MI) results from a complete coronary artery blockage. It produces a relatively homogenous injury and an infarct pattern that travels in a "wavefront" from the endocardium to the epicardium [277]. Another type of AMI, microembolization, can occur naturally due to debris escaping downstream from a partly disintegrated thrombus or iatrogenically during catheter interventions [278]. Microembolization particles produce multitudes of small ischemic territories [36] unavailable for reperfusion, yielding a patchy infarct pattern. This lends the hypothesis that these two types of AMIs may affect the longitudinal pumping and disturb the coupling of AVPD and stroke volume (SV) differently. Therefore, we investigated the relationship between AVPD and SV during the cardiac cycle, before and after AMI during the first week.

Table 4.1 shows baseline and post-AMI data for the two groups, I/R and ME. At baseline, the I/R group was slightly larger than the ME group, evident in larger end-diastolic volume (EDV), SV, end-systolic volume (ESV) (all $p<0.01$), and weight. As AVPD measurements and other cardiac function variables did not differ, this should not preclude the conclusions.

Post AMI, the ischemic injuries affected the groups slightly differently. In the I/R group, EDV decreased while ESV and heart rate increased. In the ME group, EDV and ESV increased while heart rate dropped. The decrease in EDV most likely pertains to the increased heart rate in the I/R group due to increased systemic stress. The discrepancy in heart rates between groups also impacted CO such that the I/R group decreased less

Parameters	Ischemia-Reperfusion (n = 14)			Microembolization (n = 12)		
	Baseline	Post AMI	Δ % change	Baseline	Post AMI	Δ % change
LV AVPD, mm	10.0 ± 1.8	7.2 ± 2.1***	−29 ± 14	9.3 ± 1.7	7.7 ± 1.5*	−15 ± 18‡
LV AVPD anteroseptal, mm	9.8 ± 1.3	6.7 ± 2.0***	−32 ± 15	8.9 ± 1.7	7.2 ± 1.6**	−17 ± 19‡
LV AVPD remote, mm	11.3 ± 2.4	8.5 ± 2.1***	−25 ± 11	10.5 ± 1.9	8.7 ± 1.7**	−16 ± 17
LV stroke volume, mL	48 ± 11	33 ± 10***	−33 ± 13	37 ± 5‡‡	26 ± 4***	−31 ± 11
Basal epicardial area, cm^2	27.9 ± 1.9	26.7 ± 1.9**	−4 ± 6	24.9 ± 1.2	25.7 ± 1.7*	3 ± 5‡‡‡
Long. contribution to SV, %	59 ± 13	59 ± 9	0 ± 10	62 ± 15	78 ± 14***	15 ± 11‡‡‡
LV ejection fraction, %	48 ± 6	36 ± 7***	−12 ± 6	49 ± 5	31 ± 5***	−18 ± 6‡
LV end-diastolic volume, mL	100 ± 14	91 ± 18***	−10 ± 9	76 ± 9‡‡‡	83 ± 10***	9 ± 6‡‡‡
LV end-systolic volume, mL	52 ± 7	58 ± 12*	12 ± 15	39 ± 6‡‡‡	58 ± 9***	49 ± 19‡‡‡
Heart rate, beats/min	80 ± 12	98 ± 34	23 ± 40	91 ± 16	80 ± 9*	−10 ± 17‡
Cardiac output, L/min	3.9 ± 1.0	3.0 ± 0.9*	−17 ± 30	3.4 ± 0.8	2.1 ± 0.4***	−37 ± 19
Wall thickening anteroseptal, %	48 ± 13	16 ± 12***	−32 ± 15	36 ± 9	23 ± 9***	−13 ± 7‡‡‡
Wall thickening remote, %	47 ± 15	52 ± 18	5 ± 16	38 ± 11	38 ± 13	1 ± 12
Infarct size, % LV		26 ± 11			8 ± 2‡‡‡	

Values are means ± SD for n animals. AMI, acute myocardial infarction; AVPD, atrioventricular plane displacement; LV, left ventricular; SV, stroke volume. *$P \leq 0.05$, **$P \leq 0.01$, ***$P \leq 0.001$ compared with baseline. ‡$P \leq 0.05$, ‡‡$P \leq 0.01$, ‡‡‡$P \leq 0.001$ compared with the Ischemia-Reperfusion group.

Table 4.1: Baseline and post-AMI data in Ischemia/Reperfusion and Microembolization groups.

(–17±30%; p<0.05) than the ME group (–37±19%; p<0.001) compared to baseline values. EF also decreased in both groups (I/R: –12±6% vs. ME: –18±6%; p=0.02). The more acute stress imposed on the heart in an I/R event than microembolization is a likely reason for the differing hemodynamic responses. This would explain the slight (but not statistically significant) increased wall thickening in remote regions in the I/R group and the opposite reactions in heart rate.

The I/R group showed a reduction in mean AVPD (–29±14%), anteroseptal AVPD ($AVPD_{antsep}$) (–32±15%), and remote AVPD ($AVPD_{remote}$) (–25±11%; all p<0.001). The ME group's AVPD reductions were not of the same magnitude: mean AVPD (–15±18%); $AVPD_{antsep}$ (–17±19%); $AVPD_{remote}$ (–16±17%; all p<0.05). In contrast, decreases in SV were similar for both groups (I/R: –33±13%; ME: –31±11%) (Figure 4.1). With the basal epicardial slices shifting in parallel with EDV, the percentage of longitudinal SV to total SV remained the same in the I/R group (0±10%; p=0.95) and increased slightly in the ME group (15±11%; p<0.001). Unlike ME infarcts, a stable longitudinal contribution of SV in I/R infarction agree with previous investigations [79].

Our findings that a global impact on ventricular longitudinal function from a regional injury corroborate earlier results from an investigation in patients (n=177) within a week after ST-elevation myocardial infarction (STEMI) [167]. An explanation for the global decrease is the anatomical factor. *Stoylen* stated that the rigid annulus fibrosus interconnecting all four AV-valves could prohibit regional differences in AVPD [279]. In addition, the interconnected and continuously branching network of myocytes and their helical architectural organization is another possible contributing factor.

A central result in this study was the close concordance between AVPD and SV during the initial week, where a decline with a nadir at 24 hours and a near-baseline recovery at seven days was seen (Figure 4.2). Moreover, the coupling between AVPD and SV was investigated at the individual level in regression analyses (Figure 4.3). The I/R group's re-

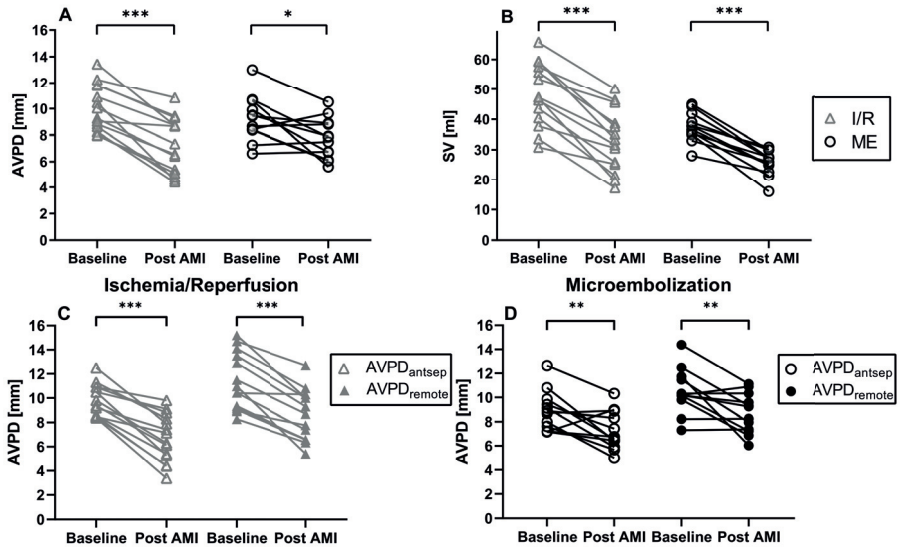

Figure 4.1: The Ischemia/Reperfusion (I/R) group displayed a larger decrease in atrioventricular plane displacement (AVPD) after acute myocardial infarction (AMI) (P<0.001) than the Microembolization (ME) group (P<0.05) (A), whereas SV decreased to a similar extent in both groups (P<0.001 for both; B). C & D: Both group displayed reduced AVPD for anteroseptal and remote regions.

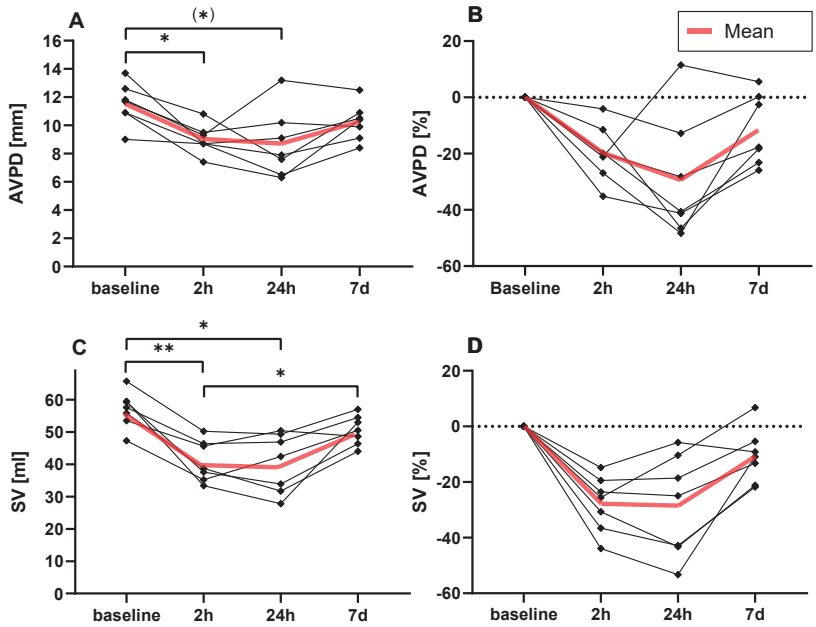

Figure 4.2: The chronological evolutions of atrioventricular plane displacement (AVPD) and stroke volume (SV) were investigated in a subset of animals in the Ischemia/Reperfusion group (n=7) during the first week. AVPD (A & B) and SV (C & D) show a similar initial decrease during the first day after ischemia, which recuperates to near-baseline values on day 7. (*)P=0.084, *P<0.05, **P<0.01.

gression slope ($0.65x + 13.6$) was steeper than the ME group ($0.39x + 24.9$) with similar regression coefficients ($r = 0.67 - 0.68$). This means that the connection is present in both groups, although slightly different mechanisms seem to be at play. The "patchy" microembolization infarcts have a greater initial decrease in SV regardless of AVPD reduction. They then carry a greater impact on longitudinal wall motion relative to each % decrease in SV than homogenous infarcts, where decreases are more equal between AVPD and SV throughout the spectrum.

Infarct sizes differed considerably between groups, and the I/R group had significantly larger infarct sizes measured with LGE (26±11% of left ventricular mass (LVM)) than the ME group (8±2% of LVM). There was a correlation between infarct size and AVPD reduction in the I/R group ($r = 0.53$; p=0.05), whereas none existed for the ME group ($r = 0.16$; p=0.61) (Figure 4.4). Interestingly, despite the slight variability in ME infarct sizes, wall motion, SV, and CO were significantly affected in both groups, again indicating that slightly different pathophysiological mechanisms are at play in the two types of AMIs.

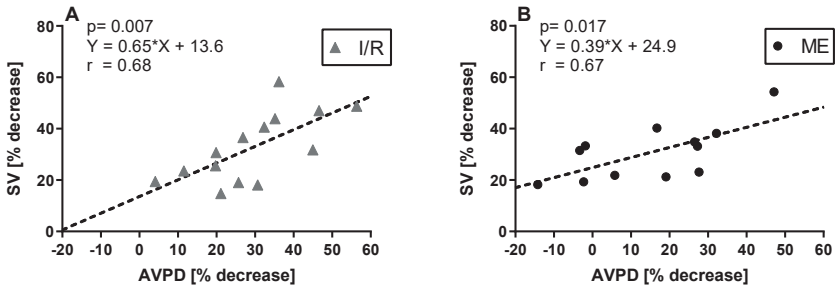

Figure 4.3: The relationship between the individual %−change in stroke volume (SV) and atrioventricular plane displacement (AVPD) before and after acute myocardial infarction in the Ischemia/Reperfusion (I/R) group (A) and the Microembolization (ME) group (B).

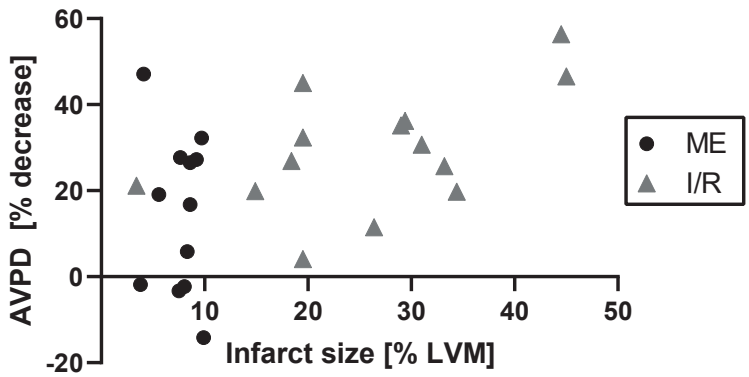

Figure 4.4: Percent decrease in atrioventricular plane displacement (AVPD) before and 2h after acute myocardial infarction plotted against infarct size in % of left ventricular mass (LVM) for the Ischemia/Reperfusion (I/R) and Microembolization (ME) groups. There is moderate evidence for the I/R group toward larger infarcts yielding larger decreases in AVPD ($r = 0.53$, P=0.05). How microembolization infarcts affected AVPD varied greatly, as shown by the large vertical spread with simultaneous small variance in infarct sizes.

The diastolic properties of ventricular longitudinal function were also assessed with reference to the diastasis [74, 78]. The early diastolic filling phase (Doppler E-wave), dependent on ventricular diastolic suction, is completed at diastasis. By extension, the first component of diastolic AVPD is dependent on restoring recoiling forces (E-wave AVPD). Thus, the subsequent atrial kick is responsible for the last longitudinal movement (A-wave AVPD). The results showed that E-wave AVPD, but not A-wave AVPD, is diminished after an AMI ($p<0.001$). This result is physiologically congruent, considering that the AMI only affects the ventricular myocardium, whereas the atrial myocardium is unaffected. Hence, the lesser ventricular systolic contraction is the cause of the decreased E-wave AVPD. These findings confirm the clinical observations by *Kranidis et. al.* [280].

In summary, *study I* investigated the link between ventricular longitudinal function, AVPD, and SV in an experimental AMI model. The results showed that SV adheres closely to changes in AVPD, both before and after AMI, in this experimental setting. This connection was persistent acutely and during the first week in I/R injuries and to a lesser and differing extent in ME injuries. Furthermore, AVPD was bludgeoned equally in remote myocardium as myocardial regions directly at risk from ischemia. Finally, after an AMI, the lesser systolic ventricular function could be deduced as decreased E-wave AVPD, while A-wave AVPD was preserved.

4.2 Study II

AMI is a severe but common event, and any improvement in cardioprotection could lead to massive cardiovascular health benefits for patients. Hypothermia is a possible therapeutic approach for reducing ischemic injuries associated with AMI. It is known that lowering the internal temperature reduces the enzymatic kinetics, i.e., the metabolic demands, of the heart and body [281] and limits damages from myocardial ischemia and reperfusion [117, 118]. Despite hypothermia's firm physiological basis, results from preclinical and clinical trials of therapeutic hypothermia have been ambiguous in realizing its potential cardioprotective effects [128, 130, 282]. With this in mind, our understanding of the protective effects of hypothermia remains incomplete due to prior studies lacking serial observations.

Previous studies have primarily focused on infarct quantification. Though the specific endpoint of infarction size is essential, a sole focus on infarction carries a risk of overlooking global effects on cardiac function. A PV loop framework is the gold standard for assessing cardiac performance, but the common invasive approach limits its clinical use. A non-invasive PV loop method, recently developed in-house, could therefore be of utility [272, 273]. Altogether, analyses of cardiac energy mechanics by non-invasive PV loops during hypothermia in I/R may add novel perspectives on the cardioprotective mechanisms involved.

Fourteen out of nineteen animals completed the full one-week study protocol and were included in the final analysis. Both groups, Hypothermia and Normothermia, consisted of seven animals, and non-invasive PV loops could be measured in all. The rapid (<5 min) cooling procedure reduced the internal temperature from 38°C at baseline to 34.5±0.5°C at reperfusion in the Hypothermia group ($p=0.002$), while the temperature was unchanged in the Normothermia group.

Though this study's protocol is similar to that by *Götberg et. al.* [123, 124, 131], which investigated the optimal timing of hypothermia and its effect on infarct size, we extended the protocol to four cardiac magnetic resonance (CMR) imaging sessions to assess the vicissitudes of cardiac function post-ischemia and their modulation by hypothermia. In our study, the infarct size (IS) and myocardiium at risk (MaR) were smaller in the Hypothermia group but not significantly (IS: 10±8% vs. 15±8%, $p=0.32$; MaR: 17±10% vs. 24±11%, $p=0.25$). The high variability in IS and MaR strongly contributed to the non-significant results. The previously mentioned studies reported significantly smaller infarcts [123, 124, 131], but we could only replicate these findings partially. This discrepancy could be attributed to lower blood pressures and heart rate (HR) at reperfusion than in prior experiments (mean arterial pressure (MAP): approximately 60 vs. 100 mmHg; HR: approximately 80 vs. 100 bpm). Increased pressure work and frequency during and after ischemia burdens the heart by increasing metabolic demand and instills more severe damages from ischemia. On a similar note, MaR was also smaller in the Hypothermia group. This finding could be due to chance. However, clinical and experimental data support that

Variables	Baseline		2h		24h		Day 7	
	Normothermia	Hypothermia	Normothermia	Hypothermia	Normothermia	Hypothermia	Normothermia	Hypothermia
EDV [ml]	110 ± 8.2	100 ± 10	110 ± 13	110 ± 14	110 ± 12	100 ± 13	110 ± 10	100 ± 8.5
ESV [ml]	55 ± 5.7	53 ± 5.4	61 ± 15	57 ± 8.2	63 ± 14	55 ± 7.9	56 ± 10	50 ± 7.4
SV [ml]	58 ± 5	52 ± 8	47 ± 10	51 ± 10	44 ± 9	49 ± 12	56 ± 8	53 ± 5
EF [%]	51 ± 3	50 ± 4	44 ± 9	47 ± 5	41 ± 9	47 ± 7	50 ± 7	51 ± 5
Cardiac Output [l/min]	4.7 ± 0.5	4.2 ± 0.6	3.7 ± 1.1	3.8 ± 0.9	3.2 ± 0.4	4.2 ± 1.0	5.2 ± 0.8	5.0 ± 0.5
Heart rate [bpm]	82 ± 9	81 ± 10	78 ± 21	75 ± 10	75 ± 9	86 ± 19	94 ± 9	96 ± 8
Infarct size T1-w [%LVM]							15 ± 8	10 ± 8
Myocardium at risk [%LVM]							24 ± 11	17 ± 10
Microvascular obstruction [%LVM]							2 ± 2	2 ± 3
Myocardial salvage [%]							41 ± 33	52 ± 26
MAP [mmHg]	63 ± 10	67 ± 6	61 ± 9	55 ± 6	57 ± 8	59 ± 5	58 ± 2	59 ± 6
Stroke work [J]	0.50 ± 0.11	0.49 ± 0.10	0.39 ± 0.12	0.39 ± 0.13	0.32 ± 0.13	0.38 ± 0.10	0.46 ± 0.08	0.42 ± 0.05
Potential Energy [J]	0.28 ± 0.05	0.30 ± 0.05	0.31 ± 0.08	0.27 ± 0.06	0.30 ± 0.05	0.27 ± 0.07	0.28 ± 0.05	0.24 ± 0.05
Efficiency [%]	64 ± 3	62 ± 5	55 ± 11	58 ± 7	51 ± 11	59 ± 8	62 ± 7	64 ± 5
External Power [W]	0.71 ± 0.16	0.69 ± 0.15	0.53 ± 0.20	0.51 ± 0.18	0.41 ± 0.11	0.56 ± 0.16	0.74 ± 0.12	0.70 ± 0.10
E_{MAX} [mmHg/ml]	1.3 ± 0.2	1.5 ± 0.2	1.2 ± 0.4	1.2 ± 0.2	1.1 ± 0.4	1.2 ± 0.1	1.3 ± 0.2	1.3 ± 0.2
E_A [mmHg/ml]	1.4 ± 0.1	1.8 ± 0.3	1.9 ± 0.4	1.5 ± 0.3	1.9 ± 0.3	1.7 ± 0.5	1.5 ± 0.3	1.5 ± 0.2
Ventricular-arterial Coupling	1.1 ± 0.1	1.2 ± 0.2	1.6 ± 0.7	1.3 ± 0.3	1.8 ± 0.6	1.4 ± 0.4	1.3 ± 0.4	1.1 ± 0.2

EDV: end-diastolic volume; ESV: end-systolic volume; SV: stroke volume; EF: ejection fraction; bpm: beats per minute; T1-w: T1-weighteded; LVM: left ventricular mass; MAP; mean arterial pressure; E_{MAX}: ventricular elastance (contractility); E_A: Arterial elastance.

Table 4.2

cardioprotective approaches, potent enough to reduce irreversible myocyte damage, also limit the extent of edema after I/R injury and thus measured MaR [204].

Table 4.2 shows the variables for each time point. As can be seen in Figure 4.5, the severity of ischemic injuries was attenuated in the Hypothermia group, as manifested in smaller reductions of volumetric variables such as stroke volume (SV: p=0.77), cardiac output (CO: p=0.037), and ejection fraction (EF: p=0.13) than the Normothermia group (SV: 0.029; CO: p<0.001; EF: p=0.068). Two variables with interesting responses were MAP and HR. MAP acutely decreased after rapid cooling (baseline−2 h: p<0.001; baseline−24h: p=0.19), whereas it was consistent for all measurements in normothermic animals. HR did not differ between groups (p=0.72) and increased on day seven. These findings also diverge from the previous reporting [123, 124, 131]. Blood pressure after induced hypothermia has been reported to be unchanged or increased [124], as well as transiently increased or reduced [283]. Differences in anesthetic depths could explain this variability as anesthesia depresses sympathetically mediated shivering and stimuli induced by hypothermia. In this study, reduced blood pressure in the acute phase could be one of the cardioprotective mechanisms adjuncts to hypothermia. Reduced pressure work and more preserved ventricular volumes would reduce the wall tension needed to sustain adequate cardiac output. Still, it is unclear from these results whether vasodilating drugs, e.g., Nitrates or Ca^{2+} chan-

nel blocking drugs, alone would yield similar preservations in cardiac function or if the protective effects are construed by other mechanisms inherent to hypothermia.

A typical example from each group is shown in Figure 4.6. PV loop-derived variables followed the same pattern as their volumetric counterparts. While both groups experienced a decrease and partial recovery pattern over the initial week, the adverse effects were generally truncated in the Hypothermia group (Figure 4.7). For example, peak reductions at 24 hours in stroke work (p=0.17), external power (p=0.01), and ventricular efficiency (p=0.13) tended to be smaller in the Hypothermia group than in the Normothermia group. Both groups experienced reduced contractility (Emax) post-AMI, but the accompanying afterload reduction (Ea) following the decreased MAP in the Hypothermia group led, in this case, to a preserved ventricular-arterial (VA) coupling of 1.4±0.4. In contrast, the Normothermia group experienced an afterload mismatch of 1.8±0.6.

The optimal VA coupling, that is, energy transfer between the ventricle and arterial tree without excessive changes in pressure, is ideally near 1 [58]. Typical ratios of Ea/Emax at rest are 0.6-1.2 in humans [61], felines [284], and canines [285]. Coupled with low contractility and high neurohormonal activity, severe afterload mismatch is present in systolic heart failure patients with VA coupling ranging between 1.3-4.3 [62] and reduced ventricular efficiencies. Our data infer a likeness of the Normothermia group to systolic heart failure (VA coupling: 1.8±0.6; efficiency: 51±11%), while the Hypothermia group saw a more preserved VA coupling (1.4±0.4) and efficiency (59±8%). As stated by previous studies [286, 287], the theoretical advantage of VA-coupling over LVEF lies in examining the individual components of Ea/Emax to discern if the hemodynamic alterations are due to properties of the left ventricle, arteries, or both. It has been demonstrated that the VA coupling is strongly predictive of adverse outcomes [288, 289]. Our results indicate that Hypothermia inflicted slightly decreased contractility while markedly reducing arterial elastance, converting to a preserved VA-coupling.

Regression analyses and analysis of covariance (ANCOVA) of the change in PV loop variables from baseline to 24 hours addressed whether the two groups' differences were present when adjusting for infarction sizes. In other words, if the differences were attributable to infarction sizes or influenced by the perturbation of hypothermia. The increase in EA and, to a borderline extent, decreased external power were significantly modulated by hypothermia (ANCOVA: p=0.015; p=0.061, respectively). Though statistical power was limited, the general trend in these analyses suggests that hypothermia had protective effects on cardiac energy and mechanics, incremental to reducing infarct size (Figure 4.8). This finding could be due to a superior contractile recovery in stunned myocardium subjected to hypothermia than normothermia; this would be supported by prior experimental studies [118].

In summary, this study of a hypothermia intervention in an experimental I/R model demonstrated a significant amelioration in cardiac impairment by rapid cooling (<35°C) at reperfusion compared to normothermia during the initial week. The results suggested

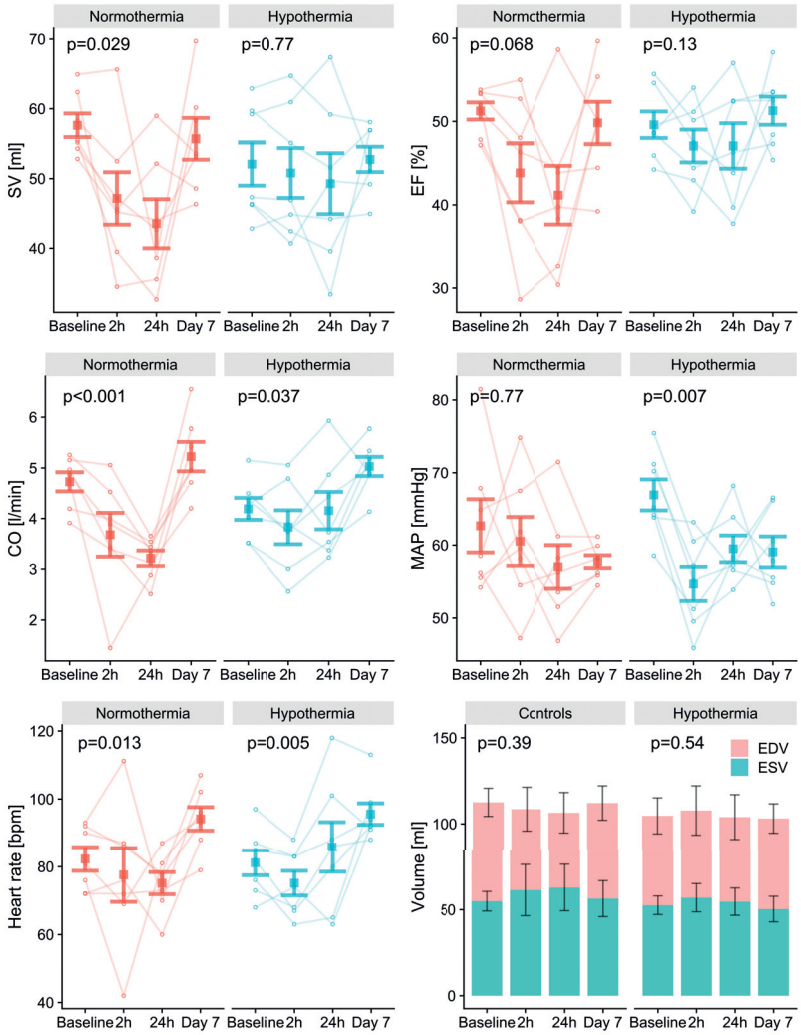

Figure 4.5: Error bar plots showing mean±standard error of the mean for stroke volume (SV), ejection fraction (EF), cardiac output (CO), mean arterial pressure (MAP), heart rate, end-diastolic volume (EDV), and end-systolic volume (ESV). The reductions in volumetric variables seen in the Normothermia group (N=7) were generally ameliorated in the Hypothermia group (N=7). MAP fell significantly in the Hypothermia group after the intervention of mild hypothermia. P values from Friedman's test compare results over four time points within each group.

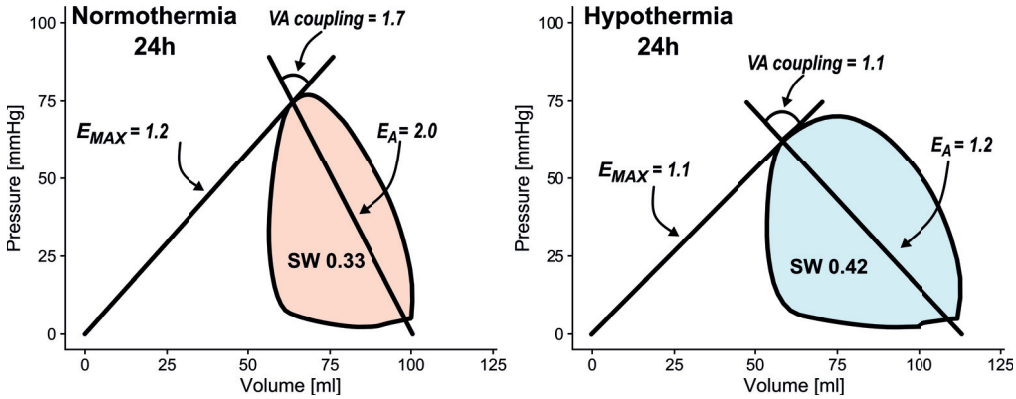

Figure 4.6: A typical example from each of the two groups, Normothermia and Hypothermia, at 24-hours after ischemia/reperfusion injury with larger ventricular-arterial(VA) decoupling in the Normothermia group compared to Hypothermia.

that hypothermia yielded favorable energy mechanics, such as higher efficiency and better matching between the ventricle and the arterial load than normothermia. Furthermore, the analyses indicated that hypothermia protected cardiac function incremental to reducing infarct size. In addition, non-invasive PV loops by CMR are clinically feasible and could help elucidate cardiovascular hemodynamic mechanisms in future studies.

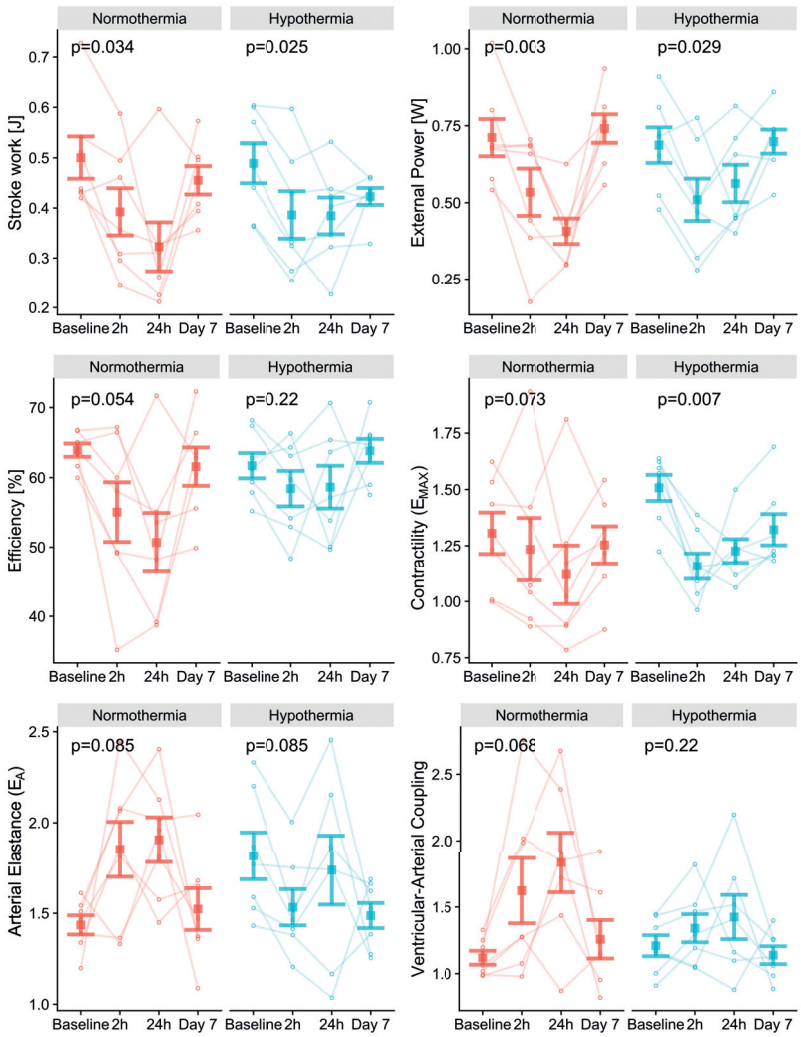

Figure 4.7: Error bar plots showing mean±standard error for stroke work, external power, efficiency, contractility (Emax), arterial elastance (Ea), and ventricular-arterial coupling. The adverse effects of ischemia/reperfusion injuries on PV loop-derived variables seen in the Normothermia group (N=7) were generally attenuated in the Hypothermia group (N=7). P values from Friedman's test compare results over four time points within each group.

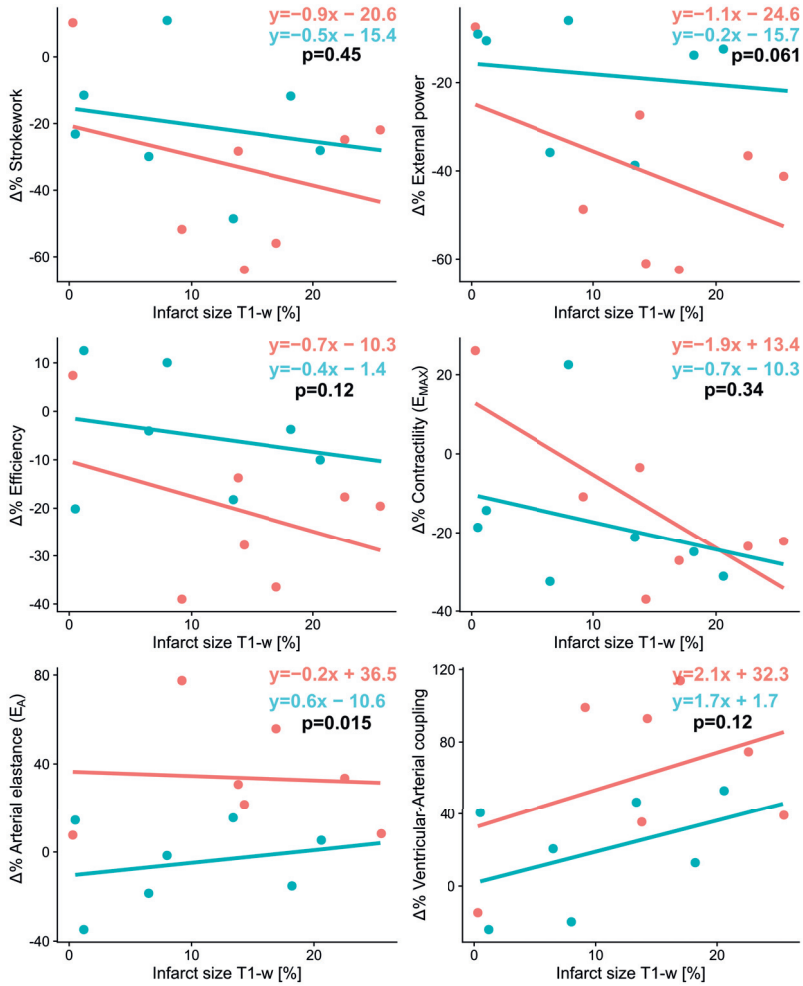

Figure 4.8: Regression analyses of the relative changes "Δ%" from baseline to 24-hours after ischemia/reperfusion with six pressure-volume (PV) loop derived measurements. If the regression lines differ in slope or offset between the Hypothermia group (N=7; *blue*) and Normothermia group (N=7; *red*), that means that hypothermia itself, in addition to the infarct size, modulates the observed results. There are slight trends in external power, efficiency, Emax, and ventricular-arterial coupling. This means that the intervention of mild hypothermia offsets and attenuates the adverse effects caused by ischemia/reperfusion. P values by the analysis of covariance tests if the relative reductions in PV loop variables between Hypothermia and Normothermia groups differ while adjusting for infarct size.

4.3 Study III

HFrEF is a severe disease, and patients experience symptoms such as shortness of breath and general fatigue. Their quality of life is often reduced [290], and HFrEF carries an excessive mortality risk comparable to many malignancies [291].

Preceding studies have found measurements of MAPSE, AVPD, and GLS to be of prognostic value in different patient populations [168, 170, 171, 184]. However, studies with a focal point on severely ill patient groups such as HFrEF are scarcer, albeit a few exist [181, 188]. Adding to this, many studies are needed to solidify the evidence base for any biomarkers before clinical or guideline implementations. For these reasons, a continued inquiry into the predictive capabilities of longitudinal ventricular function is relevant. Regarding cardiovascular (CV) and all-cause death, this study evaluates 1) AVPD and GLS as prognostic markers alone, 2) compared to established biomarkers, such as EF and LGE, and 3) the relative prognostic difference of using a single point or several averaged points for AVPD measurements.

Two hundred and ninety-five patients with HFrEF and a clinical CMR exam were considered for inclusion. Eight examinations resulted in poor image quality, resulting in 287 patients available for the final analysis (62±12 years; 78% men). All patient characteristics are found in Table 4.3. CV comorbidities and confounders included diabetes (present in 22%), hypertension (present in 30%), and smoking (present in 18%). The cause of heart failure was mainly ischemic (59%), and 47% had a functional status of New York Heart Association (NYHA) III. AVPD was higher in CV-death survivors than in non-survivors (8.0±2.4 vs. 6.4±2.0 mm, $p<0.001$). Likewise, GLS and EF were also higher in CV-death survivors than in non-survivors (–7.7±3.1 vs. –6.1±2.2%; 27.1±8.1 vs. 22.6±8.0%; both $p = 0.001$).

A large majority of patients received optimal medical treatment at the time of inclusion as >90% received Betablockers and RAAS antagonists, although only 52% received spironolactone; we did not have data on changes in prescribed medications that could impact mortality. Furthermore, newer drugs with documented survival benefits for HFrEF patients, such as SGLT2 [108] and neprilysin-inhibitor [106], were not recommended nor generally available during follow-up.

The study period was truncated to five years for the primary analysis since ventricular longitudinal shortening was expected to have less influence on prognosis beyond five years. A vast array of factors – comorbidities, lifestyle, medications, surgeries, accidents, etc. – can affect prognosis 10+ years after CMR. Regarding the 5-year follow-up, 40 CV deaths and 60 all-cause deaths occurred with median endpoint time ratios of 2.1 and 2.0, respectively. The median full follow-up time was 7.9 years (interquartile range 5.4-11.7 years), and 83 CV deaths and 134 deaths occurred with similar median endpoint time ratios.

We found that both AVPD and GLS were univariate predictors of CV death (AVPD: HR 1.30 [1.13-1.49]; GLS: HR 1.19 [1.07-1.33]) and all-cause death (AVPD: HR 1.21 [1.09-1.36]; GLS: 1.14 [1.04-1.25]). Other prominent significant risk factors for CV and

	Total	AVPD tertiles			GLS tertiles		
Characteristics	**n = 287**	**> 8.8 mm**	**6.8–8.8 mm**	**< 6.8 mm**	**< −8.4%**	**− (8.4–6.1) %**	**> −6.1%**
Age (years)	62 ± 12	63 ± 12	63 ± 12	59 ± 14	62 ± 12	63 ± 12	60 ± 14
BMI (kg/m^2)	27 ± 4	28 ± 5	27 ± 4	26 ± 5	27 ± 5	27 ± 4	27 ± 4
Male	225 (78)	67 (71)	73 (75)	85 (89)	63 (66)	76 (81)	82 (87)
ICM	168 (59)	51 (54)	63 (65)	54 (57)	51 (54)	61 (65)	53 (56)
Smoking	45 (18)	18 (22)	8 (9)	19 (22)	18 (21)	10 (12)	17 (20)
Hypertension	77 (30)	29 (34)	31 (35)	17 (20)	29 (33)	23 (27)	22 (26)
Diabetes	57 (22)	14 (17)	22 (24)	21 (24)	13 (15)	24 (28)	17 (20)
NYHA							
I	20 (9)	14 (20)	4 (6)	2 (3)	13 (17)	4 (6)	3 (4)
II	63 (29)	31 (44)	17 (24)	15 (20)	24 (32)	28 (41)	9 (13)
III	101 (47)	25 (35)	36 (51)	40 (53)	31 (41)	29 (42)	40 (59)
IV	32 (15)	1 (1)	13 (19)	18 (24)	8 (11)	8 (12)	16 (24)
Betablockers	241 (92)	75 (88)	83 (92)	83 (97)	80 (92)	78 (92)	80 (94)
RAAS antagonists	236 (90)	77 (91)	83 (92)	76 (88)	78 (90)	79 (93)	75 (88)
Spironolactone	133 (52)	36 (43)	48 (53)	49 (58)	41 (48)	39 (46)	51 (61)
eGFR (ml/min/1.73 m^2)	68 ± 20	71 ± 18	66 ± 21	69 ± 21	68 ± 20	69 ± 19	68 ± 22
NT-proBNP (ng/l), median (IQR)	1604 (695–3405)	596 (333–1501)	1730 (740–3008)	2531 (1416–5469)	737 (430–1697)	1728 (583–3417)	2531 (1416–5508)
LGE presence	220 (77)	69 (73)	75 (77)	76 (80)	67 (71)	77 (82)	72 (77)
EDV (ml)	300 ± 93	278 ± 75	292 ± 90	327 ± 106	261 ± 77	291 ± 74	348 ± 106
ESV (ml)	225 ± 88	193 ± 62	214 ± 82	269 ± 99	178 ± 62	216 ± 63	283 ± 101
SV (ml)	75 ± 22	87 ± 19	77 ± 19	61 ± 18	83 ± 21	76 ± 21	66 ± 20
CO (l/min)	4.7 ± 1.5	5.4 ± 1.4	4.7 ± 1.3	3.9 ± 1.6	5.1 ± 1.5	4.7 ± 1.2	4.1 ± 1.7
EDV index (ml/m^2)	150 ± 43	138 ± 32	148 ± 43	165 ± 50	131 ± 33	147 ± 36	174 ± 49
ESV index (ml/m^2)	113 ± 42	95 ± 27	109 ± 39	135 ± 47	89 ± 27	109 ± 31	142 ± 48
SV index (ml/m^2)	38 ± 10	43 ± 9	39 ± 9	31 ± 9	42 ± 9	38 ± 10	33 ± 10
CI (l/min/m^2)	2.4 ± 0.7	2.7 ± 0.7	2.4 ± 0.6	2.0 ± 0.8	2.6 ± 0.7	2.4 ± 0.6	2.1 ± 0.8
Left atrial volume (ml)	127 ± 45	122 ± 43	119 ± 42	140 ± 48	118 ± 48	122 ± 38	142 ± 46
EF (%)	27 ± 8	32 ± 6	28 ± 7	20 ± 6	33 ± 6	27 ± 6	20 ± 7
Mean AVPD (mm)	7.8 ± 2.4	10.4 ± 1.4	7.7 ± 0.6	5.1 ± 1.1	9.8 ± 1.9	7.9 ± 1.6	5.5 ± 1.6
GLS (%)	− 7.5 ± 3.0	− 10.0 ± 1.4	− 7.5 ± 1.9	− 5.1 ± 2.1	− 10.8 ± 2.1	− 7.2 ± 0.7	− 4.4 ± 1.4
TAPSE (mm)	18.5 ± 6.3	22.7 ± 5.0	18.3 ± 5.6	14.5 ± 5.5	20.5 ± 6.1	19.2 ± 6.1	15.5 ± 5.6

Baseline characteristics stratified by AVPD and GLS tertiles. Data are expressed as mean ± standard deviation or as absolute numbers and percentages in parentheses unless otherwise stated. *BMI* body mass index, *ICM* ischemic cardiomyopathy, *NYHA* New York Heart Association, *RAAS* renin–angiotensin–aldosterone-system, *IQR* inter-quartile range, *LGE* late gadolinium enhancement, *EDV* end-diastolic volume, *ESV* end-systolic volume, *SV* stroke volume, *CO* cardiac output, *CI* cardiac index, *EF* ejection fraction, *AVPD* atrioventricular plane displacement, *GLS* global longitudinal strain, *TAPSE* tricuspid annular plane systolic excursion.

Table 4.3

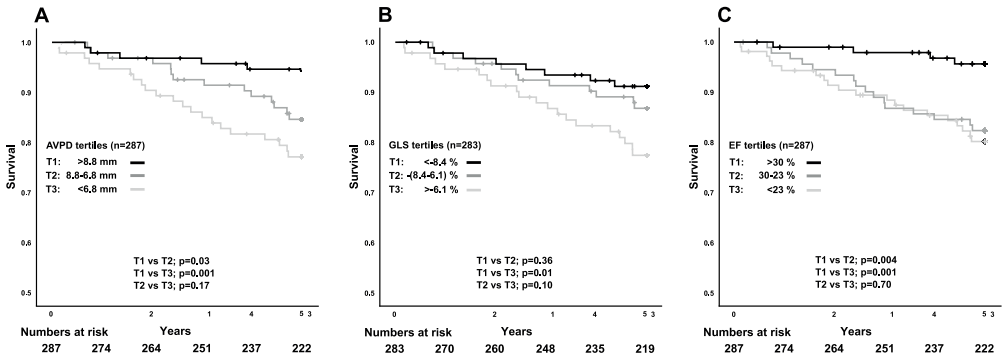

Figure 4.9: Kaplan–Meier curves showing survival from *cardiovascular death* stratified by tertiles for (A) atrioventricular plane displacement (AVPD), (B) global longitudinal strain (GLS) and (C) ejection fraction (EF) for the 5-year follow-up in panels. T1, upper tertile; T2, middle tertile; T3, lower tertile.

all-cause death, respectively, were age (HR 1.05 & 1.04), N-terminal pro-brain natriuretic peptide (NT-proBNP) (HR 1.17 & 1.17), etiology of HF (HR 2.59 & 2.26), LGE presence (2.89 & 2.43), diabetes (HR 2.39 & 3.05), EF (1.06 & 1.04), and TAPSE (HR 1.09 & 1.09).

Kaplan-Meier analyses of AVPD, GLS, and EF tertiles found decreasing survival probabilities with worsened longitudinal ventricular function and EF (Figure 4.9 & 4.10). Of note, the survival rates were the most uniformly separated with AVPD, indicating a slight predictive edge for AVPD over GLS and EF. The central results show that AVPD, unlike GLS, persisted as an independent predictor of CV death (33% increased mortality incidence per 1 mm decrease) when adjusting for a priori clinical risk factors (age, sex, body mass index (BMI), etiology of HF, LGE presence, EF, and EDVi). Both AVPD and GLS remained independent predictors of all-cause death when adjusting for the same confounders (AVPD: HR 1.24; GLS: HR 1.15) (Table 4.4). When considering the similar event distribution of AVPD and GLS, their interrelatedness, measurement variability, and sample size distinct discrimination between these variables' predictive values cannot be made with our study. Thus, we deem our results not to contradict GLS as a significant predictor of outcome in heart disease [170, 184, 185, 220, 292].

This study focuses on HFrEF patients, implying a low ventricular longitudinal function, a severely reduced systolic function, and excessive mortality. This means that the lion's share of systolic deterioration would already have occurred. Prior studies' results on ventricular longitudinal function include significant prognostic values in outpatients referred for clinical CMR [168], for patients with EF below 50% [171, 184], and patients with hypertension [172]. It is not evident that GLS or AVPD would have prognostic importance when the global function measured as EF is severely reduced. One of this study's main

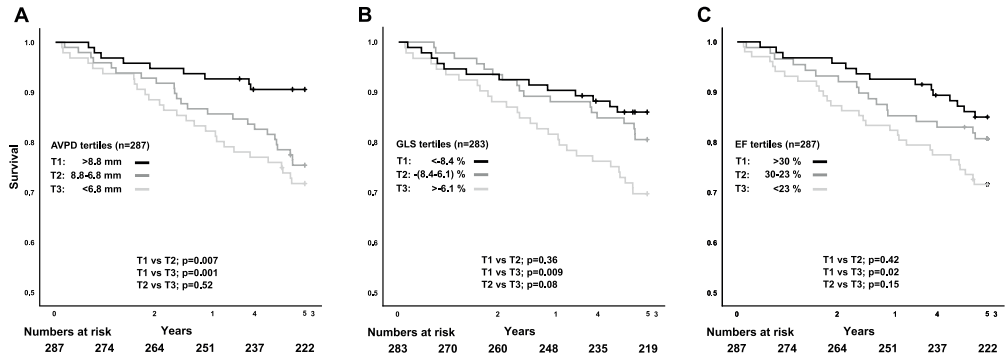

Figure 4.10: Kaplan–Meier curves showing survival from *all-cause death* stratified by tertiles for (A) atrioventricular plane displacement (AVPD), (B) global longitudinal strain (GLS) and (C) ejection fraction (EF) for the 5-year follow-up. T1, upper tertile; T2, middle tertile; T3, lower tertile.

findings is that ventricular longitudinal shortening retains its independent predictive value in this patient population.

Several factors could vary the degree of prognostic implication of ventricular longitudinal function variables. Three factors worth discussing include population characteristics, length of follow-up, and measurement location.

First, the intrinsic mortality risk in a study population determines the event rates and, consequently, the number of events needed for statistical analyses. Our 5-year total mortality of 21% was approximately 40% higher than the three studies from *Romano et. al.* [171, 172, 184]. In these three populations, mean EF ranged from 33 to 59% compared to our number of 26.5%, which likely explains differing mortality.

Second, a successful predictive biomarker can discern patients likely to survive longer. A longer follow-up carries more information and could aid in distinguishing prognostic information among homogenous groups with minor differences. However, longer follow-up times expose patients to an increasing number of confounding factors that are impossible to control sufficiently. In line with added information and confounding factors, we found a non-proportional hazard of AVPD during the extended follow-up period. This indicates that the influence of AVPD on mortality decreases with time. This was also seen in a Swedish HF population, which showed that AVPD predicted CV mortality in a time-dependent non-proportional fashion [293].

Third, we show that measurement location influences the hazard ratios. This can depend on methodological and pathophysiological reasons and is important to consider when comparing prognostic studies. Attention to the normal range of a variable, its reproducibility, reported increment, and what constitutes clinically significant changes are essential. Efforts to report dimensionless comparisons include increments of standard deviations, likelihood-derived or χ^2 values, but this might not aid interpretation. This study included

	Cardiovascular death		All-cause death	
Multivariate Cox regression 5-year follow-up	**HR (95% CI)**	**p value**	**HR (95% CI)**	**p value**
Model 1—AVPD (n = 287)	**LR test p < 0.001**		**LR test p < 0.001**	
Age, per 1 year	**1.06 (1.02–1.09)**	**0.001**	**1.04 (1.02–1.07)**	**< 0.001**
Sex, male	1.11 (0.44–2.77)	0.83[1]	1.36 (0.63–2.91)	0.44[4]
BMI, per 1 kg/m^2	0.96 (0.88–1.04)	0.29[4]	0.94 (0.88–1.01)	0.06[6]
Etiology, ICM	1.93 (0.86–4.37)	0.11[5]	0.63 (0.34–1.17)	0.15[5]
LGE presence	1.40 (0.43–4.56)	0.58[2]	1.34 (0.53–3.35)	0.54[3]
EF, per 1%	1.02 (0.96–1.09)	0.47[3]	1.00 (0.95–1.05)	1.00[1]
EDVi, per 10 ml/m^2	1.05 (0.98–1.13)	0.15[6]	1.01 (0.94–1.08)	0.78[2]
Mean AVPD, per 1 mm	**1.33 (1.16–1.53)**	**< 0.001**	**1.24 (1.11–1.39)**	**< 0.001**
Model 2—GLS (n = 283)	LR test p = 0.26 (GLS not significant)		**LR test p = 0.002**	
Age, per 1 year	**1.06 (1.03–1.10)**	**< 0.001**	**1.04 (1.02–1.07)**	**0.001**
Sex, male	0.95 (0.38–2.37)	0.91[1]	1.31 (0.61–2.84)	0.49[3]
BMI, per 1 kg/m^2	0.95 (0.88–1.03)	0.24[5]	0.94 (0.88–1.01)	0.08[6]
Etiology, ICM	1.87 (0.85–4.01)	0.12[6]	1.68 (0.89–3.17)	0.11[5]
LGE presence	1.49 (0.45–4.90)	0.52[3]	1.26 (0.49–3.24)	0.63[2]
EF, per 1%	**1.08 (1.04–1.13)**	**< 0.001**	1.02 (0.98–1.06)	0.28[4]
EDVi, per 10 ml/m^2	1.01 (0.93–1.10)	0.82[2]	0.99 (0.91–1.06)	0.72[1]
GLS, per 1%	1.07 (0.93–1.23)	0.37[4]	**1.15 (1.05–1.25)**	**0.003**

Multivariate modeling for death in HFrEF. Bold text indicates statistical significance. *HR* hazard ratio, *CI* confidence interval, *LR* likelihood ratio, *BMI* body mass index, *NYHA* New York Heart Association, *ICM* ischemic cardiomyopathy, *LGE* late gadolinium enhancement, *EF* ejection fraction, *EDVi* end-diastolic volume indexed to body surface area, *AVPD* atrioventricular plane displacement, *GLS* global longitudinal strain. Log-likelihood ratio (LR)-tests assess the added prognostic values compared with nested models without AVPD (Model 1) and GLS (Model 2). Numbers in superscript represents the last step before elimination for that variable.

Table 4.4

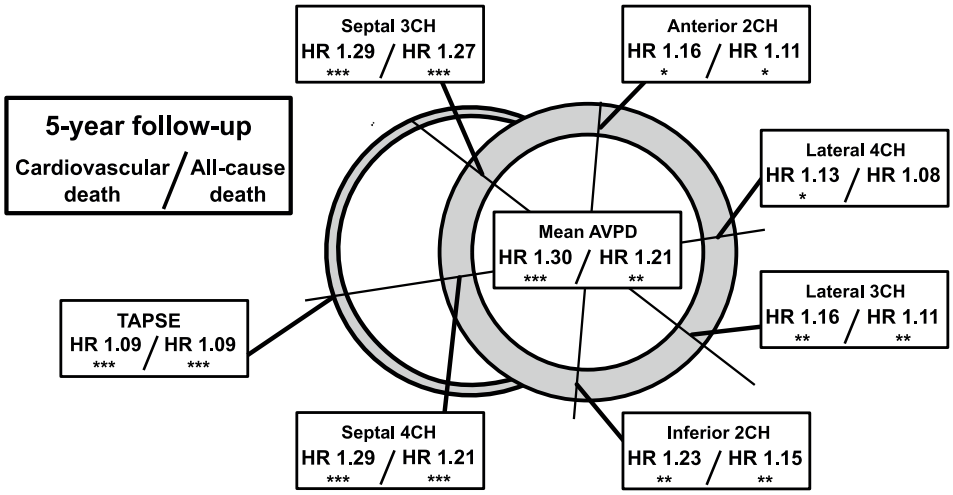

Figure 4.11: Prognostic values by measurement location. Univariate Cox regression analyses of the six different atrioventricular plane displacement (AVPD) locations. The short-axis slice illustrates hazard ratios (HR) for cardiovascular death and all-cause death at the 5-year follow-up for each location. Septal and average locations indicate higher HR values than lateral, anterior and inferior points. Asterisks represent *p<0.05, **p<0.01, ***p<0.001. TAPSE, tricuspid annular plane systolic excursion.

a relative comparison of each AVPD measurement location (Figure 4.11). Likely reasons for mean AVPD to yield the highest HR are minimizing variability by averaging multiple measurements and a stronger connection to longitudinal pumping mechanics and thus physiology.

Supplementary analyses were performed to isolate the impact of AVPD and GLS in either HF etiology. First, when adding etiology to age-adjusted models of AVPD and GLS in the total population, there are insubstantial changes in hazard ratios (Both AVPD and GLS: ΔHR 0.01). Next, when patients were separated into ischemic cardiomyopathy (ICM) and non-ischemic cardiomyopathy (NICM) groups, the number of subjects and events decreased significantly, such that the ICM-group had 31 CV deaths and the NICM-group nine CV deaths. Since statistical power here is limited, the multivariate analyses warrant cautious interpretation. AVPD and GLS were significantly predictive of CV mortality with similar HR values in the ICM-group and borderline to moderately significant in the NICM-group. A fact to account for is that the baseline hazard for ICM is considerably higher than for NICM etiology (5-year all-cause mortality of 27% vs. 13%). In essence, these findings comply with the primary analyses' results.

To summarize, this study shows that longitudinal ventricular shortening variables are prominent predictors of CV and all-cause mortality in patients with HFrEF independently

after adjusting for well-known clinical risk factors. Furthermore, the measurement location influences the predictive results. Mean AVPD achieved the highest hazard ratios indicating that it appears to be the most suitable variable for determining prognosis in HFrEF.

4.4 Study IV

Over 1 million hospitalizations annually have heart failure (HF) as the primary diagnosis in the United States, and around 2 million have HF as the secondary diagnosis [88]. Repeating hospitalizations increase the risk of mortality [294] but remain, unfortunately, fundamental parts of the typical and progressive trajectory for the HF patient. Continuous research efforts are warranted to increase pathophysiological understanding, improve detection of HF, better predict patients at highest risk, and develop efficacious therapies. In many studies on CV diseases, especially those focusing on HF, patients can repeatedly experience events of interest during the observational period. These events are referred to as reoccurring. Important to realize is that standard statistical methods mainly used today in the cardiovascular research domain, such as Kaplan-Meier and Cox proportional hazards (PH) regression analyses, focus on the first event and ignore data beyond this single event.

Patients with heart failure with a reduced ejection fraction (HFrEF) are at high risk for cardiac events and death and carry approximately 40% higher risk than other forms of HF [295]. We previously showed that ventricular longitudinal function could predict mortality in an HFrEF population (*study III* [187]). Just as mortality is essential, so is morbidity since its detrimental impact on patients' quality of life and wellbeing [290]. Therefore, this study aimed to assess the ability of the ventricular longitudinal function to predict HF-associated morbidity and mortality while considering several available events.

We identified 295 patients with HFrEF that underwent CMR. Eight patients lacked images with sufficient quality and were excluded, resulting in 287 for the final analysis. Four additional cases were excluded for GLS measurements resulting in 283 patients.

The mean age was 62 years; 78% were male; the mean left ventricular ejection fraction (EF) was 26.5%. Almost 60% of patients had ischemic heart failure as etiology of HF, and about half were in NYHA functional class III. Hypertension was present in 37%, diabetes in 23%, history of atrial fibrillation or flutter in 20% of the patients, a record of prior revascularization in 39%, AMI in 34%, or stroke in 5%. Medications included beta-blockers and RAAS inhibitors in 92% of patients (Table 4.5).

One hundred fifty-five (54%) patients experienced an adverse cardiovascular event. Of these patients, 110 (71%) had three or fewer events. The 5-year follow-up period comprised 578 events, and HF hospitalizations (n=418) were predominant. The other most common events were revascularizations (n=64), CV deaths (n=40), and MIs (n=21). The three first events accounted for 51% (n=295) of all events. Subjects in the lowest tertile of AVPD or GLS experienced more than three times as many events as subjects in the highest tertile (Figure 4.12). The bottom tertile also faced more CV deaths, HF hospitalizations, and myocardial infarctions. Consequently, they spent more time hospitalized from HF (AVPD: 19 vs. 8 days; GLS 19 vs. 5 days; $p=0.001$ for both) and overall (AVPD: 21 vs. 9 days; GLS: 22 vs. 7 days; $p=0.001$ for both).

Patients who experienced cardiovascular events vs. event-free patients had a higher degree of ischemic HF (an increase of 23%, $p<0.001$), and they were more likely to have

Baseline characteristics		No events (N = 132)	With events (N = 155)	P-value
Sex	Male	100 (76%)	125 (81%)	0.39
Age, years	Mean (SD)	61.4 (12.3)	61.9 (12.7)	0.77
Smoking (n = 255)	Yes	18 (15%)	27 (20%)	0.38
Aetiology of heart failure	ICM	61 (46%)	107 (69%)	<**0.001**
LGE presence	Yes	93 (71%)	127 (82%)	**0.03**
Hypertension	Yes	51 (39%)	54 (35%)	0.59
Diabetes	Yes	23 (17%)	43 (28%)	0.05
History of atrial fib. or flutter	Yes	23 (17%)	35 (23%)	0.35
NYHA class (n = 216)	NYHA I	10 (10%)	10 (9%)	0.26
	NYHA II	36 (35%)	27 (24%)	
	NYHA III	45 (44%)	56 (50%)	
	NYHA IV	12 (11%)	20 (17%)	
Prior stroke	Yes	6 (5%)	7 (5%)	0.99
Prior revascularization	Yes	49 (37%)	62 (40%)	0.71
Prior AMI	Yes	31 (24%)	66 (43%)	**0.001**
RAAS inhibitor (n = 261)	Yes	111 (92%)	125 (89%)	0.65
Beta-blocker (n = 261)	Yes	109 (90%)	132 (94%)	0.30
Aldosterone inhibitor (n = 258)	Yes	65 (54%)	68 (49%)	0.51
Diuretics (n = 261)	Yes	79 (65%)	93 (66%)	0.95
Device, ICD or CRT	Yes	81 (61%)	80 (52%)	0.12
NT-proBNP, ng/L (n = 170)	Median [IQR]	1010 [503–2200]	2210 [1180–4110]	0.13
eGFR, mL/min/1.73 m^2 (n = 254)	Mean (SD)	68.7 (18.4)	68.6 (22.0)	0.96
EDV index, mL/m^2	Mean (SD)	144 (44.0)	156 (42.4)	**0.02**
ESV index, mL/m^2	Mean (SD)	105 (41.4)	120 (41.8)	**0.004**
SV index, mL/m^2	Mean (SD)	38.7 (10.6)	36.9 (9.94)	0.15
Cardiac index, L/min/m^2	Mean (SD)	2.37 (0.85)	2.34 (0.64)	0.81
Ejection fraction, %	Mean (SD)	28.3 (7.78)	24.8 (7.93)	<**0.001**
GLS, % (n = 283)	Mean (SD)	−8.57 (3.25)	−6.60 (2.49)	<**0.001**
LV AVPD, mm	Mean (SD)	8.37 (2.55)	7.23 (2.20)	<**0.001**
LV s′, cm/s	Mean (SD)	−3.65 (1.01)	−3.30 (0.99)	**0.004**
LV e′, cm/s	Mean (SD)	3.73 (1.56)	3.42 (1.49)	0.09
LV a′, cm/s	Mean (SD)	3.46 (1.78)	3.23 (1.76)	0.27

Number of patients with available data are shown in parentheses, and bold numbers indicate statistical significance.
ICM, ischaemic cardiomyopathy; NICM, non-ischaemic cardiomyopathy; LGE, late gadolinium enhancement; NYHA, New York Heart Association; AMI, acute myocardial infarction; RAAS, renin angiotensin aldosterone system; ICD, implantable cardioverter-defibrillator; CRT, cardiac resynchronizing therapy; NT-proBNP, n-terminal pro brain natriuretic peptide; IQR, interquartile range; eGFR, estimated glomerular filtration rate; EDV, end-diastolic volume; ESV, end-systolic volume; SV, stroke volume; GLS, global longitudinal strain; LV, left-ventricular; AVPD, atrioventricular plane displacement.

Table 4.5

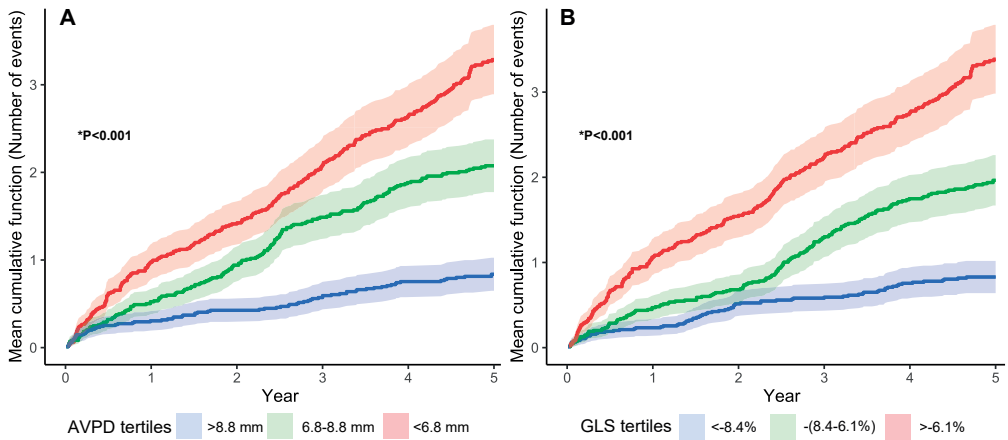

Figure 4.12: Mean cumulative function (MCF) of events by tertiles of (A) atrioventricular plane displacement (AVPD) and (B) global longitudinal strain (GLS). The horizontal axes show the time since the study entry and the vertical axes show the average number of events an individual had experienced during follow-up. Each colour displays the MCF and predicted confidence intervals for each tertile. On average, a patient in the lowest tertile of ventricular longitudinal function (*red*) had over 3 times as many events during follow up compared with the highest tertile (*blue*). *Two-sample pseudo-score test, variance estimator: Poisson.

Variables	HR	95% CI	Wald	*P*-value
LGE presence	1.56	1.14–2.13	7.82	0.005
Aetiology of heart failure, ICM	1.54	1.19–1.98	9.99	0.002
Sex, male	1.56	1.15–2.11	8.33	0.004
NYHA	1.33	1.12–1.57	11.14	0.001
Prior stroke	1.33	0.76–2.33	1	0.317
Prior revascularization	1.14	0.89–1.47	1.05	0.305
Atrial fib or flutter	1.23	0.92–1.65	1.95	0.162
Hypertension	0.92	0.71–1.19	0.38	0.538
Diabetes	1.37	1.04–1.79	5.1	0.024
Smoking	0.78	0.57–1.06	2.54	0.111
Hyponatremia, <135 mmol/L	1.88	1.34–2.65	13.15	<0.001
Age, 10 years	1.08	0.97–1.2	2.04	0.153
NT-proBNP, log (ng/L)	1.72	1.22–2.43	9.46	0.002
eGFR, mL/1.73m^2	0.98	0.91–1.05	0.42	0.517
LV EDV index, 10 mL/m^2	1.05	1.02–1.08	10.97	0.001
LV ESV index, 10 mL/m^2	1.06	1.03–1.09	14.19	<0.001
LV SV index, 10 mL/m^2	0.94	0.82–1.07	1.01	0.316
Cardiac index, L/min/m^2	0.97	0.75–1.26	0.05	0.821
Ejection fraction, 5%	1.18	1.1–1.27	19.07	<0.001
LV AVPD, mm	1.14	1.09–1.21	24.92	<0.001
GLS, %	1.14	1.1–1.19	38.54	<0.001
LV s′, cm/s	1.3	1.13–1.49	14.23	<0.001
LV e′, cm/s	0.86	0.79–0.95	9.84	0.002
LV a′, cm/s	0.9	0.84–0.97	7.64	0.006
BMI	0.98	0.96–1.01	1.54	0.215

LGE, late gadolinium enhancement; ICM, ischaemic cardiomyopathy; NYHA, New York Heart Association; NT-proBNP, N-terminal pro brain natriuretic peptide; eGFR, estimated glomerular filtration rate; LV, left-ventricular; EDV, end-diastolic volume; ESV, end-systolic volume; SV, stroke volume; GLS, global longitudinal strain; AVPD, atrioventricular plane displacement; BMI, body mass index.

Table 4.6: Univariate analysis according to Prentice, William & Peterson-total time—up to third event (295 events in total).

LGE presence (an increase of 11%, p=0.03). They had more often prior AMIs, larger left ventricles (increased LV ESV and EDV index), and worse systolic function (lower EF; LV s'; AVPD; higher GLS; p<0.004 for all).

The Prentice, William & Peterson-total time model was applied to the first three events in the primary analyses. The ventricular longitudinal variables, including AVPD (HR 1.14 per-mm-decrease), GLS (1.14 per-%-increase), and LV s' (1.3 per-cm/s-decrease), were the strongest univariate predictors of adverse cardiac events. EF (1.18 per-5%-decrease) was also a significant predictor. The other important univariate predictors were higher LV ESV and EDV index, hyponatremia (<135 mmol/L), higher NYHA classification, ischemic etiology, presence of LGE, higher levels of NT-proBNP, and male sex (Table 4.6).

In multivariate analyses, AVPD (HR 1.12 per-mm-decrease) and GLS (1.13 per-%-increase) retained their prognostic value in each model after variable selection, establishing their independence as relevant predictors for the combined endpoint of CV morbidity and mortality (Table 4.7). Other covariates included in the final models were hyponatremia, etiology of HF, and LV EDV index. Using AVPD and GLS in the final models yielded incremental predictive values compared with reduced models (likelihood ratio test: p<0.001 for both). However, only GLS managed to produce a significant discriminatory value by the concordant index (AVPD: 0.60 (CI95% 0.56-0.64) to 0.62 (CI95% 0.58-0.66); GLS: 0.58 (CI95% 0.54-0.62) to 0.63 (CI95% 0.59-0.67)) (Table 4.8).

The concordance index assesses the probability that a random pair from the sample has a concordant prediction, that is, the observation conforms to the forecast. The GLS

Variables	Multivariate stepwise			
	HR	95% CI	Wald	*P*-value
GLS				
LV GLS, %	1.13	1.09–1.18	32.96	<0.001
Hyponatremia, <135 mmol/L	1.8	1.28–2.53	11.59	0.001
Aetiology of heart failure, ICM	1.51	1.17–1.95	8.51	0.004
AVPD				
LV AVPD, mm	1.12	1.06–1.18	15.28	<0.001
Hyponatremia, <135 mmol/L	2.01	1.48–2.72	20.03	<0.001
Aetiology of heart failure, ICM	1.73	1.34–2.26	14.19	<0.001
LV EDV index, 10 mL/m^2	1.05	1.01–1.08	8.42	0.004

GLS, global longitudinal strain; ICM, ischaemic cardiomyopathy; AVPD, atrioventricular plane displacement; LV, left-ventricular; EDV, end-diastolic volume.

Table 4.7: Multivariate analysis according to Prentice, William & Peterson-total time (forward selection) – up to the third event

	Likelihood ratio test		Concordance index (95% CI)
	χ^2	*P*-value	
AVPD			
Model without AVPD	Reference	Reference	0.60 (0.56–0.64)
AVPD	16.83	<0.001	0.62 (0.58–0.66)
GLS			
Model without GLS	Reference	Reference	0.58 (0.54–0.62)
GLS	30.6	<0.001	0.63 (0.59–0.67)

AVPD, atrioventricular plane displacement; GLS, global longitudinal strain.

Table 4.8: Prentice, William & Peterson-total time – model fit – (forward selection) – up to the third event

model's 0.63 was the same as the average number found in a systematic review listing 117 HF models and 249 unique variables [296]. This review also lists sodium among frequently used variables with the highest predictive prognostic values, corroborating our results.

Because we only included people who had been referred to undergo CMR imaging, our study is subject to referral bias. Patients with atrial fibrillation, renal failure, and implanted devices are likely not included with the same proportion present in the general HF population. This could explain why these variables failed to predict events in our study.

GLS by echocardiography has prognostic value in patients with HFrEF [181, 188]. However, it is not established that adding GLS measured on an echocardiography examination to a GLS derived from CMR adds prognostic information beyond what can be obtained from a single modality. This is especially true when the echocardiography examination is of adequate quality. Unfortunately, inter-vendor and inter-modality differences exist, and reference values and thus distinctions of clinically significant values are needed for each combination [189]. Theoretically, it should be possible to assess GLS by either echocardiography or CMR at an index exam and proceed with a follow-up examination with any modality or vendor. Meanwhile, this study shows that the excursion of the basal portion of the ventricle as a proxy for global longitudinal function has a similar predictive ability as GLS for HF-associated morbidity, with good reproducibility and without needing specialized software.

To summarize, AVPD and GLS independently predicted the combined endpoint of cardiovascular mortality and heart failure-associated morbidity. Low AVPD and GLS were associated with a significantly impaired prognosis, such as an increased number of hospitalizations and days hospitalized due to cardiovascular causes. As AVPD and GLS reflect the global ventricular longitudinal function, this study corroborates previous research highlighting them as more relevant variables than LVEF to stratify patients with chronic HF and severe systolic dysfunction.

Chapter 5

Conclusions

The overall thesis aims to further the pathophysiological understanding of heart failure (HF) and acute myocardial infarction (AMI), ultimately providing beneficial insights to better identify, prognosticate, and treat patients with heart failure and myocardial infarction. Specific areas studied were ventricular longitudinal function, hypothermia, and Pressure-Volume (PV) loops.

The major conclusions from studies I-IV were:

I atrioventricular plane displacement (AVPD) is depressed after AMI and is linked to decreased stroke volume (SV). The coupling between decreased AVPD and SV is present in microembolization infarcts and likely to a greater degree in ischemia/reperfusion infarcts. Both AVPD and SV evolve in concordance during the first week after AMI. This study's findings shed light on the physiological significance of AVPD when assessing acute and subacute myocardial infarction.

II The protective effects of hypothermia at reperfusion are quantified by serial cardiac magnetic resonance (CMR) imaging from a perspective of cardiac energy and mechanics. This study suggests that blood flow restoration in ischemic myocardium at hypothermia has ameliorating effects on ventricular performance besides reducing infarct size. Additionally, non-invasive PV loops by CMR are feasible and could help elucidate cardiovascular hemodynamic mechanisms in future larger studies.

III Ventricular longitudinal shortening variables are predictors of cardiovascular and all-cause death in patients with heart failure with a reduced ejection fraction (HFrEF) and remain independently prognostic even after adjusting for well-known clinical risk factors. AVPD measured in the septum and mean AVPD demonstrated the highest hazard ratio indicating that measurement location influences the predictive

values. Measurements of AVPD are quick, do not require specialized software, and can be performed at one or several points. AVPD, therefore, appeared to be clinically more favorable than global longitudinal strain (GLS) for predicting mortality prognosis in HFrEF.

IV AVPD and GLS are independent predictors of cardiovascular morbidity and mortality. Furthermore, a low ventricular longitudinal function is associated with an increased number of events and extended in-hospital stay. We suggest that ventricular longitudinal function is valuable in HFrEF patients to predict cardiovascular mortality and morbidity outcome.

Chapter 6

Future Directions

Hopefully, this thesis will have broadened the perspectives of ventricular longitudinal function and non-invasive PV loops in health and disease. I have learned a great deal when writing this thesis, and I hope that this book can serve as a condensed guide aimed at future Ph.D. students when undertaking these subjects. There have also arisen several new thoughts and ideas during the writing process. Ideas not expanded upon in this section are often alluded to in the thesis itself, such as further exploring multi-event analyses in survival studies, extended validations of non-invasive with invasive PV loops in different disease conditions, and further studying therapeutic hypothermia with increased cooling or with an intracoronary approach. For conciseness, I will briefly discuss a few ideas, as I hope they might inspire some new thoughts in researchers and students alike.

6.1 Longitudinal Pumping and Mechanical Circulatory Support Devices

The requirement of additional alternatives for patients with end-stage heart failure is much needed. The number of new patients diagnosed with heart failure and patients who reach end-stage conditions increases [297]. While younger patients might be suitable for a curable heart transplant, the availability is poor due to a scarcity of organs. Recent advances in gene-modified xenotransplantation [298] could increase the supply of organs in the future, but the shortages of organs are not likely to pass. The first human receiving a gene-modified pig heart died two months after transplantation surgery, and a porcine cytomegalovirus infection was found to be a likely precipitant of the patient's death. The mean age for transplant recipients is 55 years. However, since most heart failure patients are in their 70s and above, a significant mismatch in supply and demand exists. This void is a suitable target for mechanical circulatory assist devices.

Today's most common indication for implanting a mechanical circulatory support device is when continuous use of intravenous inotropic support is needed [299]. Some heart

failure patients show progressive declines despite intravenous drug support. Some still progress to critical circulatory shock conditions. About 45% of implantations are left ventricular assist devices (LVADs), but only 1% are total artificial hearts (TAH) [300].

The current thesis has provided evidence that the atrioventricular plane displacement (AVPD) significantly contributes to the pumping capacity in normal and diseased states. Furthermore, the AVPD is substantially reduced and sometimes to the point of being eradicated in late-stage heart failure. In addition, AVPD is predictive of both mortality and morbidity. This information makes longitudinal pumping a valid target for mechanical assistance. Nevertheless, the critical question is whether an AVPD-augmenting device will improve cardiac pumping and ultimately reduce mortality and morbidity for patients.

The mimicry of cardiac longitudinal pumping has been the basis of a selected few mechanical circulatory support devices since the advent of the innovative ideas from the late *Stig Lundbäck* in the 1980s. At the beginning of the millennium, two Swedish cardiac support device companies, *Syntach AB* and *Scandinavian Real Heart AB*, began their enterprises. Both have clearly expressed that their foundations lay upon the importance of the AV plane and longitudinal pumping and could vanguard a new category of cardiac and circulatory support devices. Both companies explicitly aim to mimic the heart's longitudinal pumping and thereby provide an energy-efficient cardiac throughput while producing a physiologic pulsatile flow and minimizing the risk of blood clots and strokes. Both technologies differ considerably and should perhaps not be viewed as competitors. Syntach develops a fully implantable system that anchors to the mitral plane and augments the existing heart's longitudinal function. In contrast, Realheart develops a total artificial heart aiming to replace and substitute the diseased heart's function with the Realheart device. As I personally do not have any proprietary knowledge of the Realheart device, I am here oblivious to which considerable challenges remain.

A few exciting research questions pertaining to the Syntach device are:

- How will a long-term use impact the reverse remodeling of dilated hearts?
- Could an increased longitudinal pumping significantly improve the outcome for HFpEF patients with restrictive filling patterns, for which current assist device alternatives are awfully scarce?
- What are the assist's optimal timing, amplitude, and force?
- How is the myocardial stretch reflex, also known as stretch activation and its complementary phenomenon of shortening deactivation [301, 302], affected by externally forced longitudinal shortening?

In the coming years, we will learn if these companies, or still unknown ones, will be able to traverse the preclinical and clinical trials and acquire a significant market adoption to reach their goals of saving patients' lives.

6.2 Longitudinal Pumping in Valve Pathologies

Prior knowledge showed that the left ventricle has approximately 60% longitudinal contribution to stroke volume. This number varies between individuals – and even be above 100 percent when the lateral walls exhibit paradoxical wall motion. Valve insufficiencies can disturb the atrioventricular (AV) coupling and the natural energy-efficient pumping mechanism – in ways that are not fully elucidated yet. An experimental study investigating the alterations in longitudinal pumping prior, during, and after isolated pulmonary regurgitation found that a leaking pulmonary valve abated right ventricular longitudinal function [303]. There was simultaneously a compensatory right ventricular septal pumping. The left ventricle responded with increased longitudinal and reduced septal contributions to stroke volume. While there are clinical studies investigating longitudinal function in patients with mitral regurgitation [304, 305], there are no studies focused on the changes in longitudinal contribution to stroke volume in valve diseases. Investigative studies of the mechanistic alterations of longitudinal pumping in valve diseases would further our current understanding.

Mitral regurgitation (MR) can be caused by ventricular enlargement by annular dilatation and tethering to translocated papillary muscles. Patients with MR may exhibit escalated left ventricular dilatation, increased wall stress, and systolic and diastolic dysfunction despite a lack of overt symptoms. Left ventricular ejection fraction (EF) is currently used to make medical decisions relating to patients with MR. However, while EF represents the transition of volume between end-diastole and end-systole, it does not accurately characterize the intrinsic function of the heart muscle. Assessment of left-ventricular systolic function is further complicated because MR causes increased preload and decreased afterload, which may mask impaired LV function. After corrective surgery, however, patients with MR show a decrease in LV EF and global strain, reflecting altered loading conditions. LV FE and global strain often improve significantly in the long term [304].

Considering the previous section, the implication of valve insufficiencies for future mechanical assist devices aiming to augment ventricular longitudinal function is unknown. This is an essential question since MR is a common comorbidity in heart failure and future eligible patients receiving mechanical assist devices. These devices should likely seek to minimize valve insufficiencies to maintain the natural AV coupling. Speculatively, any regurgitant volume is equally deleterious for the operating mechanism of the device, such that, even with an excessive augmenting function, the valve insufficiency could increase to the same extent and neutralize the device's benefit.

6.3 Implementation of Ventricular Longitudinal Biomarkers into Clinical Routine

This thesis has brought up the theoretical and physiological basis and the current view of ventricular longitudinal function. One of the logical next steps is to explore the possibility

of implementing these measures into the clinical routine. GLS is more widely used and reported in clinical reports, especially in echocardiographic examinations. GLS has replaced the role of AVPD or MAPSE in clinical echocardiography exams partly because the reproducibility of MAPSE has been questioned. The variability of our reported AVPD and GLS measurements were low (AVPD: Intraclass correlation (ICC) 0.95-92, Coefficient of Variation (CoV) 10-13%; GLS: ICC 0.90, CoV: 19%). Still, the clinical significance of these small discrepancies could be impactful if integrated into the clinical routine. However, automated efforts could be an important key to unbiased results and broad adoption.

Artificial intelligence (AI) is being used at the forefront of medical imaging to advance our understanding of ventricular mechanics and accelerate the clinical use of cardiac MRI. This is good news. The fact that CMR AVPD measurements are becoming more automated means that they could be more reproducible and reliable in the future. A recently published study supports that using artificial intelligence to automate CMR measurements has higher reproducibility and prognostic value than manual CMR measurements [306]. Ultimately, this will help drive the clinical adoption of longitudinal ventricular function measurements. On a broader scale, compelling trends indicate that AI in CMR will become potent accessories for clinicians, researchers, and MRI physicists in developing novel methods of detecting, diagnosing, and imaging disease.

Large randomized clinical trials (RCTs) financed by pharmacologic industries are common for cardiovascular drugs. The impetus of positive trials showing safety and effectiveness leads to official adjudication and integration into guidelines. Large RCTs for imaging biomarkers are scarcer, especially for deciding on therapy. For instance, the recent ESC guidelines for diagnosing heart failure include but one prospective therapy-guiding RCT [307]. This compared GLS and EF for cardiotoxicity surveillance during cancer treatment and showed fewer patients developing cardiac dysfunction with GLS-surveillance. A glance at currently registered clinical trials reveals hundreds of studies mentioning strain. Only a handful are therapy-guiding and primarily for surveilling cardiotoxicity for cancer treatmentsvery few mention mitral annular plane systolic excursion (MAPSE). Trials with imaging biomarkers might pale compared to large heavy-hitting RCTs cardiologists are accustomed to. Still, RCTs of imaging-guided decisions, e.g., by titrating drug dosage, can have a meaningful impact and answer clinically relevant questions.

Finally, there has historically not been a stringent qualification process for imaging biomarkers. Although, my view is that this seems to have improved over the last few decades. Biomarkers need multiple studies showing them useable, accurate, precise, reproducible, and validated. This should advocate researchers to continually report reliability metrics when studying imaging biomarkers.

6.4 Non-Invasive Pressure-Volume Loops in Future Studies

Invasive Pressure-Volume (PV) loops constitute the “gold standard” of hemodynamic assessment [39]. Non-invasive PV algorithms by cardiac magnetic resonance (CMR), such

as the one employed in this thesis, provide similar information and could be employed without significant difficulty on standard clinical examinations. The echocardiographic single-beat method by *Chen et. al.* [308] has been used in several studies [287] but does not carry the volumetric precision of CMR. Nevertheless, non-invasive methods would allow more extensive studies to study pathophysiology on an epidemiological level, evaluate new therapies, or predict prognosis in a broader set of cardiac diseases such as hypertension, coronary artery disease, and heart failure. It would also be interesting to evaluate the non-invasive PV loop methods in valvular heart diseases, where regular filling and ejection patterns are disturbed.

Speculatively, as CMR can assess other physiological phenomena, there is potential to develop hybrid PV loop methods. For example, this could mean integration with regional strain to quantify regional work, similar to echo-based stress-strain loops [309, 310], with CMR elastography [311] for integration of myocardial stiffness, or with CMR-flow measurements to incorporating energy loss from valvular diseases.

In summary, the adoption of non-invasive PV loops is potentially in its embryonal stage, and future studies utilizing assessments of cardiac energetics and work in a wide range of cardiovascular diseases are warranted and welcomed.

Acknowledgements

Without the support and contribution of many people, the work of this thesis would not have been accomplished. I would like to send my deepest appreciation for the support you all have provided me throughout the years that I have been a Ph.D. student.

First of all, I would like to thank my supervisor **Marcus Carlsson** for continuous support. I'm always amazed at the wisdom you bring, and you have been the most important contributor to this thesis. You have been an inspiration, both as a person and a researcher.

My co-supervisor, **Håkan Arheden**. Thank you for all the valuable and thought-inspiring lessons and dialogues, from how to get things done to how to rise above stress and conflict. You have kindled a flame that I aim to sustain.

My co-supervisor, **Kristian Solem**. Thank you for all the exciting discussions about still unknown physiology that we stumbled upon in the lab. Thank you for being a great travel companion. Thank you for your input on my work from an outsider's and engineer's view.

My co-supervisor, **Einar Heiberg**. Thank you for being a great collaborator, a joy to be around, and doing cool stuff. Thank you for always coming up with solutions to all emerging technical or software problems.

Thank you **Robert Jablonowski** and **David Nordlund** for introducing me to the experimental group and for being great collaborators. To **Petter Frieberg**, for always listening and being present. **Jonas Liefke**, for being a great friend. To **Anthony Lindholm**, **Daniel Ryd**, **Per Arvidsson**, **Björn Östensson**, **Tom Gyllenhammar**, for exciting discussions and reflections. To **Sebastian Bidhult**, for taking your time to explain physics and CMR. To **Felicia Seeman**, for the great collaboration. To **Jane Tufvesson** for being helpful.

Thank you **all the rest of the Ph.D. students and researchers** in the Cardiac MR group for creating a wonderful research group.

A very special thanks to **David Nordlund**, **Robert Jablonowski**, **Per Arvidsson**, **Anthony Lindholm**, **Björn Östensson**, **Julius Åkesson**, for helping me improve my thesis summary.

I am sorry *(not sorry)* to all future Ph.D. students for writing such a long thesis…

Thank you for your support to all the rest of my colleagues in the Cardiac MR Group, the Department of Clinical Physiology, and collaborators in other departments.

To all my colleagues and friends at *Syntach*. Thank you **Jan Solem**, for sharing your ingenuity, expertise, wisdom, and many fascinating stories from your life as a cardiac surgeon. **Daniel Engvall**, for showing expert project management, always asking questions, and never giving up. **Victoria Kruger**, for your assistance in the lab, from all assistance during interventions and surgeries, persistent data management, and showing contagious discipline. **Gunnar Malmkvist**, for interesting discussions about physiology and allowing me to vex you with my questions. Thank you **André Spånberg**, **Martin Wolff**, **Lazar Milosovic**, **Andreas Arvidsson**, **David Karlsson**, **Christian Cedervall** for trying to teach me some engineering, electronics, math, chemistry, and for many thought-inspiring conversations, and for having a good time.

To my beloved wife **Lovisa** for always being my biggest supporter, enduring the sometimes very long workdays for the last years (especially the last weeks) and creating a beautiful family with me. To my lovely daughters **Agnes** and **Hedvig** for being everything I could wish for. To my parents, **Ulrika**, for always listening and providing a mother's advice, and my father, **Göran**, for being conscientious and witty and always supporting me. To my sister **Madeleine** with family, it's always a joy to spend time with you.

Bibliography

[1] E. A. Hoffman and E. L. Ritman. “Heart-lung interaction: Effect on regional lung air content and total heart volume”. In: *Annals of Biomedical Engineering* 15.3-4 (1987), pp. 241–257.

[2] E. A. Waters, A. W. Bowman, and S. J. Kovács. “MRI-determined left ventricular ”crescent effect”: A consequence of the slight deviation of contents of the pericardial sack from the constant-volume state”. In: *American Journal of Physiology - Heart and Circulatory Physiology* 288.2 57-2 (2005), pp. 848–853.

[3] S. Lundbäck. “Cardiac pumping and function of the ventricular septum”. eng. In: *Acta Physiologica Scandinavica. Supplementum* 550 (1986), pp. 1–101.

[4] V. Wykes and R. Vindlacheruvu. “Intracranial pressure, cerebral blood flow and brain oedema”. In: *Surgery (United Kingdom)* 33.8 (2015), pp. 355–362.

[5] R. A. Greenbaum, S. Y. Ho, D. G. Gibson, A. E. Becker, and R. H. Anderson. “Left ventricular fibre architecture in man”. In: *British Heart Journal* 45.3 (1981), pp. 248–263.

[6] A. F. Huxley and R. Niedergerke. “Structural changes in muscle during contraction”. In: *Nature* 4412.4412 (1954), pp. 971–973.

[7] H. HUXLEY and J. HANSON. “Changes in the cross-striations of muscle during contraction and stretch and their structural interpretation.” In: *Nature* 173.4412 (May 1954), pp. 973–6.

[8] H. L. Granzier and T. C. Irving. “Passive tension in cardiac muscle: contribution of collagen, titin, microtubules, and intermediate filaments”. In: *Biophysical Journal* 68.3 (1995), pp. 1027–1044.

[9] H. Granzier and S. Labeit. “Cardiac titin: An adjustable multi-functional spring”. In: *Journal of Physiology* 541.2 (2002), pp. 335–342.

[10] D. H. MacLennan and E. G. Kranias. “Phospholamban: A crucial regulator of cardiac contractility”. In: *Nature Reviews Molecular Cell Biology* 4.7 (2003), pp. 566–577.

[11] W. C. Hunter. “Role of myofilaments and calcium handling in left ventricular relaxation.” In: *Cardiology clinics* 18.3 (Aug. 2000), pp. 443–57.

[12] E. A. Sallin. “Fiber orientation and ejection fraction in the human left ventricle.” In: *Biophysical journal* 9.7 (1969), pp. 954–64.

[13] J. Cosín Aguilar. “Francisco Torrent-Guasp (1931-2005)”. In: *Revista Española de Cardiología (English Edition)* 58.6 (June 2005), pp. 759–760.

[14] D. H. MacIver, R. S. Stephenson, B. Jensen, P. Agger, D. Sánchez-Quintana, J. C. Jarvis, J. B. Partridge, and R. H. Anderson. “The end of the unique myocardial band: Part I. Anatomical considerations”. In: *European Journal of Cardio-thoracic Surgery* 53.1 (2018), pp. 112–119.

[15] D. H. MacIver, R. S. Stephenson, B. Jensen, P. Agger, D. Sánchez-Quintana, J. C. Jarvis, J. B. Partridge, and R. H. Anderson. “The end of the unique myocardial band: Part II clinical and functional considerations”. In: *European Journal of Cardio-thoracic Surgery* 53.1 (2018), pp. 112–119.

[16] L. Axel, V. J. Wedeen, and D. B. Ennis. “Probing dynamic myocardial microstructure with cardiac magnetic resonance diffusion tensor imaging”. In: *Journal of Cardiovascular Magnetic Resonance* 16.1 (2014), pp. 1–7.

[17] S. Nielles-Vallespin, A. Scott, P. Ferreira, Z. Khalique, D. Pennell, and D. Firmin. “Cardiac Diffusion: Technique and Practical Applications”. In: *Journal of Magnetic Resonance Imaging* 52.2 (Aug. 2020), pp. 348–368.

[18] P. J. Basser, J. Mattiello, and D. Lebihan. *Estimation of the Effective Self-Diffusion Tensor from the NMR Spin Echo*. 1994.

[19] P. Helm, M. F. Beg, M. I. Miller, and R. L. Winslow. “Measuring and mapping cardiac fiber and laminar architecture using diffusion tensor MR imaging”. In: *Annals of the New York Academy of Sciences* 1047 (2005), pp. 296–307.

[20] P. F. Ferreira et al. “In vivo cardiovascular magnetic resonance diffusion tensor imaging shows evidence of abnormal myocardial laminar orientations and mobility in hypertrophic cardiomyopathy”. In: *Journal of Cardiovascular Magnetic Resonance* 16.1 (2014), pp. 1–16.

[21] S. Nielles-Vallespin et al. “Assessment of Myocardial Microstructural Dynamics by In Vivo Diffusion Tensor Cardiac Magnetic Resonance.” eng. In: *Journal of the American College of Cardiology* 69.6 (Feb. 2017), pp. 661–676.

[22] D. D. Streeter, H. M. Spotnitz, D. P. Patel, J. Ross, and E. H. Sonnenblick. “Fiber orientation in the canine left ventricle during diastole and systole.” In: *Circulation research* 24.3 (1969), pp. 339–347.

[23] I. J. LeGrice, B. H. Smaill, L. Z. Chai, S. G. Edgar, J. B. Gavin, and P. J. Hunter. "Laminar structure of the heart: ventricular myocyte arrangement and connective tissue architecture in the dog." eng. In: *The American journal of physiology* 269.2 Pt 2 (Aug. 1995), pp. 571–82.

[24] K. D. Costa, Y. Takayama, A. D. McCulloch, and J. W. Covell. "Laminar fiber architecture and three-dimensional systolic mechanics in canine ventricular myocardium". In: *American Journal of Physiology - Heart and Circulatory Physiology* 276.2 45-2 (1999), pp. 595–607.

[25] H. Ashikaga, J. C. Criscione, J. H. Omens, J. W. Covell, and N. B. Ingels. "Transmural left ventricular mechanics underlying torsional recoil during relaxation". In: *American Journal of Physiology-Heart and Circulatory Physiology* 286.2 (Feb. 2004), H640–H647.

[26] S. H. Gilbert, D. Benoist, A. P. Benson, E. White, S. F. Tanner, A. V. Holden, H. Dobrzynski, O. Bernus, and A. Radjenovic. "Visualization and quantification of whole rat heart laminar structure using high-spatial resolution contrast-enhanced MRI". In: *American Journal of Physiology - Heart and Circulatory Physiology* 302.1 (2012), pp. 287–298.

[27] P. W. Hales, J. E. Schneider, R. A. Burton, B. J. Wright, C. Bollensdorff, and P. Kohl. "Histo-anatomical structure of the living isolated rat heart in two contraction states assessed by diffusion tensor MRI". In: *Progress in Biophysics and Molecular Biology* 110.2-3 (Oct. 2012), pp. 319–330.

[28] C. Mekkaoui et al. "Fiber architecture in remodeled myocardium revealed with a quantitative diffusion CMR tractography framework and histological validation". In: *Journal of Cardiovascular Magnetic Resonance* 14.1 (Dec. 2012), p. 70.

[29] E. X. Wu, Y. Wu, J. M. Nicholls, J. Wang, S. Liao, S. Zhu, C. P. Lau, and H. F. Tse. "MR diffusion tensor imaging study of postinfarct myocardium structural remodeling in a porcine model". In: *Magnetic Resonance in Medicine* 58.4 (2007), pp. 687–695.

[30] C. Mekkaoui, M. P. Jackowski, W. J. Kostis, C. T. Stoeck, A. Thiagalingam, T. G. Reese, V. Y. Reddy, J. N. Ruskin, S. Kozerke, and D. E. Sosnovik. "Myocardial scar delineation using diffusion tensor magnetic resonance tractography". In: *Journal of the American Heart Association* 7.3 (2018), pp. 1–10.

[31] M. R. Pfaller, J. M. Hörmann, M. Weigl, A. Nagler, R. Chabiniok, C. Bertoglio, and W. A. Wall. "The importance of the pericardium for cardiac biomechanics: from physiology to computational modeling". In: *Biomechanics and Modeling in Mechanobiology* 18.2 (2019), pp. 503–529.

[32] S. W. Ubbink, P. H. Bovendeerd, T. Delhaas, T. Arts, and F. N. van de Vosse. "Towards model-based analysis of cardiac MR tagging data: Relation between left ventricular shear strain and myofiber orientation". In: *Medical Image Analysis* 10.4 (2006), pp. 632–641.

[33] Z. Khalique, P. F. Ferreira, A. D. Scott, S. Nielles-Vallespin, D. N. Firmin, and D. J. Pennell. "Diffusion Tensor Cardiovascular Magnetic Resonance Imaging: A Clinical Perspective". In: *JACC: Cardiovascular Imaging* 13.5 (2020), pp. 1235–1255.

[34] G. Baroldi and G. Scomazzoni. *Coronary circulation in the normal and the pathologic heart*. Vol. 35. Office of the Surgeon General, Department of the Army, 1967.

[35] J. Reig and M. Petit. "Main trunk of the left coronary artery: anatomic study of the parameters of clinical interest." In: *Clinical anatomy (New York, N.Y.)* 17.1 (Jan. 2004), pp. 6–13.

[36] N. M. Malyar, M. Gössl, P. E. Beighley, and E. L. Ritman. "Relationship between arterial diameter and perfused tissue volume in myocardial microcirculation: a micro-CT-based analysis." In: *American journal of physiology. Heart and circulatory physiology* 286 (2004), H2386–H2392.

[37] V. Sequeira and J. van der Velden. "Historical perspective on heart function: the Frank–Starling Law". In: *Biophysical Reviews* 7.4 (Dec. 2015), pp. 421–447.

[38] C. S. Chung, M. Karamanoglu, and S. J. Kovács. "Duration of diastole and its phases as a function of heart rate during supine bicycle exercise". In: *American Journal of Physiology - Heart and Circulatory Physiology* 287.5 56-5 (2004), pp. 2003–2008.

[39] D. Burkhoff, I. Mirsky, and H. Suga. "Assessment of systolic and diastolic ventricular properties via pressure-volume analysis: A guide for clinical, translational, and basic researchers". In: *American Journal of Physiology - Heart and Circulatory Physiology* 289.2 58-2 (2005).

[40] G. Blaudszun and D. R. Morel. "Relevance of the volume-axis intercept, V0, compared with the slope of end-systolic pressure-volume relationship in response to large variations in inotropy and afterload in rats". In: *Experimental Physiology* 96.11 (2011), pp. 1179–1195.

[41] D. A. Kass, R. Beyar, E. Lankford, M. Heard, W. L. Maughan, and K. Sagawa. "Influence of contractile state on curvilinearity of in situ end-systolic pressure-volume relations". In: *Circulation* 79.1 (1989), pp. 167–178.

[42] D. Burkhoff, S. Sugiura, D. T. Yue, and K. Sagawa. "Contractility-dependent curvilinearity of end-systolic pressure-volume relations". In: *American Journal of Physiology-Heart and Circulatory Physiology* 252.6 (June 1987), H1218–H1227.

[43] M. A. Habigt, M. Krieger, J. Gesenhues, M. Ketelhut, M. Mechelinck, and M. Hein. "Non-linearity of end-systolic pressure–volume relation in afterload increases is caused by an overlay of shortening deactivation and the Frank–Starling mechanism". In: *Scientific Reports* 11.1 (2021), pp. 1–11.

[44] M. F. O'Rourke and M. G. Taylor. "Vascular Impedance of the Femoral Bed". In: *Circulation Research* 18.2 (1966), pp. 126–139.

[45] E. Ben-Assa et al. "Ventricular stroke work and vascular impedance refine the characterization of patients with aortic stenosis". In: *Science Translational Medicine* 11.509 (2019).

[46] W. L. Maughan, K. Sunagawa, D. Burkhoff, W. L. Graves, W. C. Hunter, and K. Sagawa. "Effect of heart rate on the canine end-systolic pressure-volume relationship". In: *Circulation* 72.3 (1985), pp. 654–659.

[47] S. Klotz, I. Hay, M. L. Dickstein, G. H. Yi, J. Wang, M. S. Maurer, D. A. Kass, and D. Burkhoff. "Single-beat estimation of end-diastolic pressure-volume relationship: A novel method with potential for noninvasive application". In: *American Journal of Physiology - Heart and Circulatory Physiology* 291.1 (2006), pp. 403–412.

[48] K. Sunagawa, W. L. Maughan, D. Burkhoff, and K. Sagawa. "Left ventricular interaction with arterial load studied in isolated canine ventricle". In: *American Journal of Physiology - Heart and Circulatory Physiology* 14.5 (1983).

[49] K. B. Campbell, R. D. Kirkpatrick, G. G. Knowlen, and J. A. Ringo. "Late-systolic pumping properties of the left ventricle. Deviation from elastance-resistance behavior". In: *Circulation Research* 66.1 (1990), pp. 218–233.

[50] W. C. Hunter. "End-systolic pressure as a balance between opposing effects of ejection". In: *Circulation Research* 64.2 (1989), pp. 265–275.

[51] D. Burkhoff, P. P. De Tombe, and W. C. Hunter. "Impact of ejection on magnitude and time course of ventricular pressure-generating capacity". In: *American Journal of Physiology-Heart and Circulatory Physiology* 265.3 (Sept. 1993), H899–H909.

[52] D. Burkhoff, P. P. De Tombe, W. C. Hunter, and D. A. Kass. "Contractile strength and mechanical efficiency of left ventricle are enhanced by physiological afterload". In: *American Journal of Physiology - Heart and Circulatory Physiology* 260.2 29-2 (1991).

[53] H. Suga. "Total mechanical energy of a ventricle model and cardiac oxygen consumption." In: *The American journal of physiology* 236.3 (1979).

[54] H. Suga, K. Sagawa, and A. A. Shoukas. "Load independence of the instantaneous pressure-volume ratio of the canine left ventricle and effects of epinephrine and heart rate on the ratio." In: *Circulation research* 32.3 (1973), pp. 314–322.

[55] H. Suga, T. Hayashi, and M. Shirahata. "Ventricular systolic pressure-volume area as predictor of cardiac oxygen consumption". In: *American Journal of Physiology-Heart and Circulatory Physiology* 240.1 (Jan. 1981), H39–H44.

[56] J. A. Chirinos. "Ventricular-arterial coupling: Invasive and non-invasive assessment". In: *Artery Research* 7.1 (2013), pp. 2–14.

[57] H. Suga. "Global cardiac function: Mechano-energetico-informatics". In: *Journal of Biomechanics* 36.5 (2003), pp. 713–720.

[58] P. P. De Tombe, S. Jones, D. Burkhoff, W. C. Hunter, and D. A. Kass. "Ventricular stroke work and efficiency both remain nearly optimal despite altered vascular loading". In: *American Journal of Physiology - Heart and Circulatory Physiology* 264.6 33-6 (1993).

[59] S. Sasayama and H. Asanoi. "Coupling between the heart and arterial system in heart failure." In: *The American journal of medicine* 90.5B (May 1991), 14S–18S.

[60] D. Burkhoff and K. Sagawa. "Ventricular efficiency predicted by an analytical model". In: *American Journal of Physiology - Regulatory Integrative and Comparative Physiology* 250.6 (19/6) (1986), pp. 1021–1027.

[61] M. R. Starling. "Left ventricular-arterial coupling relations in the normal human heart". In: *American Heart Journal* 125.6 (1993), pp. 1659–1666.

[62] H. Asanoi, S. Sasayama, and T. Kameyama. "Ventriculoarterial coupling in normal and failing heart in humans." In: *Circulation Research* 65.2 (Aug. 1989), pp. 483–493.

[63] B. A. Borlaug and D. A. Kass. "Ventricular-vascular interaction in heart failure." In: *Heart failure clinics* 4.1 (Jan. 2008), pp. 23–36.

[64] J. L. Robotham, M. Takata, M. Berman, and Y. Harasawa. "Ejection fraction revisited." In: *Anesthesiology* 74.1 (Jan. 1991), pp. 172–83.

[65] P. D. Chantler, E. G. Lakatta, and S. S. Najjar. "Arterial-ventricular coupling: Mechanistic insights into cardiovascular performance at rest and during exercise". In: *Journal of Applied Physiology* 105.4 (2008), pp. 1342–1351.

[66] B. Wandt. "Long-Axis Contraction of the Ventricles: A Modern Approach , but Described Already by Leonardo da Vinci". In: (2000), pp. 699–706.

[67] W. F. Hamilton and J. H. Rompf. "Movements of the base of the ventricle and the relative constancy of the cardiac volume". In: *American Journal of Physiology-Legacy Content* 102.3 (1932), pp. 559–565.

[68] A. Zaky, L. Grabhorn, and H. Feigenbaum. "Movement of the mitral ring: A study in ultrasoundcardiography". In: *Cardiovascular Research* 1.2 (1967), pp. 121–131.

[69] E. A. Hoffman and E. L. Ritman. "Invariant total heart volume in the intact thorax." eng. In: *The American journal of physiology* 249.4 Pt 2 (Oct. 1985), pp. 883–90.

[70] K. Steding-Ehrenborg, M. Carlsson, S. Stephensen, and H. Arheden. "Atrial aspiration from pulmonary and caval veins is caused by ventricular contraction and secures 70% of the total stroke volume independent of resting heart rate and heart size." In: *Clinical physiology and functional imaging* 33.3 (May 2013), pp. 233–40.

[71] M. Carlsson, P. Cain, C. Holmqvist, F. Stahlberg, S. Lundback, and H. Arheden. "Total heart volume variation throughout the cardiac cycle in humans". In: *AJP: Heart and Circulatory Physiology* 287.1 (Apr. 2004), H243–H250.

[72] M. Carlsson, M. Ugander, E. Heiberg, and H. Arheden. "The quantitative relationship between longitudinal and radial function in left, right, and total heart pumping in humans." In: *American journal of physiology. Heart and circulatory physiology* 293.1 (2007), pp. 636–44.

[73] M. Ugander, M. Carlsson, and H. Arheden. "Short-axis epicardial volume change is a measure of cardiac left ventricular short-axis function, which is independent of myocardial wall thickness". In: *American Journal of Physiology-Heart and Circulatory Physiology* 298.2 (Feb. 2010), H530–H535.

[74] A. W. Bowman and S. J. Kovács. "Assessment and consequences of the constant-volume attribute of the four-chambered heart." In: *American journal of physiology. Heart and circulatory physiology* 285.5 (Nov. 2003), pp. 2027–33.

[75] M. Carlsson, A. Rosengren, M. Ugander, U. Ekelund, P. A. Cain, and H. Arheden. "Center of volume and total heart volume variation in healthy subjects and patients before and after coronary bypass surgery". In: *Clinical Physiology and Functional Imaging* 25.4 (July 2005), pp. 226–233.

[76] A. W. Bowman and S. J. Kovács. "Left atrial conduit volume is generated by deviation from the constant-volume state of the left heart: A combined MRI-echocardiographic study". In: *American Journal of Physiology - Heart and Circulatory Physiology* 286.6 55-6 (2004), pp. 2416–2424.

[77] M. M. Riordan and S. J. Kovács. "Absence of diastolic mitral annular oscillations is a marker for relaxation-related diastolic dysfunction". In: *American Journal of Physiology - Heart and Circulatory Physiology* 292.6 (2007), pp. 2952–2958.

[78] W. Zhang, C. Chung, L. Shmuylovich, S. Kovacs, and M. Yildiz. "Is left ventricular volume during diastasis the real equilibrium volume, and what is its relationship to diastolic suction?" In: *Journal of applied physiology (Bethesda, Md. : 1985)* 105.3 (2008), 1018, author reply 1019.

[79] D. Asgeirsson, E. Hedström, J. Jögi, U. Pahlm, K. Steding-Ehrenborg, H. Engblom, H. Arheden, and M. Carlsson. "Longitudinal shortening remains the principal component of left ventricular pumping in patients with chronic myocardial infarction even when the absolute atrioventricular plane displacement is decreased." In: *BMC cardiovascular disorders* 17.1 (2017), p. 208.

[80] M. Carlsson, M. Ugander, H. Mosén, T. Buhre, and H. Arheden. "Atrioventricular plane displacement is the major contributor to left ventricular pumping in healthy adults, athletes, and patients with dilated cardiomyopathy." In: *American journal of physiology. Heart and circulatory physiology* 292.3 (Mar. 2007), pp. 1452–9.

[81] A. Støylen, H. E. Mølmen, and H. Dalen. "Relation between Mitral Annular Plane Systolic Excursion and Global longitudinal strain in normal subjects: The HUNT study". In: *Echocardiography* 35.5 (2018), pp. 603–610.

[82] B. Wandt, L. Bojö, and B. Wranne. "Influence of body size and age on mitral ring motion". In: *Clinical Physiology* 17.6 (1997), pp. 635–646.

[83] M. M. Ochs, T. Fritz, F. André, J. Riffel, D. Mereles, M. Müller-Hennessen, E. Giannitsis, H. A. Katus, M. G. Friedrich, and S. J. Buss. "A comprehensive analysis of cardiac valve plane displacement in healthy adults: age-stratified normal values by cardiac magnetic resonance". In: *International Journal of Cardiovascular Imaging* 33.5 (2017), pp. 721–729.

[84] A. Støylen, H. E. Mølmen, and H. Dalen. "Over all variability of mitral annular plane peak systolic velocity and peak global longitudinal strain rate in relation to age, body size, and sex: The HUNT Study". In: *Echocardiography* 37.4 (2020), pp. 578–585.

[85] T. M. Stokke, N. E. Hasselberg, M. K. Smedsrud, S. I. Sarvari, K. H. Haugaa, O. A. Smiseth, T. Edvardsen, and E. W. Remme. "Geometry as a Confounder When Assessing Ventricular Systolic Function: Comparison Between Ejection Fraction and Strain". In: *Journal of the American College of Cardiology* 70.8 (2017), pp. 942–954.

[86] G. Pedrizzetti, J. Mangual, and G. Tonti. "On the geometrical relationship between global longitudinal strain and ejection fraction in the evaluation of cardiac contraction". In: *Journal of Biomechanics* 47.3 (2014), pp. 746–749.

[87] A. Tower-Rader, D. Mohananey, A. To, H. M. Lever, Z. B. Popovic, and M. Y. Desai. "Prognostic Value of Global Longitudinal Strain in Hypertrophic Cardiomyopathy: A Systematic Review of Existing Literature". In: *JACC: Cardiovascular Imaging* 12.10 (2019), pp. 1930–1942.

[88] E. J. Benjamin et al. "Heart Disease and Stroke Statistics-2018 Update: A Report From the American Heart Association." In: *Circulation* 137.12 (Mar. 2018), e67–e492.

[89] P. Ponikowski et al. “2016 ESC Guidelines for the diagnosis and treatment of acute and chronic heart failure: The Task Force for the diagnosis and treatment of acute and chronic heart failure of the European Society of Cardiology (ESC). Developed with the special contribution ”. In: *European journal of heart failure* 18.8 (2016), pp. 891–975.

[90] R. W. Nesto and G. J. Kowalchuk. “The ischemic cascade: Temporal sequence of hemodynamic, electrocardiographic and symptomatic expressions of ischemia”. In: *The American Journal of Cardiology* 59.7 (1987).

[91] A. Maznyczka, S. Sen, C. Cook, and D. P. Francis. “The ischaemic constellation: an alternative to the ischaemic cascade—implications for the validation of new ischaemic tests”. In: *Open Heart* 2.1 (2015), e000178.

[92] E. Larose et al. “Predicting Late Myocardial Recovery and Outcomes in the Early Hours of ST-Segment Elevation Myocardial Infarction. Traditional Measures Compared With Microvascular Obstruction, Salvaged Myocardium, and Necrosis Characteristics by Cardiovascular Magnetic R”. In: *Journal of the American College of Cardiology* 55.22 (2010), pp. 2459–2469.

[93] E. Hedström, H. Engblom, F. Frogner, K. Ålström-Olsson, H. Öhlin, S. Jovinge, and H. Arheden. “Infarct evolution in man studied in patients with first-time coronary occlusion in comparison to different species - Implications for assessment of myocardial salvage”. In: *Journal of Cardiovascular Magnetic Resonance* 11.1 (2009), pp. 1–10.

[94] E. M. Antman et al. “2007 Focused Update of the ACC/AHA 2004 Guidelines for the Management of Patients With ST-Elevation Myocardial Infarction: a report of the American College of Cardiology/American Heart Association Task Force on Practice Guidelines: developed in collaborat”. In: *Circulation* 117.2 (Jan. 2008), pp. 296–329.

[95] M. Ugander, P. A. Cain, P. Johnsson, J. Palmer, and H. Arheden. “Chronic non-transmural infarction has a delayed recovery of function following revascularization”. In: *BMC Cardiovascular Disorders* 10 (2010).

[96] R. O. Bonow. “Identification of Viable Myocardium”. In: *Circulation* 94.11 (Dec. 1996), pp. 2674–2680.

[97] W. Wijns, S. F. Vatner, and P. G. Camici. “Hibernating Myocardium”. In: *New England Journal of Medicine* 339.3 (July 1998). Ed. by F. H. Epstein, pp. 173–181.

[98] G. Heusch, R. Schulz, and S. H. Rahimtoola. “Myocardial hibernation: a delicate balance”. In: *American Journal of Physiology-Heart and Circulatory Physiology* 288.3 (Mar. 2005), H984–H999.

[99] P. Woudstra, M. J. Grundeken, T. P. van de Hoef, L. Wallentin, K. A. Fox, R. J. de Winter, and P. Damman. "Prognostic relevance of PCI-related myocardial infarction." In: *Nature reviews. Cardiology* 10.4 (Apr. 2013), pp. 231–6.

[100] E. C. Keeley, J. A. Boura, and C. L. Grines. "Primary angioplasty versus intravenous thrombolytic therapy for acute myocardial infarction: A quantitative review of 23 randomised trials". In: *Lancet* 361.9351 (2003), pp. 13–20.

[101] T. A. McDonagh et al. "2021 ESC Guidelines for the diagnosis and treatment of acute and chronic heart failure". In: *European Heart Journal* 42.36 (2021), pp. 3599–3726.

[102] G. N. Levine et al. *2016 ACC/AHA Guideline Focused Update on Duration of Dual Antiplatelet Therapy in Patients with Coronary Artery Disease: A Report of the American College of Cardiology/American Heart Association Task Force on Clinical Practice Guidelines*. Vol. 134. 10. 2016, e123–e155.

[103] M. Packer, M. R. Bristow, J. N. Cohn, W. S. Colucci, M. B. Fowler, E. M. Gilbert, and N. H. Shusterman. "The Effect of Carvedilol on Morbidity and Mortality in Patients with Chronic Heart Failure". In: *New England Journal of Medicine* 334.21 (1996), pp. 1349–1355.

[104] B. Pitt, R. Segal, F. A. Martinez, G. Meurers, A. J. Cowley, I. Thomas, P. C. Deedwania, D. E. Ney, D. B. Snavely, and P. I. Chang. "Randomised trial of losartan versus captopril in patients over 65 with heart failure (Evaluation of Losartan in the Elderly Study, ELITE)". In: *Lancet* 349.9054 (1997), pp. 747–752.

[105] J. a. Cairns, S. J. Connolly, R. Roberts, and M. Gent. "Randomised trial of outcome after myocardial infarction in patients with frequent or repetitive ventricular premature depolarisations: CAMIAT. Canadian Amiodarone Myocardial Infarction Arrhythmia Trial Investigators." In: *Lancet (London, England)* 349.9053 (Mar. 1997), pp. 675–82.

[106] J. J. McMurray et al. "Angiotensin–Neprilysin Inhibition versus Enalapril in Heart Failure". In: *New England Journal of Medicine* 371.11 (Sept. 2014), pp. 993–1004.

[107] S. D. Solomon et al. "Angiotensin–Neprilysin Inhibition in Heart Failure with Preserved Ejection Fraction". In: *New England Journal of Medicine* 381.17 (2019), pp. 1609–1620.

[108] F. Zannad et al. "SGLT2 inhibitors in patients with heart failure with reduced ejection fraction: a meta-analysis of the EMPEROR-Reduced and DAPA-HF trials". In: *The Lancet* 396.10254 (2020), pp. 819–829.

[109] S. D. Anker et al. "Empagliflozin in Heart Failure with a Preserved Ejection Fraction". In: *New England Journal of Medicine* 385.16 (2021), pp. 1451–1461.

[110] F. Okamoto, B. S. Allen, and G. D. Buckberg. "Studies of controlled reperfusion after ischemia. XIV. Reperfusion conditions: Importance of ensuring gentle versus sudden reperfusion during relief of coronary occlusion". In: *Journal of Thoracic and Cardiovascular Surgery* 92.3 II (1986), pp. 613–620.

[111] Z. Q. Zhao, J. S. Corvera, M. E. Halkos, F. Kerendi, N. P. Wang, R. A. Guyton, and J. Vinten-Johansen. "Inhibition of myocardial injury by ischemic postconditioning during reperfusion: Comparison with ischemic preconditioning". In: *American Journal of Physiology - Heart and Circulatory Physiology* 285.2 54-2 (2003), pp. 579–588.

[112] D. Garcia-Dorado and H. M. Piper. "Postconditioning: reperfusion of "reperfusion injury" after hibernation." In: *Cardiovascular research* 69.1 (Jan. 2006), pp. 1–3.

[113] D. J. Hausenloy, H. E. Botker, T. Engstrom, D. Erlinge, G. Heusch, B. Ibanez, R. A. Kloner, M. Ovize, D. M. Yellon, and D. Garcia-Dorado. "Targeting reperfusion injury in patients with ST-segment elevation myocardial infarction: Trials and tribulations". In: *European Heart Journal* 38.13 (2017), pp. 935–941.

[114] D. M. Yellon and D. J. Hausenloy. "Myocardial Reperfusion Injury". In: *New England Journal of Medicine* 357.11 (Sept. 2007), pp. 1121–1135.

[115] T.-T. Cung et al. "Cyclosporine before PCI in Patients with Acute Myocardial Infarction". In: *New England Journal of Medicine* 373.11 (2015), pp. 1021–1031.

[116] A. P. Halestrap and P. Pasdois. "The role of the mitochondrial permeability transition pore in heart disease". In: *Biochimica et Biophysica Acta (BBA) - Bioenergetics* 1787.11 (2009), pp. 1402–1415.

[117] R. Tissier, M. Chenoune, B. Ghaleh, M. V. Cohen, J. M. Downey, and A. Berdeaux. "The small chill: Mild hypothermia for cardioprotection?" In: *Cardiovascular Research* 88.3 (2010), pp. 406–414.

[118] R. Tissier, B. Ghaleh, M. V. Cohen, J. M. Downey, and A. Berdeaux. "Myocardial protection with mild hypothermia". In: *Cardiovascular Research* 94.2 (2012), pp. 217–225.

[119] S. L. Hale, R. H. Dave, and R. A. Kloner. "Regional hypothermia reduces myocardial necrosis even when instituted after the onset of ischemia". In: *Basic Research in Cardiology* 92.5 (1997), pp. 351–357.

[120] L. M. Schwartz, S. G. Verbinski, R. S. Vander Heide, and K. A. Reimer. "Epicardial temperature is a major predictor of myocardial infarct size in dogs." eng. In: *Journal of molecular and cellular cardiology* 29.6 (June 1997), pp. 1577–1583.

[121] H. Hamamoto et al. "Very Mild Hypothermia During Ischemia and Reperfusion Improves Postinfarction Ventricular Remodeling". In: *Annals of Thoracic Surgery* 87.1 (2009), pp. 172–177.

[122] D. J. Duncker, C. L. Klassen, Y. Ishibashi, S. H. Herrlinger, T. J. Pavek, and R. J. Bache. "Effect of temperature on myocardial infarction in swine." eng. In: *The American journal of physiology* 270.4 Pt 2 (Apr. 1996), pp. 1189–99.

[123] M. Götberg, G. K. Olivecrona, H. Engblom, M. Ugander, J. van der Pals, E. Heiberg, H. Arheden, and D. Erlinge. "Rapid short-duration hypothermia with cold saline and endovascular cooling before reperfusion reduces microvascular obstruction and myocardial infarct size". In: *BMC Cardiovascular Disorders* 8 (2008), pp. 1–10.

[124] M. Götberg et al. "Optimal timing of hypothermia in relation to myocardial reperfusion". In: *Basic Research in Cardiology* 106.5 (2011), pp. 697–708.

[125] A. R. Panchal et al. *Part 3: Adult Basic and Advanced Life Support: 2020 American Heart Association Guidelines for Cardiopulmonary Resuscitation and Emergency Cardiovascular Care*. Vol. 142. 16 2. 2020, S366–S468.

[126] J. P. Nolan et al. "European Resuscitation Council and European Society of Intensive Care Medicine Guidelines 2021: Post-resuscitation care". In: *Resuscitation* 161 (2021), pp. 220–269.

[127] M. Hay, D. W. Thomas, J. L. Craighead, C. Economides, and J. Rosenthal. "Clinical development success rates for investigational drugs". In: *Nature Biotechnology* 32.1 (2014), pp. 40–51.

[128] P. A. Villablanca et al. "Therapeutic hypothermia in ST elevation myocardial infarction: A systematic review and meta-analysis of randomised control trials". In: *Heart* 102.9 (2016), pp. 712–719.

[129] I. S. Kang, I. Fumiaki, and W. B. Pyun. "Therapeutic hypothermia for cardioprotection in acute myocardial infarction". In: *Yonsei Medical Journal* 57.2 (2016), pp. 291–297.

[130] M. El Farissi et al. "Hypothermia for Cardioprotection in Patients with St-Elevation Myocardial Infarction: Do Not Give It the Cold Shoulder Yet!" In: *Journal of Clinical Medicine* 11.4 (2022), p. 1082.

[131] M. Götberg, G. K. Olivecrona, S. Koul, M. Carlsson, H. Engblom, M. Ugander, J. Van Der Pals, L. Algotsson, H. Arheden, and D. Erlinge. "A pilot study of rapid cooling by cold saline and endovascular cooling before reperfusion in patients with ST-elevation myocardial infarction". In: *Circulation: Cardiovascular Interventions* 3.5 (2010), pp. 400–407.

[132] D. Erlinge et al. "Rapid endovascular catheter core cooling combined with cold saline as an adjunct to percutaneous coronary intervention for the treatment of acute myocardial infarction: The CHILL-MI trial: A randomized controlled study of the use of central venous cathete". In: *Journal of the American College of Cardiology* 63.18 (2014), pp. 1857–1865.

[133] G. Nichol et al. “Prospective, Multicenter, Randomized, Controlled Pilot Trial of Peritoneal Hypothermia in Patients with ST-Segment - Elevation Myocardial Infarction”. In: *Circulation: Cardiovascular Interventions* 8.3 (2015), pp. 1–8.

[134] C. Testori, D. Beitzke, A. Mangold, F. Sterz, C. Loewe, C. Weiser, T. Scherz, H. Herkner, and I. Lang. “Out-of-hospital initiation of hypothermia in ST-segment elevation myocardial infarction: A randomised trial”. In: *Heart* 105.7 (2019), pp. 531–537.

[135] L. A. P. Dallan et al. “Cooling as an Adjunctive Therapy to Percutaneous Intervention in Acute Myocardial Infarction: COOL-MI InCor Trial”. In: *Therapeutic Hypothermia and Temperature Management* 11.3 (Sept. 2021), pp. 135–144.

[136] M. Noc et al. “A multicentre, prospective, randomised controlled trial to assess the safety and effectiveness of cooling as an adjunctive therapy to percutaneous intervention in patients with acute myocardial infarction: the COOL AMI EU Pivotal Trial.” eng. In: *EuroIntervention : journal of EuroPCR in collaboration with the Working Group on Interventional Cardiology of the European Society of Cardiology* 17.6 (Aug. 2021), pp. 466–473.

[137] D. Erlinge, M. Götberg, C. Grines, S. Dixon, K. Baran, D. Kandzari, and G. K. Olivecrona. “A pooled analysis of the effect of endovascular cooling on infarct size in patients with ST-elevation myocardial infarction”. eng. In: *EuroIntervention : journal of EuroPCR in collaboration with the Working Group on Interventional Cardiology of the European Society of Cardiology* 8.12 (2013), pp. 1435–1440.

[138] L. C. Otterspoor, L. X. van Nunen, T. T. Rosalina, M. van’t Veer, S. Van Tuijl, M. Stijnen, M. C. Rutten, F. N. van de Vosse, and N. H. Pijls. “Intracoronary hypothermia for acute myocardial infarction in the isolated beating pig heart”. In: *American Journal of Translational Research* 9.2 (2017), pp. 558–568.

[139] M. El Farissi et al. “Safety of Selective Intracoronary Hypothermia During Primary Percutaneous Coronary Intervention in Patients With Anterior STEMI.” In: *JACC. Cardiovascular interventions* 14.18 (2021), pp. 2047–2055.

[140] S. L. Jackson, X. Tong, R. J. King, F. Loustalot, Y. Hong, and M. D. Ritchey. “National Burden of Heart Failure Events in the United States, 2006 to 2014”. In: *Circulation. Heart failure* 11.12 (2018), e004873.

[141] A. L. Bui, T. B. Horwich, and G. C. Fonarow. “Epidemiology and risk profile of heart failure”. In: *Nature Reviews Cardiology* 8.1 (2011), pp. 30–41.

[142] M. Gheorghiade and A. Mebazaa. “Introduction to Acute Heart Failure Syndromes”. In: *The American Journal of Cardiology* 96.6 (Sept. 2005), pp. 1–4.

[143] W. J. Paulus and E. Dal Canto. “Distinct Myocardial Targets for Diabetes Therapy in Heart Failure With Preserved or Reduced Ejection Fraction”. In: *JACC: Heart Failure* 6.1 (2018), pp. 1–7.

[144] J. Tromp, M. A. Khan, I. T. Klip, S. Meyer, R. A. de Boer, T. Jaarsma, H. Hillege, D. J. van Veldhuisen, P. van der Meer, and A. A. Voors. "Biomarker profiles in heart failure patients with preserved and reduced ejection fraction". In: *Journal of the American Heart Association* 6.4 (2017).

[145] S. F. Mohammed, S. Hussain, S. A. Mirzoyev, W. D. Edwards, J. J. Maleszewski, and M. M. Redfield. "Coronary microvascular rarefaction and myocardial fibrosis in heart failure with preserved ejection fraction". In: *Circulation* 131.6 (2015), pp. 550–559.

[146] B. Bozkurt et al. "Universal Definition and Classification of Heart Failure". In: *Journal of Cardiac Failure* 27.4 (Apr. 2021), pp. 387–413.

[147] J. S. Forrester, G. Diamond, K. Chatterjee, and H. J. C. Swan. "Medical Therapy of Acute Myocardial Infarction by Application of Hemodynamic Subsets". In: *New England Journal of Medicine* 295.24 (Dec. 1976), pp. 1356–1362.

[148] E. J. Velazquez et al. "Coronary-Artery Bypass Surgery in Patients with Ischemic Cardiomyopathy". In: *New England Journal of Medicine* 374.16 (2016), pp. 1511–1520.

[149] S. Cazeau et al. "Effects of Multisite Biventricular Pacing in Patients with Heart Failure and Intraventricular Conduction Delay". In: *New England Journal of Medicine* 344.12 (Mar. 2001), pp. 873–880.

[150] S. J. Connolly et al. "Metal-analysis of the implantable cardioverter defibrillator secondary prevention trials". In: *European Heart Journal* 21.24 (2000), pp. 2071–2078.

[151] A. Vahanian and F. Beyersdorf. "2021 ESC/EACTS Guidelines for the management of valvular heart disease". In: *European Journal of Cardio-thoracic Surgery* 60.4 (2021), pp. 727–800.

[152] L. H. Lund et al. "The Registry of the International Society for Heart and Lung Transplantation: Thirtieth Official Adult Heart Transplant Report—2013; Focus Theme: Age". In: *The Journal of Heart and Lung Transplantation* 32.10 (Oct. 2013), pp. 951–964.

[153] E. V. Potapov et al. "2019 EACTS Expert Consensus on long-term mechanical circulatory support". In: *European Journal of Cardio-thoracic Surgery* 56.2 (2019), pp. 230–270.

[154] M. Y. Henein and D. G. Gibson. "Long axis function in disease". In: *Heart* 81.3 (1999), pp. 229–231.

[155] C. Höglund, M. Alam, and C. Thorstrand. "Effects of acute myocardial infarction on the displacement of the atrioventricular plane: an echocardiographic study". In: *Journal of Internal Medicine* 226.4 (1989), pp. 251–256.

[156] M. Alam. "The atrioventricular plane displacement as a means of evaluating left ventricular systolic function in acute myocardial infarction". In: *Clin Cardiol* 14.7 (1991), pp. 588–594.

[157] M. Alam and C. Höglund. "Serial echocardiographic studies following thrombolytic treatment in myocardial infarction with special reference to the atrioventricular valve plane displacement". In: *Clinical Cardiology* 15.1 (1992), pp. 30–36.

[158] M. Alam, C. Höglund, C. Thorstrand, and C. Hellekant. "Haemodynamic significance of the atrioventricular plane displacement in patients with coronary artery disease." In: *European heart journal* 13.2 (Feb. 1992), pp. 194–200.

[159] M. Alam, C. Höglund, C. Thorstrand, and A. Philip. "Atrioventricular plane displacement in severe congestive heart failure following dilated cardiomyopathy or myocardial infarction." In: *Journal of internal medicine* 228.6 (Dec. 1990), pp. 569–75.

[160] R. Willenheimer, B. Israelsson, C. Cline, E. Rydberg, K. Broms, and L. Erhardt. "Left atrioventricular plane displacement is related to both systolic and diastolic left ventricular performance in patients with chronic heart failure." In: *European heart journal* 20.8 (Apr. 1999), pp. 612–8.

[161] E. Rydberg, P. Gudmundsson, L. Kennedy, L. Erhardt, and R. Willenheimer. "Left atrioventricular plane displacement but not left ventricular ejection fraction is influenced by the degree of aortic stenosis". In: *Heart* 90.10 (2004), pp. 1151–1155.

[162] R. Willenheimer, C. Cline, L. Erhardt, and B. Israelsson. "Left ventricular atrioventricular plane displacement: An echocardiographic technique for rapid assessment of prognosis in heart failure". In: *Heart* 78.3 (1997), pp. 230–236.

[163] B. Brand, E. Rydberg, G. Ericsson, P. Gudmundsson, and R. Willenheimer. "Prognostication and risk stratification by assessment of left atrioventricular plane displacement in patients with myocardial infarction". In: *International Journal of Cardiology* 83.1 (2002), pp. 35–41.

[164] E. Rydberg, M. Arlbrandt, P. Gudmundsson, L. Erhardt, and R. Willenheimer. "Left atrioventricular plane displacement predicts cardiac mortality in patients with chronic atrial fibrillation". In: *International Journal of Cardiology* 91.1 (2003), pp. 1–7.

[165] E. Rydberg, L. Erhardt, B. Brand, and R. Willenheimer. "Left atrioventricular plane displacement determined by echocardiography: A clinically useful, independent predictor of mortality in patients with stable coronary artery disease". In: *Journal of Internal Medicine* 254.5 (2003), pp. 479–485.

[166] J. Berg, R. Jablonowski, D. Nordlund, S. Kopic, S. Bidhult, C. G. Xanthis, M. Saeed, K. Solem, H. Arheden, and M. Carlsson. "Decreased atrioventricular plane displacement after acute myocardial infarction yields a concomitant decrease in stroke volume". In: *Journal of Applied Physiology* 128.2 (Feb. 2020), pp. 252–263.

[167] U. Pahlm et al. "Longitudinal left ventricular function is globally depressed within a week of STEMI." In: *Clinical physiology and functional imaging* (2018), pp. 1–9.

[168] V. Rangarajan, S. J. Chacko, S. Romano, J. Jue, N. Jariwala, J. Chung, and A. Farzaneh-Far. "Left ventricular long axis function assessed during cine cardiovascular magnetic resonance is an independent predictor of adverse cardiac events". In: *Journal of Cardiovascular Magnetic Resonance* 18.1 (Dec. 2016), p. 35.

[169] A. Mayr et al. "Mitral annular plane systolic excursion by cardiac MR is an easy tool for optimized prognosis assessment in ST-elevation myocardial infarction". In: *European Radiology* 30.1 (2020), pp. 620–629.

[170] M. Holzknecht et al. "Global longitudinal strain improves risk assessment after ST-segment elevation myocardial infarction: a comparative prognostic evaluation of left ventricular functional parameters". In: *Clinical Research in Cardiology* 0123456789 (2021).

[171] S. Romano, R. M. Judd, R. J. Kim, H. W. Kim, I. Klem, J. F. Heitner, D. J. Shah, J. Jue, and A. Farzaneh-Far. "Left Ventricular Long-Axis Function Assessed with Cardiac Cine MR Imaging is an Independent Predictor of All-Cause Mortality in Patients with Reduced Ejection Fraction: A Multicenter Study". In: *Radiology* 286.2 (Sept. 2017), p. 170529.

[172] S. Romano et al. "Prognostic Implications of Mitral Annular Plane Systolic Excursion in Patients with Hypertension and a Clinical Indication for Cardiac Magnetic Resonance Imaging". In: *JACC: Cardiovascular Imaging* 12.9 (Sept. 2019), pp. 1769–1779.

[173] O. Gjesdal et al. "Reduced long axis strain is associated with heart failure and cardiovascular events in the multi-ethnic study of Atherosclerosis". In: *Journal of Magnetic Resonance Imaging* 44.1 (2016), pp. 178–185.

[174] M. B. Harbo, E. S. Nordén, J. Narula, I. Sjaastad, and E. K. S. Espe. "Quantifying left ventricular function in heart failure: What makes a clinically valuable parameter?" In: *Progress in Cardiovascular Diseases* 63.5 (2020), pp. 552–560.

[175] E. Kraigher-Krainer et al. "Impaired systolic function by strain imaging in heart failure with preserved ejection fraction". In: *Journal of the American College of Cardiology* 63.5 (2014), pp. 447–456.

[176] K. Kalam, P. Otahal, and T. H. Marwick. "Prognostic implications of global LV dysfunction: a systematic review and meta-analysis of global longitudinal strain and ejection fraction." In: *Heart (British Cardiac Society)* 100.21 (Nov. 2014), pp. 1673–80.

[177] N. E. Hasselberg, K. H. Haugaa, S. I. Sarvari, L. Gullestad, A. K. Andreassen, O. A. Smiseth, and T. Edvardsen. "Left ventricular global longitudinal strain is associated with exercise capacity in failing hearts with preserved and reduced ejection fraction". In: *European Heart Journal - Cardiovascular Imaging* 16.2 (Feb. 2015), pp. 217–224.

[178] G. Korosoglou et al. "Fast Strain-Encoded Cardiac Magnetic Resonance for Diagnostic Classification and Risk Stratification of Heart Failure Patients". In: *JACC: Cardiovascular Imaging* 14.6 (2021), pp. 1177–1188.

[179] S. Romano, I. N. Mansour, M. Kansal, H. Gheith, Z. Dowdy, C. A. Dickens, C. Buto-Colletti, J. M. Chae, H. H. Saleh, and T. D. Stamos. "Left Ventricular global longitudinal strain predicts heart failure readmission in acute decompensated heart failure". In: *Cardiovascular Ultrasound* 15.1 (2017), pp. 1–6.

[180] J. Berg, J. Åkesson, R. Jablonowski, K. Solem, E. Heiberg, R. Borgquist, H. Arheden, and M. Carlsson. "Ventricular longitudinal function by cardiovascular magnetic resonance predicts cardiovascular morbidity in HFrEF patients". In: *ESC Heart Failure* March (Apr. 2022).

[181] A. Mignot, E. Donal, A. Zaroui, P. Reant, A. Salem, C. Hamon, S. Monzy, R. Roudaut, G. Habib, and S. Lafitte. "Global longitudinal strain as a major predictor of cardiac events in patients with depressed left ventricular function: A multicenter study". In: *Journal of the American Society of Echocardiography* 23.10 (2010), pp. 1019–1024.

[182] S. Romano, B. Romer, K. Evans, M. Trybula, C. Shenoy, R. Y. Kwong, and A. Farzaneh-Far. "Prognostic Implications of Blunted Feature-Tracking Global Longitudinal Strain During Vasodilator Cardiovascular Magnetic Resonance Stress Imaging". In: *JACC: Cardiovascular Imaging* 13.1 (Jan. 2020), pp. 58–65.

[183] A. Gozdzik, T. H. Marwick, M. Przewlocka-Kosmala, E. A. Jankowska, P. Ponikowski, and W. Kosmala. "Comparison of left ventricular longitudinal systolic function parameters in the prediction of adverse outcome in heart failure with preserved ejection fraction". In: *ESC Heart Failure* 8.2 (2021), pp. 1531–1540.

[184] S. Romano et al. "Feature-Tracking Global Longitudinal Strain Predicts Death in a Multicenter Population of Patients With Ischemic and Nonischemic Dilated Cardiomyopathy Incremental to Ejection Fraction and Late Gadolinium Enhancement". In: *JACC: Cardiovascular Imaging* 11.10 (Oct. 2018), pp. 1419–1429.

[185] S. J. Buss et al. “Assessment of myocardial deformation with Cardiac magnetic resonance strain imaging improves risk stratification in patients with dilated cardiomyopathy”. In: *European Heart Journal Cardiovascular Imaging* 16.3 (2015), pp. 307–315.

[186] J. J. Park, J. B. Park, J. H. Park, and G. Y. Cho. “Global Longitudinal Strain to Predict Mortality in Patients With Acute Heart Failure”. In: *Journal of the American College of Cardiology* 71.18 (2018), pp. 1947–1957.

[187] J. Berg, R. Jablonowski, M. Mohammad, K. Solem, R. Borgquist, E. Ostenfeld, H. Arheden, and M. Carlsson. “Ventricular longitudinal shortening is an independent predictor of death in heart failure patients with reduced ejection fraction”. In: *Scientific Reports* 11.1 (Dec. 2021), p. 20280.

[188] M. Sengeløv, P. G. Jørgensen, J. S. Jensen, N. E. Bruun, F. J. Olsen, T. Fritz-Hansen, K. Nochioka, and T. Biering-Sørensen. “Global Longitudinal Strain is a Superior Predictor of All-Cause Mortality in Heart Failure with Reduced Ejection Fraction”. In: *JACC: Cardiovascular Imaging* 8.12 (2015), pp. 1351–1359.

[189] K. E. Farsalinos, A. M. Daraban, S. Ünlü, J. D. Thomas, L. P. Badano, and J.-U. Voigt. “Head-to-Head Comparison of Global Longitudinal Strain Measurements among Nine Different Vendors: The EACVI/ASE Inter-Vendor Comparison Study.” eng. In: *Journal of the American Society of Echocardiography : official publication of the American Society of Echocardiography* 28.10 (Oct. 2015), pp. 1171–1181.

[190] D. Liu, C. Wagner, K. Hu, B. Lengenfelder, G. Ertl, S. Frantz, and P. Nordbeck. “Prognostic value of global longitudinal strain versus mitral annular plane systolic excursion in patients with ischemic heart failure”. In: *European Heart Journal* 41.Supplement_2 (2020), p. 2020.

[191] M. Reindl et al. “Prognostic Implications of Global Longitudinal Strain by Feature-Tracking Cardiac Magnetic Resonance in ST-Elevation Myocardial Infarction”. In: *Circulation. Cardiovascular imaging* 12.11 (2019), e009404.

[192] O. Bieri and K. Scheffler. “Fundamentals of balanced steady state free precession MRI”. In: *Journal of Magnetic Resonance Imaging* 38.1 (2013), pp. 2–11.

[193] L. C. Amado, B. L. Gerber, S. N. Gupta, D. W. Rettmann, G. Szarf, R. Schock, K. Nasir, D. L. Kraitchman, and J. A. Lima. “Accurate and objective infarct sizing by contrast-enhanced magnetic resonance imaging in a canine myocardial infarction model”. In: *Journal of the American College of Cardiology* 44.12 (2004), pp. 2383–2389.

[194] R. Jablonowski, D. Nordlund, M. Kanski, J. Ubachs, S. Koul, E. Heiberg, H. Engblom, D. Erlinge, H. Arheden, and M. Carlsson. "Infarct quantification using 3D inversion recovery and 2D phase sensitive inversion recovery; validation in patients and ex vivo". In: *BMC Cardiovascular Disorders* 13 (2013).

[195] H. Arheden, M. Saeed, C. B. Higgins, D. W. Gao, J. Bremerich, R. Wyttenbach, M. W. Dae, and M. F. Wendland. "Measurement of the distribution volume of gadopentetate dimeglumine at echo-planar MR imaging to quantify myocardial infarction: comparison with 99mTc-DTPA autoradiography in rats." eng. In: *Radiology* 211.3 (June 1999), pp. 698–708.

[196] O. P. Simonetti, R. J. Kim, D. S. Fieno, H. B. Hillenbrand, E. Wu, J. M. Bundy, J. P. Finn, and R. M. Judd. "An improved MR imaging technique for the visualization of myocardial infarction." eng. In: *Radiology* 218.1 (Jan. 2001), pp. 215–223.

[197] P. Kellman and A. E. Arai. "Cardiac imaging techniques for physicians: Late enhancement". In: *Journal of Magnetic Resonance Imaging* 36.3 (2012), pp. 529–542.

[198] J. P. Cleutjens, M. J. Verluyten, J. F. Smits, and M. J. Daemen. "Collagen remodeling after myocardial infarction in the rat heart". In: *American Journal of Pathology* 147.2 (1995), pp. 325–338.

[199] M. Dobaczewski, M. Bujak, P. Zymek, G. Ren, M. L. Entman, and N. G. Frangogiannis. "Extracellular matrix remodeling in canine and mouse myocardial infarcts". In: *Cell and Tissue Research* 324.3 (2006), pp. 475–488.

[200] R. J. Kim, E. L. Chen, J. A. Lima, and R. M. Judd. "Myocardial Gd-DTPA kinetics determine MRI contrast enhancement and reflect the extent and severity of myocardial injury after acute reperfused infarction." eng. In: *Circulation* 94.12 (Dec. 1996), pp. 3318–3326.

[201] S. J. Flacke, S. E. Fischer, and C. H. Lorenz. "Measurement of the gadopentetate dimeglumine partition coefficient in human myocardium in vivo: normal distribution and elevation in acute and chronic infarction." eng. In: *Radiology* 218.3 (Mar. 2001), pp. 703–710.

[202] R. J. Kim, E. Wu, A. Rafael, E. L. Chen, M. A. Parker, O. Simonetti, F. J. Klocke, R. O. Bonow, and R. M. Judd. "The use of contrast-enhanced magnetic resonance imaging to identify reversible myocardial dysfunction." In: *The New England journal of medicine* 343.20 (Nov. 2000), pp. 1445–53.

[203] K. C. Wu, E. A. Zerhouni, R. M. Judd, C. H. Lugo-Olivieri, L. A. Barouch, S. P. Schulman, R. S. Blumenthal, and J. A. C. Lima. "Prognostic Significance of Microvascular Obstruction by Magnetic Resonance Imaging in Patients With Acute Myocardial Infarction". In: *Circulation* 97.8 (Mar. 1998), pp. 765–772.

[204] B. Ibanez et al. “Cardiac MRI Endpoints in Myocardial Infarction Experimental and Clinical Trials: JACC Scientific Expert Panel”. In: *Journal of the American College of Cardiology* 74.2 (2019), pp. 238–256.

[205] P. W. Doherty, M. J. Lipton, W. H. Berninger, C. G. Skioldebrand, E. Carlsson, and R. W. Redington. “Detection and quantitation of myocardial infarction in vivo using transmission computed tomography”. In: *Circulation* 63.3 (1981), pp. 597–606.

[206] H. W. Eichstaedt, R. Felix, F. C. Dougherty, M. Langer, W. Rutsch, and H. Schmutzler. “Magnetic resonance imaging (MRI) in different stages of myocardial infarction using the contrast agent gadolinium□DTPA”. In: *Clinical Cardiology* 9.11 (1986), pp. 527–535.

[207] P. Kellman, A. E. Arai, E. R. McVeigh, and A. H. Aletras. “Phase-sensitive inversion recovery for detecting myocardial infarction using gadolinium-delayed hyperenhancement”. In: *Magnetic Resonance in Medicine* 47.2 (2002), pp. 372–383.

[208] A. Huber, C. Hayes, B. Spannagl, J. Rieber, V. Klauss, S. O. Schoenberg, M. Reiser, and B. J. Wintersperger. “Phase-Sensitive Inversion Recovery Single-Shot Balanced Steady-State Free Precession for Detection of Myocardial Infarction During a Single Breathhold”. In: *Academic Radiology* 14.12 (2007), pp. 1500–1508.

[209] P. Kellman and A. Larson. “Motion□corrected free□breathing delayed enhancement imaging of myocardial infarction”. In: *Magnetic Resonance in Medicine* 53.1 (2005), pp. 194–200.

[210] M. J. Ledesma-Carbayo, P. Kellman, A. E. Arai, and E. R. McVeigh. “Motion corrected free-breathing delayed-enhancement imaging of myocardial infarction using nonrigid registration”. In: *Journal of Magnetic Resonance Imaging* 26.1 (2007), pp. 184–190.

[211] K. M. Piehler et al. “Free-breathing, motion-corrected late gadolinium enhancement is robust and extends risk stratification to vulnerable patients”. In: *Circulation: Cardiovascular Imaging* 6.3 (2013), pp. 423–432.

[212] P. Kellman, H. Xue, L. J. Olivieri, R. R. Cross, E. K. Grant, M. Fontana, M. Ugander, J. C. Moon, and M. S. Hansen. “Dark blood late enhancement imaging”. In: *Journal of Cardiovascular Magnetic Resonance* 18.1 (2016), pp. 1–11.

[213] L. Y. Hsu, A. Natanzon, P. Kellman, G. A. Hirsch, A. H. Aletras, and A. E. Arai. “Quantitative myocardial infarction on delayed enhancement MRI. Part I: Animal validation of an automated feature analysis and combined thresholding infarct sizing algorithm”. In: *Journal of Magnetic Resonance Imaging* 23.3 (2006), pp. 298–308.

[214] R. J. Kim, D. S. Fieno, T. B. Parrish, K. Harris, E. L. Chen, O. Simonetti, J. Bundy, J. P. Finn, F. J. Klocke, and R. M. Judd. "Relationship of MRI delayed contrast enhancement to irreversible injury, infarct age, and contractile function". In: *Circulation* 100.19 (1999), pp. 1992–2002.

[215] L. J. Acierno and L. T. Worrell. "Inge Edler: father of echocardiography." In: *Clinical cardiology* 25.4 (Apr. 2002), pp. 197–9.

[216] I. Edler and C. H. Hertz. "The Use of Ultrasonic Reflectoscope for the Continuous Recording of the Movements of Heart Walls." In: *Clinical Physiology and Functional Imaging* 24.3 (May 2004), pp. 118–136.

[217] R. S. Bhatia, J. V. Tu, D. S. Lee, P. C. Austin, J. Fang, A. Haouzi, Y. Gong, and P. P. Liu. "Outcome of Heart Failure with Preserved Ejection Fraction in a Population-Based Study". In: *New England Journal of Medicine* 355.3 (2006), pp. 260–269.

[218] K. Hogg, K. Swedberg, and J. McMurray. "Heart Failure with Preserved Left Ventricular Systolic Function: Epidemiology, Clinical Characteristics, and Prognosis". In: *Journal of the American College of Cardiology* 43.3 (2004), pp. 317–327.

[219] A. M. Shah, B. Claggett, N. K. Sweitzer, S. J. Shah, I. S. Anand, L. Liu, B. Pitt, M. A. Pfeffer, and S. D. Solomon. "Prognostic importance of impaired systolic function in heart failure with preserved ejection fraction and the impact of spironolactone". In: *Circulation* 132.5 (2015), pp. 402–414.

[220] A. A. Kammerlander et al. "Global Longitudinal Strain by CMR Feature Tracking Is Associated With Outcome in HFPEF". In: *JACC: Cardiovascular Imaging* 12.8P1 (2019), pp. 1585–1587.

[221] M. S. Amzulescu, M. De Craene, H. Langet, A. Pasquet, D. Vancraeynest, A. C. Pouleur, J. L. Vanoverschelde, and B. L. Gerber. "Myocardial strain imaging: review of general principles, validation, and sources of discrepancies". In: *European Heart Journal - Cardiovascular Imaging* 32 (2019), pp. 605–619.

[222] K. K. Kadappu and L. Thomas. "Tissue doppler imaging in echocardiography: Value and limitations". In: *Heart Lung and Circulation* 24.3 (2015), pp. 224–233.

[223] H. Blessberger and T. Binder. "Two dimensional speckle tracking echocardiography: Clinical applications". In: *Heart* 96.24 (2010), pp. 2032–2040.

[224] S. Stephensen, K. Steding-Ehrenborg, P. Munkhammar, E. Heiberg, H. Arheden, and M. Carlsson. "The relationship between longitudinal, lateral, and septal contribution to stroke volume in patients with pulmonary regurgitation and healthy volunteers". In: *AJP: Heart and Circulatory Physiology* 306.6 (2014), H895–H903.

[225] A. Fyrdahl, J. G. Ramos, M. J. Eriksson, K. Caidahl, M. Ugander, and A. Sigfridsson. "Sector-wise golden-angle phase contrast with high temporal resolution for evaluation of left ventricular diastolic dysfunction". In: *Magnetic Resonance in Medicine* 83.4 (2020), pp. 1310–1321.

[226] A. A. Young, L. Axel, L. Dougherty, D. K. Bogen, and C. S. Parenteau. "Validation of tagging with MR imaging to estimate material deformation." In: *Radiology* 188.1 (July 1993), pp. 101–108.

[227] S. B. Yeon, N. Reichek, B. A. Tallant, J. A. Lima, L. P. Calhoun, N. R. Clark, E. A. Hoffman, K. K. Ho, and L. Axel. "Validation of in vivo myocardial strain measurement by magnetic resonance tagging with sonomicrometry". In: *Journal of the American College of Cardiology* 38.2 (2001), pp. 555–561.

[228] E. A. Zerhouni, D. M. Parish, W. J. Rogers, A. Yang, and E. P. Shapiro. "Human heart: Tagging with MR imaging - A new method for noninvasive assessment of myocardial motion". In: *Radiology* 169.1 (1988), pp. 59–63.

[229] N. F. Osman, W. S. Kerwin, E. R. McVeigh, and J. L. Prince. "Cardiac motion tracking using CINE harmonic phase (HARP) magnetic resonance imaging." In: *Magnetic resonance in medicine* 42.6 (Dec. 1999), pp. 1048–60.

[230] N. F. Osman, S. Sampath, E. Atalar, and J. L. Prince. "Imaging longitudinal cardiac strain on short-axis images using strain-encoded MRI". In: *Magnetic Resonance in Medicine* 46.2 (2001), pp. 324–334.

[231] A. H. Aletras, S. Ding, R. S. Balaban, and H. Wen. "DENSE: Displacement Encoding with Stimulated Echoes in Cardiac Functional MRI". In: *Journal of Magnetic Resonance* 137.1 (Mar. 1999), pp. 247–252.

[232] L. Pan, M. Stuber, D. L. Kraitchman, D. L. Fritzges, W. D. Gilson, and N. F. Osman. "Real-time imaging of regional myocardial function using fast-SENC". In: *Magnetic Resonance in Medicine* 55.2 (2006), pp. 386–395.

[233] Yudong Zhu, M. Drangova, and N. Pelc. "Estimation of deformation gradient and strain from cine-PC velocity data [cardiac magnetic resonance imaging]". In: *IEEE Transactions on Medical Imaging* 16.6 (1997), pp. 840–851.

[234] P. Bucius et al. "Comparison of feature tracking, fast-SENC, and myocardial tagging for global and segmental left ventricular strain." In: *ESC heart failure* 7.2 (2020), pp. 523–532.

[235] T. Hoskin. "Parametric and nonparametric: Demystifying the terms". In: *Mayo Clinic*. Vol. 5. 1. 2012, pp. 1–5.

[236] T. R. Fleming and D. Y. Lin. "Survival Analysis in Clinical Trials: Past Developments and Future Directions". In: *Biometrics* 56.4 (Dec. 2000), pp. 971–983.

[237] E. L. Kaplan and P. Meier. "Nonparametric Estimation from Incomplete Observations". In: *Journal of the American Statistical Association* 53.282 (June 1958), pp. 457–481.

[238] N. Mantel. "Evaluation of survival data and two new rank order statistics arising in its consideration." In: *Cancer chemotherapy reports* 50.3 (Mar. 1966), pp. 163–70.

[239] D. R. Cox. "Regression Models and Life-Tables". In: *Journal of the Royal Statistical Society: Series B (Methodological)* 34.2 (Jan. 1972), pp. 187–202.

[240] F. Zannad et al. "Clinical outcome endpoints in heart failure trials: A European Society of Cardiology Heart Failure Association consensus document". In: *European Journal of Heart Failure* 15.10 (2013), pp. 1082–1094.

[241] M. Wolbers, M. T. Koller, V. S. Stel, B. Schaer, K. J. Jager, K. Leffondre, and G. Heinze. "Competing risks analyses: Objectives and approaches". In: *European Heart Journal* 35.42 (2014), pp. 2936–2941.

[242] M. Huebner, M. Wolkewitz, M. Enriquez-Sarano, and M. Schumacher. "Competing risks need to be considered in survival analysis models for cardiovascular outcomes". In: *Journal of Thoracic and Cardiovascular Surgery* 153.6 (2017), pp. 1427–1431.

[243] R. J. Gray. "A Class of K-Sample Tests for Comparing the Cumulative Incidence of a Competing Risk". In: *The Annals of Statistics* 16.3 (Sept. 1988).

[244] J. P. Fine and R. J. Gray. "A Proportional Hazards Model for the Subdistribution of a Competing Risk". In: *Journal of the American Statistical Association* 94.446 (1999), pp. 496–509.

[245] C. A. Ariti, J. G. Cleland, S. J. Pocock, M. A. Pfeffer, K. Swedberg, C. B. Granger, J. J. McMurray, E. L. Michelson, J. Östergren, and S. Yusuf. "Days alive and out of hospital and the patient journey in patients with heart failure: Insights from the Candesartan in Heart failure: Assessment of Reduction in Mortality and morbidity (CHARM) program". In: *American Heart Journal* 162.5 (2011), pp. 900–906.

[246] S. J. Pocock, C. A. Ariti, T. J. Collier, and D. Wang. "The win ratio: A new approach to the analysis of composite endpoints in clinical trials based on clinical priorities". In: *European Heart Journal* 33.2 (2012), pp. 176–182.

[247] J. F. Lawless and C. Nadeau. "Some Simple Robust Methods for the Analysis of Recurrent Events". In: *Technometrics* 37.2 (May 1995), pp. 158–168.

[248] L. T. Yang, E. Yamashita, Y. Nagata, Y. Kado, S. Oshima, Y. Otsuji, and M. Takeuchi. "Prognostic value of biventricular mechanical parameters assessed using cardiac magnetic resonance feature-tracking analysis to predict future cardiac events". In: *Journal of Magnetic Resonance Imaging* 45.4 (2017), pp. 1034–1045.

[249] R. L. Prentice, B. J. Williams, and A. V. Peterson. "On the regression analysis of multivariate failure time data". In: *Biometrika* 68.2 (1981), pp. 373–379.

[250] P. K. Andersen and R. D. Gill. "Cox's Regression Model for Counting Processes: A Large Sample Study". In: *The Annals of Statistics* 10.4 (Dec. 1982).

[251] L. J. Wei, D. Y. Lin, and L. Weissfeld. "Regression Analysis of Multivariate Incomplete Failure Time Data by Modeling Marginal Distributions". In: *Journal of the American Statistical Association* 84.408 (Dec. 1989), pp. 1065–1073.

[252] P. K. Andersen and N. Keiding. “Multi-state models for event history analysis”. In: *Statistical Methods in Medical Research* 11.2 (2002), pp. 91–115.

[253] J. K. Rogers, S. J. Pocock, J. J. McMurray, C. B. Granger, E. L. Michelson, J. Östergren, M. A. Pfeffer, S. D. Solomon, K. Swedberg, and S. Yusuf. “Analysing recurrent hospitalizations in heart failure: a review of statistical methodology, with application to CHARM-Preserved”. In: *European Journal of Heart Failure* 16.5 (May 2014), pp. 592–592.

[254] A. C. Alba, T. Agoritsas, M. Walsh, S. Hanna, A. Iorio, P. J. Devereaux, T. McGinn, and G. Guyatt. “Discrimination and calibration of clinical prediction models: Users’ guides to the medical literature”. In: *JAMA - Journal of the American Medical Association* 318.14 (2017), pp. 1377–1384.

[255] A. J. Vickers, A. M. Cronin, and C. B. Begg. “One statistical test is sufficient for assessing new predictive markers”. In: *BMC Medical Research Methodology* 11 (2011), pp. 1–7.

[256] F. E. Harrell. “Evaluating the Yield of Medical Tests”. In: *JAMA: The Journal of the American Medical Association* 247.18 (May 1982), p. 2543.

[257] E. Longato, M. Vettoretti, and B. Di Camillo. “A practical perspective on the concordance index for the evaluation and selection of prognostic time-to-event models”. In: *Journal of Biomedical Informatics* 108.June (2020), p. 103496.

[258] P. Royston and D. G. Altman. “External validation of a Cox prognostic model: principles and methods”. In: *BMC Medical Research Methodology* 13.1 (Dec. 2013), p. 33.

[259] M. J. Pencina, R. B. D’ Agostino, R. B. D’ Agostino, and R. S. Vasan. “Evaluating the added predictive ability of a new marker: From area under the ROC curve to reclassification and beyond”. In: *Statistics in Medicine* 27.2 (Jan. 2008), pp. 157–172.

[260] M. J. Pencina, R. B. D’Agostino, and O. V. Demler. “Novel metrics for evaluating improvement in discrimination: net reclassification and integrated discrimination improvement for normal variables and nested models”. In: *Statistics in Medicine* 31.2 (Jan. 2012), pp. 101–113.

[261] J. C. Garber. *Guide for the Care and Use of Laboratory Animals*. Eight edit. National research council of the national academies, 2011, 2011, pp. 1–220.

[262] P. P. Lelovas, N. G. Kostomitsopoulos, and T. T. Xanthos. “A comparative anatomic and physiologic overview of the porcine heart.” In: *Journal of the American Association for Laboratory Animal Science : JAALAS* 53.5 (2014), pp. 432–8.

[263] M. A. Genain, A. Morlet, M. Herrtage, H. Muresian, F. Anselme, C. Latremouille, F. Laborde, L. Behr, and N. Borenstein. "Comparative anatomy and angiography of the cardiac coronary venous system in four species: human, ovine, porcine, and canine". In: *Journal of Veterinary Cardiology* 20.1 (2018), pp. 33–44.

[264] H. Engblom et al. "A new automatic algorithm for quantification of myocardial infarction imaged by late gadolinium enhancement cardiovascular magnetic resonance: Experimental validation and comparison to expert delineations in multi-center, multi-vendor patient data". In: *Journal of Cardiovascular Magnetic Resonance* 18.1 (2016), pp. 1–13.

[265] M. Carlsson, D. Saloner, A. J. Martin, P. C. Ursell, and M. Saeed. "Heterogeneous microinfarcts caused by coronary microemboli: evaluation with multidetector CT and MR imaging in a swine model." In: *Radiology* 254.3 (2010), pp. 718–28.

[266] M. Carlsson, M. Wilson, A. J. Martin, and M. Saeed. "Myocardial microinfarction after coronary microembolization in swine: MR imaging characterization." In: *Radiology* 250.3 (2009), pp. 703–13.

[267] R. Y. Kwong and A. Farzaneh-Far. "Measuring myocardial scar by CMR". In: *JACC: Cardiovascular Imaging* 4.2 (2011), pp. 157–160.

[268] E. Heiberg, J. Sjögren, M. Ugander, M. Carlsson, H. Engblom, and H. Arheden. "Design and validation of Segment - freely available software for cardiovascular image analysis". In: *BMC Medical Imaging* 10 (2010), pp. 1–13.

[269] R. M. Lang et al. "Recommendations for chamber quantification: A report from the American Society of Echocardiography's guidelines and standards committee and the Chamber Quantification Writing Group, developed in conjunction with the European Association of Echocardiograph". In: *Journal of the American Society of Echocardiography* 18.12 (2005), pp. 1440–1463.

[270] F. Seemann et al. "Time-resolved tracking of the atrioventricular plane displacement in Cardiovascular Magnetic Resonance (CMR) images". In: *BMC Medical Imaging* 17.19 (2017), p. 19.

[271] B. Heyde, R. Jasaityte, D. Barbosa, V. Robesyn, S. Bouchez, P. Wouters, F. Maes, P. Claus, and J. D'hooge. "Elastic image registration versus speckle tracking for 2-D myocardial motion estimation: a direct comparison in vivo." In: *IEEE transactions on medical imaging* 32.2 (Feb. 2013), pp. 449–59.

[272] F. Seemann, P. Arvidsson, D. Nordlund, S. Kopic, M. Carlsson, H. Arheden, and E. Heiberg. "Noninvasive Quantification of Pressure-Volume Loops From Brachial Pressure and Cardiovascular Magnetic Resonance". In: *Circulation. Cardiovascular imaging* 12.1 (2019), e008493.

[273] P. Sjöberg, F. Seemann, H. Arheden, and E. Heiberg. "Non-invasive quantification of pressure-volume loops from cardiovascular magnetic resonance at rest and during dobutamine stress." In: *Clinical physiology and functional imaging* 41.5 (Sept. 2021), pp. 467–470.

[274] M. B. Bastos et al. "Invasive left ventricle pressure-volume analysis: Overview and practical clinical implications". In: *European Heart Journal* 41.12 (2020), pp. 1286–1297.

[275] J. Bland and D. Altman. "Statistical methods for assessing agreement between two methods of clinical measurement". In: *Lancet* 8;1(8476): (1986), pp. 307–10.

[276] K. P. Vatcheva and M. Lee. "Multicollinearity in Regression Analyses Conducted in Epidemiologic Studies". In: *Epidemiology: Open Access* 06.02 (2016).

[277] K. A. Reimer, J. E. Lowe, M. M. Rasmussen, and R. B. Jennings. "The wavefront phenomenon of ischemic cell death. 1. Myocardial infarct size vs duration of coronary occlusion in dogs." In: *Circulation* 56.5 (Nov. 1977), pp. 786–794.

[278] I. Porto, J. B. Selvanayagam, W. J. Van Gaal, F. Prati, A. Cheng, K. Channon, S. Neubauer, and A. P. Banning. "Plaque Volume and Occurrence and Location of Periprocedural Myocardial Necrosis After Percutaneous Coronary Intervention". In: *Circulation* 114.7 (Aug. 2006), pp. 662–669.

[279] A. Stoylen. *Regional functional imaging*.

[280] A. Kranidis et al. "Analysis of Left Atrioventricular Plane Movement during Diastole in Ischemic Heart Disease." In: *Japanese Heart Journal* 36.5 (1995), pp. 545–556.

[281] P. J. Kennelly and V. W. Rodwell. "Enzymes: Kinetics". In: *Harper's Illustrated Biochemistry, 30e*. Ed. by V. W. Rodwell, D. A. Bender, K. M. Botham, P. J. Kennelly, and P. A. Weil. New York, NY: McGraw-Hill Education, May 2016.

[282] D. Erlinge. "A Review of Mild Hypothermia as an Adjunctive Treatment for ST-Elevation Myocardial Infarction". In: *Therapeutic Hypothermia and Temperature Management* 1.3 (2011), pp. 129–141.

[283] O. Prec, R. Rosenman, K. Braun, S. Rodbard, and L. N. Katz. "The cardiovascular effects of acutely induced hypothermia". In: *Journal of Clinical Investigation* 28.2 (Mar. 1949), pp. 293–300.

[284] G. J. van den Horn, N. Westerhof, and G. Elzinga. "Optimal power generation by the left ventricle. A study in the anesthetized open thorax cat." In: *Circulation Research* 56.2 (Feb. 1985), pp. 252–261.

[285] W. C. Little and C. P. Cheng. "Effect of exercise on left ventricular-arterial coupling assessed in the pressure-volume plane". In: *American Journal of Physiology-Heart and Circulatory Physiology* 264.5 (May 1993), H1629–H1633.

[286] T. Bombardini, M. F. Costantino, R. Sicari, Q. Ciampi, L. Pratali, and E. Picano. "End-systolic elastance and ventricular-arterial coupling reserve predict cardiac events in patients with negative stress echocardiography". In: *BioMed Research International* 2013 (2013).

[287] F. Antonini-Canterin, S. Poli, O. Vriz, D. Pavan, V. Bello, and G. Nicolosi. "The ventricular-arterial coupling: From basic pathophysiology to clinical application in the echocardiography laboratory". In: *Journal of Cardiovascular Echography* 23.4 (2013), pp. 91–95.

[288] B. Ky et al. "Ventricular-arterial coupling, remodeling, and prognosis in chronic heart failure". In: *Journal of the American College of Cardiology* 62.13 (2013), pp. 1165–1172.

[289] A. Milewska, A. Minczykowski, T. Krauze, J. Piskorski, J. Heathers, A. Szczepanik, A. Banaszak, P. Guzik, and A. Wykretowicz. "Prognosis after acute coronary syndrome in relation with ventricular–arterial coupling and left ventricular strain". In: *International Journal of Cardiology* 220 (2016), pp. 343–348.

[290] F. D. Hobbs, J. E. Kenkre, A. K. Roalfe, R. C. Davis, R. Hare, and M. K. Davies. "Impact of heart failure and left ventricular systolic dysfunction on quality of life: A cross-sectional study comparing common chronic cardiac and medical disorders and a representative adult population". In: *European Heart Journal* 23.23 (2002), pp. 1867–1876.

[291] R. Zarrinkoub, B. Wettermark, P. W??ndell, M. Mejhert, R. Szulkin, G. Ljunggren, and T. Kahan. "The epidemiology of heart failure, based on data for 2.1 million inhabitants in Sweden". In: *European Journal of Heart Failure* 15.9 (2013), pp. 995–1002.

[292] F. Fröjdh et al. "Extracellular Volume and Global Longitudinal Strain Both Associate With Outcomes But Correlate Minimally". In: *JACC: Cardiovascular Imaging* 13.11 (Nov. 2020), pp. 2343–2354.

[293] J. Berg, P. Lindgren, T. Kahan, O. Schill, H. Persson, M. Edner, and M. Mejhert. "Health-related quality of life and long-term morbidity and mortality in patients hospitalised with systolic heart failure". In: *JRSM Cardiovascular Disease* 3 (2014), p. 204800401454873.

[294] S. Setoguchi, L. W. Stevenson, and S. Schneeweiss. "Repeated hospitalizations predict mortality in the community population with heart failure". In: *American Heart Journal* 154.2 (2007), pp. 260–266.

[295] Meta-analysis Global Group in Chronic Heart Failure (MAGGIC). "The survival of patients with heart failure with preserved or reduced left ventricular ejection fraction: an individual patient data meta-analysis." In: *European heart journal* 33.14 (July 2012), pp. 1750–7.

[296] W. Ouwerkerk, A. A. Voors, and A. H. Zwinderman. "Factors influencing the predictive power of models for predicting mortality and/or heart failure hospitalization in patients with heart failure." In: *JACC. Heart failure* 2.5 (Oct. 2014), pp. 429–36.

[297] R. E. S. Bowen, T. J. Graetz, D. A. Emmert, and M. S. Avidan. "Statistics of heart failure and mechanical circulatory support in 2020". In: *Annals of Translational Medicine* 8.13 (July 2020), pp. 827–827.

[298] S. Reardon. "First pig-to-human heart transplant: what can scientists learn?" In: *Nature* 601.7893 (Jan. 2022), pp. 305–306.

[299] D. J. Goldstein, B. Meyns, R. Xie, J. Cowger, S. Pettit, T. Nakatani, I. Netuka, S. Shaw, M. Yanase, and J. K. Kirklin. "Third Annual Report From the ISHLT Mechanically Assisted Circulatory Support Registry: A comparison of centrifugal and axial continuous-flow left ventricular assist devices". In: *Journal of Heart and Lung Transplantation* 38.4 (2019), pp. 352–363.

[300] K. K. Khush et al. "The International Thoracic Organ Transplant Registry of the International Society for Heart and Lung Transplantation: Thirty-sixth adult heart transplantation report — 2019; focus theme: Donor and recipient size match". In: *Journal of Heart and Lung Transplantation* 38.10 (2019), pp. 1056–1066.

[301] A. K. Loya, S. K. Van Houten, B. M. Glasheen, and D. M. Swank. "Shortening deactivation: quantifying a critical component of cyclical muscle contraction". In: *American Journal of Physiology-Cell Physiology* 322.4 (Dec. 2021), pp. C653–C665.

[302] J. K. Leach, D. V. Priola, L. A. Grimes, and B. J. Skipper. "Shortening deactivation of cardiac muscle: physiological mechanisms and clinical implications." In: *Journal of investigative medicine : the official publication of the American Federation for Clinical Research* 47.8 (Sept. 1999), pp. 369–77.

[303] S. Kopic, S. S. Stephensen, E. Heiberg, H. Arheden, P. Bonhoeffer, M. Ersbøll, N. Vejlstrup, L. Søndergaard, and M. Carlsson. "Isolated pulmonary regurgitation causes decreased right ventricular longitudinal function and compensatory increased septal pumping in a porcine model". In: *Acta Physiologica* 221.3 (2017), pp. 163–173.

[304] T. G. Witkowski et al. "Changes in left ventricular function after mitral valve repair for severe organic mitral regurgitation". In: *Annals of Thoracic Surgery* 93.3 (2012), pp. 754–760.

[305] V. Kamperidis, N. A. Marsan, V. Delgado, and J. J. Bax. "Left ventricular systolic function assessment in secondary mitral regurgitation: Left ventricular ejection fraction vs. speckle tracking global longitudinal strain". In: *European Heart Journal* 37.10 (2016), pp. 811–816.

[306] H. Xue et al. “Automated Inline Artificial Intelligence Measured Global Longitudinal Shortening and Mitral annular plane systolic excursion: Reproducibility and Prognostic Significance”. In: *Journal of the American Heart Association* Accepted. (Feb. 2022).

[307] P. Thavendiranathan et al. “Strain-Guided Management of Potentially Cardiotoxic Cancer Therapy”. In: *Journal of the American College of Cardiology* 77.4 (2021), pp. 392–401.

[308] C. H. Chen, B. Fetics, E. Nevo, C. E. Rochitte, K. R. Chiou, P. A. Ding, M. Kawaguchi, and D. A. Kass. “Noninvasive single-beat determination of left ventricular end-systolic elastance in humans.” In: *Journal of the American College of Cardiology* 38.7 (Dec. 2001), pp. 2028–34.

[309] S. Urheim, S. I. Rabben, H. Skulstad, E. Lyseggen, H. Ihlen, and O. A. Smiseth. “Regional myocardial work by strain Doppler echocardiography and LV pressure: a new method for quantifying myocardial function”. In: *American Journal of Physiology-Heart and Circulatory Physiology* 288.5 (May 2005), H2375–H2380.

[310] A. Hubert, V. Le Rolle, C. Leclercq, E. Galli, E. Samset, C. Casset, P. Mabo, A. Hernandez, and E. Donal. “Estimation of myocardial work from pressure–strain loops analysis: an experimental evaluation”. In: *European Heart Journal Cardiovascular Imaging* 19.12 (2018), pp. 1372–1379.

[311] A. Kolipaka, P. A. Araoz, K. P. McGee, A. Manduca, and R. L. Ehman. “Magnetic resonance elastography as a method for the assessment of effective myocardial stiffness throughout the cardiac cycle”. In: *Magnetic Resonance in Medicine* 64.3 (2010), pp. 862–870.

Author Contributions

	Study design	Ethical application	Data collection	Statistical analysis	Figures and tables	Interpretation of results	Preparation of manuscript	Revision of manuscript	Reply to reviewers
Study I	3	0	2	2	3	3	3	3	3
Study II	3	0	3	3	3	3	3	-	-
Study III	3	1	3	3	3	3	3	3	3
Study IV	3	1	3	3	3	3	3	3	3

Not applicable	-
No contribution	0
Limited contribution	1
Moderate contribution	2
Significant contribution	3

Cardiac Long-Axis Function

Jonathan Berg was born on the 9th of May, 1992. He and his family lived in a large house in the countryside near the village of Vessigebro, municipality of Falkenberg, on the western coast of Sweden. After receiving his Upper secondary diploma in Falkenberg in 2011 while playing professional indoor volleyball, he embarked on his medical career at the Lund Medical School at Lund University the subsequent year. He graduated in the summer of 2017 and started working at the Department of Surgery in Helsingborg. However, during his final year in medical school, there was news about an upcoming Ph.D. project involving the heart. After a few months of working as a medical doctor, Jonathan applied for the project. He got registered as a Ph.D. student in September 2017 at the Department of Clinical Physiology in collaboration with the med-tech company Syntach AB. This thesis is the culmination of said Ph.D. project.

Printed by Media-Tryck, Lund 2022 NORDIC SWAN ECOLABEL 3041 0903

LUND UNIVERSITY

FACULTY OF MEDICINE

Department of clinical physiology

Lund University, Faculty of Medicine
Doctoral Dissertation Series 2022:97
ISBN 978-91-8021-258-8
ISSN 1652-8220